STUDIES ON HEAT TRANSFER CHARACTERISTICS OF HEAT PIPE HEAT EXCHANGER UNDER NATURAL CONVECTION

A Thesis
Submitted in Fulfillment of the
Requirements for the Degree of

DOCTOR OF PHILOSOPHY
in
MECHANICAL ENGINEERING

By
VIKAS KUMAR

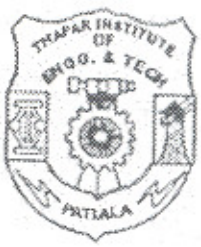

DEPARTMENT OF MECHANICAL ENGINEERING
THAPAR INSTITUTE OF ENGINEERING AND TECHNOLOGY
(DEEMED UNIVERSITY)
PATIALA, PUNJAB, INDIA
2004

CERTIFICATE

Certified that the thesis entitled **STUDIES ON HEAT TRANSFER CHARACTERISTICS OF HEAT PIPE HEAT EXCHANGER UNDER NATURAL CONVECTION** which is being submitted by **Mr. Vikas Kumar**, in fulfillment of the requirements for the award of the Degree of **Doctor of Philosophy** in the Department of Mechanical Engineering, **Thapar Institute of Engineering and Technology, Patiala (INDIA)**, is a record of candidate's own work carried out by him under our supervision and guidance. The matter embodied in this thesis has not been submitted in part or full to any other University or Institution for the award of any Degree.

D. Gangacharyulu 23/03/2005

(**D. Gangacharyulu**)
(Supervisor)
Assistant Professor
Department of Chemical Engineering

23/3

(**R.G. Tathgir**)
(Supervisor)
Professor
Department of Mechanical Engineering

ACKNOWLEDGMENTS

The author is deeply indebted to Dr. R.G. Tathgir, Professor, Mechanical Engineering and Dr. D. Gangacharyulu, Assistant Professor, Chemical Engineering, Thapar Institute of Engineering & Technology, Patiala, India for acting as supervisors and giving valuable guidance during the course of this investigation.

The author acknowledges with gratitude the help given by Director, Thapar Institute of Engineering & Technology, Patiala and Director, Thapar Centre for Industrial Research & Development, Patiala for providing facilities to execute this research work.

Thanks are also due to staff at Thapar Institute of Engineering & Technology and Thapar Centre for Industrial Research & Development for their cooperation and assistance in completing this work.

The author is thankful to management of Centre for Development of Advanced Computing (C-DAC), Pune, India for providing computing facility, encouragement and kind cooperation, which helped in completion of the thesis.

The author is grateful to his family members for all the support & encouragement extended to him during the course of this study.

Vikas Kumar

(Vikas Kumar)

23.03.05

ABSTRACT

An analytical model has been developed to evaluate the thermal performance of a heat pipe heat exchanger (HPHE) under natural convection by adopting thermal resistance approach. The model evaluates the rate of heat transport and pressure drop across evaporator system of the HPHE under natural convection. The model computes various thermal resistances of the heat pipe at the external surface of evaporator & condenser as well as at the internal surface of the heat pipe based on the correlations available in the literature. The rate of heat transport has been calculated by converting the model into a computer programme, whose solution is based on an iterative procedure.

A test rig has been developed for thermal performance evaluation of a single heat pipe under natural convective conditions as well as to do the validation of the analytical model for the same. Natural convective experimental studies have been carried out on the heat pipe at different tilt angles from the horizontal, i.e., 15°, 20°, 25°, 30°, 35°, & 90° and various temperatures of the heating fluid, i.e., 40 °C, 50 °C, 60 °C, & 70 °C at a constant flow rate of the heating fluid (laminar flow regime) in the evaporator section at an ambient temperature of about 13±1 °C. The experimental observations reveal that the tilt angle and the heating fluid temperature influence the heat transport rate of the heat pipe. The heat transport rate increases as the tilt angle of the heat pipe increases from 15° to 25°, and it starts decreasing beyond 25°. The maximum heat transport rate of the heat pipe has been obtained at a tilt angle of 25° and 70.3 °C heating fluid temperature, which may be due to the lowest overall thermal resistance at this operating condition, which is caused by the minimal external condenser thermal resistance of the finned condenser.

Some typical experimental results on different individual heat transfer coefficients have been compared with the analytical model for a single heat pipe at 25° tilt angle. The evaporator heat transfer coefficient predicted by using Dobson & Kröger's correlation has closer agreement with the experimental value as compared to Fand's correlation, therefore, the computed evaporator surface temperature is very close (within 1 °C) to the experimental value. The internal heat transfer coefficient of the heat pipe predicted by the correlation provided by Chi, is 3.5 to 4.7 times more as compared to the experimental value, therefore the predicted condenser temperature

is on the higher side by 3.1 °C to 5.6 °C as compared to the experimental value. The heat transfer coefficient on the condenser side predicted by the correlation proposed by Churchill and Chu (for all range of Rayleigh number) is close to the experimental value. Even though, there is a large deviation in the prediction of internal heat transfer coefficient of the heat pipe, the overall heat transfer coefficient predicted by the analytical model is in good agreement with the experimental value. In fact, the value of internal heat transfer coefficient is very high and it contributes little to the overall heat transfer coefficient, which is mostly governed by condenser heat transfer coefficient and to a less degree by evaporator heat transfer coefficient.

The analytical model validated on a single heat pipe has been extended to the HPHE by incorporating appropriate geometrical & heat transfer correlations. Another test rig has been developed for evaluating the thermal performance of a HPHE under natural convective cooling condition as well as for validating the analytical model. The experiments have been conducted on the HPHE under natural convective condition at different tilt angles from the horizontal (15°, 20°, 25°, 30°, & 90°) and at various heating fluid temperatures (40 °C, 50 °C, 60 °C, & 70 °C) at its evaporator inlet. The Reynolds number of heating fluid in the evaporator section varied in the range of 436 to 1380. The variation of ambient surrounding temperature was in the range of 18 °C to 22 °C. The experimental studies show that the heat transport rate of the HPHE increases marginally as the Reynolds number of heating fluid increases in the evaporator section because the condenser heat transfer coefficient does not increase significantly. The maximum heat transport rate from the HPHE has been obtained at 25° tilt angle and 70 °C heating fluid temperature.

Some typical results of heat transport rate obtained from experiments for the HPHE at 25° tilt angle have been compared with the results predicted by the analytical model. It has been observed that the heat transport rate predicted by the analytical model is 7 to 27 % more than the heat transport rate of the HPHE obtained from the experiments. The excess heat transport rate prediction is due to computation of higher value of internal heat transfer coefficient by the analytical model and the model predicts in turn higher condenser temperature. The pressure drop across tube bundle in the evaporator section of the HPHE is small in magnitude and majority of the pressure drop is due to sudden expansion & contraction of the heating fluid at the inlet & outlet of the evaporator section. The deviation in the computed pressure drop and the experimental value is within the range of 2 to 13 %.

The present investigation concludes that the developed analytical model for thermal performance evaluation of the HPHE is reasonably in good agreement with the experimental results. It is expected that the analytical model along with computer programme can be used as a design tool for thermal performance analysis and rating of the HPHE under various configurations & operating conditions for natural convective applications.

TABLE OF CONTENTS

LIST OF FIGURES

LIST OF PLATES

LIST OF TABLES

NOMENCLATURE

Symbol	Description	Unit
A	cross section area	m^2
A_c	external surface area of condenser	m^2
A_e	external surface area of evaporator	m^2
A_f	fin surface area	m^2
A_{free}	minimum free flow area in the evaporator	m^2
$A_{frontal}$	frontal area of the heat exchanger	m^2
A_h	hot fluid side heat transfer surface area	m^2
A_o	external condenser surface area without fin	m^2
A_p	heat pipe cross sectional area without fin	m^2
A_{sw}	surface area of wooden box	m^2
A_v	vapour core area	m^2
c_p	specific heat	J/(kg-K)
D_h	hydraulic diameter	m
d	wire screen diameter	m
d_i	inner diameter of heat pipe	m
$d_{f,o}$	outer diameter of fin	m
d_o	outer diameter of heat pipe	m
d_v	vapour core diameter of heat pipe	m
F	radiation shape factor	dimensionless
f	fanning friction factor	dimensionless
F_l	liquid frictional coefficient	Pa/(W-m)
F_v	vapor frictional coefficient	Pa/(W-m)
G	mass velocity of heating fluid	$kg/(s\text{-}m^2)$
Gr_L	Grashof number	dimensionless
g	acceleration due to gravity	m^2/s
h	heat transfer coefficient	$W/(m^2\text{-}K)$
$\bar{h}$	average heat transfer coefficient	$W/(m^2\text{-}K)$
h_c	external heat transfer coefficient on condenser	$W/(m^2\text{-}K)$
h_{cond}	heat transfer coefficient under condensation inside the condenser	$W/(m^2\text{-}K)$
h_{ev}	heat transfer coefficient under boiling inside the evaporator	$W/(m^2\text{-}K)$
h_h	external heat transfer coefficient on evaporator	$W/(m^2\text{-}K)$
h_w	heat transfer coefficient of wooden box	$W/(m^2\text{-}K)$
$(hA)_c$	thermal conductance of HPHE on condenser	W/K
$(hA)_h$	thermal conductance of HPHE on evaporator	W/K
J	mechanical heat equivalent	J/cal
K	wick permeability	m^2
k	thermal conductivity	W/(m-K)

$k_{e,c}$	effective thermal conductivity of liquid saturated wick at condenser	W/(m-K)
$k_{e,e}$	effective thermal conductivity of liquid saturated wick at evaporator	W/(m-K)
L	characteristic length	m
L_2	flow length of fluid	m
L_3	base width of heat exchanger	m
L_a	adiabatic length of heat pipe	m
L_c	condenser length of heat pipe	m
L_e	evaporator length of heat pipe	m
L_t	total length of heat pipe	m
m	mass of working fluid	kg
$\dot{m}$	mass flow rate of heating fluid	kg/s
N	number of heat pipes (Chapter 3)	dimensionless
N	number of wires per meter (Appendix - A)	1/m
N_L	number of rows of heat pipes in HPHE	dimensionless
Nu	Nusselt number	dimensionless
P	pressure	Pa
P_f	fin perimeter	m
P_{in}	inlet pressure	Pa
P_{pm}	mean effective pumping pressure	Pa
Pr	Prandtl number	dimensionless
Pr_s	Prandtl number at surface temperature	dimensionless
$P_{v,c}$	vapor pressure at condenser	Pa
$P_{v,e}$	vapor pressure at evaporator	Pa
Q	heat transfer rate	W
Q_{90}	heat transfer rate at 90^o, i.e., vertical	W
Q_b	boiling limit	W
Q_c	capillary heat transport limit	W
Q_e	entrainment limit	W
Q_s	sonic limit	W
Q_v	viscous limit	W
$(QL)_{c,max}$	capillary heat transport factor	W-m
Ra	Rayleigh number	dimensionless
Re	Reynolds number	dimensionless
Re_v	Reynolds number for vapour flow	dimensionless
$R_{f,c}$	cold fluid side fouling factor	$(m^2\text{-K})/W$
$R_{f,h}$	hot fluid side fouling factor	$(m^2\text{-K})/W$
R_{HP}	total thermal resistance of heat pipe	$(m^2\text{-K})/W$
r_c	capillary radius	m
$r_{h,s}$	wick surface pore hydraulic radius	m
$r_{h,v}$	vapour core hydraulic radius	m
r_i	inside radius of heat pipe	m
r_n	nucleation radius	m
r_o	outside radius of heat pipe	m
$R_{p,c}$	thermal resistance of heat pipe wall at condenser	$(m^2\text{-K})/W$
$R_{p,e}$	thermal resistance of heat pipe wall at evaporator	$(m^2\text{-K})/W$

R_v	thermal resistance of vapor flow from evaporator to condenser	$(m^2\text{-}K)/W$
r_v	vapor core radius of heat pipe	m
$R_{w,c}$	thermal resistance of wick at condenser	$(m^2\text{-}K)/W$
$R_{w,e}$	thermal resistance of wick at evaporator	$(m^2\text{-}K)/W$
S	fin spacing (Chapter 3)	m
S	crimping factor (Appendix - A)	dimensionless
S_L	lateral pitch	m
S_T	transverse pitch	m
T	temperature	°C
T_a	ambient temperature	°C
T_c	condenser surface temperature	°C
T_f	film temperature	°C
T_i	inlet temperature at evaporator jacket	°C
T_o	outlet temperature at evaporator jacket	°C
$T_{p,c}$	condenser pipe wall temperature	°C
$T_{p,e}$	evaporator pipe wall temperature	°C
T_{sat}	saturation temperature of the working fluid	K
T_{sw}	surface temperature of wooden box	°C
T_v	vapor temperature	K
$T_{w,c}$	temperature of the solid-liquid thin film interface at condenser	K
$T_{w,e}$	temperature of the solid-liquid thin film interface at evaporator	K
t_f	fin thickness	m
t_p	heat pipe wall thickness	m
t_w	wick thickness	m
U	overall heat transfer coefficient	$W/(m^2\text{-}K)$
U_c	overall heat transfer coefficient based on condenser surface area	$W/(m^2\text{-}K)$
U_h	overall heat transfer coefficient based on evaporator surface area	$W/(m^2\text{-}K)$
$U_{HP,p}$	overall heat transfer coefficient of heat pipe based on outer diameter	$W/(m^2\text{-}K)$
V_f	volumetric flow rate of heating fluid	m^3/s
v	velocity	m/s
X_l	longitudinal pitch of heat pipe	m
X_t	transverse pitch of heat pipe	m

Greek Letters

ρ	fluid density	kg/m^3
μ	dynamic viscosity	kg/(m-s)
ν	kinematic viscosity	m^2/s
λ	latent heat of vaporization	J/kg
γ_v	vapour specific heat ratio	dimensionless
η_f	overall fin surface efficiency	dimensionless
η_o	fin effectiveness	dimensionless
ΔP	pressure drop	Pa
ΔT	temperature drop	°C

σ	Stefan Boltzman constant (Chapter 3)	$W/(m^2\text{-}K^4)$
σ	surface tension (Appendix - A)	N/m
σ	standard deviation (Appendix - B-III)	dimensionless
σ_A	ratio of free flow & frontal area	dimensionless
ε	emissivity	dimensionless
ε_o	porosity of wick material	dimensionless
β	volumetric expansion coefficient	1/K
ψ	angle of inclination with horizontal	Radian
θ	angle of inclination with vertical	Degree

Subscript

ass	assumed
C	convection
c	critical
c	condenser (Appendix - C)
cal	calculated
cond	condensation
cp	circulating pipe
e	evaporator
ev	boiling
in	inlet
L	local
l	liquid
m	mean
max	maximum
out	outlet
p	pipe
R	radiation
s	surface
v	vapour
W	wood
w	wick

Units

S.I. system has been followed in the present thesis.

Abbreviation

Amb	ambient
Deg	Degree
Deg.C	Degree Celsius
Dev	deviation
gm	gram
HPHE	heat pipe heat exchanger
HVAC	heating, ventilation, & air conditioning
lph	litre per hour
lpm	litre per minute
No	number
Sl	serial
temp	temperature
Vol	volume

CHAPTER 1

INTRODUCTION

Thermal systems are commonly associated with different types of heat exchangers, based on sensible heat transfer, latent heat transfer and mixed mode of these two types. These include shell and tube type, cross flow heat exchangers, evaporators, condensers, and heat pipe heat exchangers, etc. The motivation for using heat pipe heat exchangers is to obtain high exchanger compactness in given box-volume having weight limitations [1]. Energy systems manufacturers normally offer the base systems, which are used in a variety of engineering applications. For conversion of these base systems into a complete one, the manufacturers normally depend upon the local vendors for procurement of accessories including heat exchangers, which may not be optimally designed. Since these heat exchangers are to be adopted in a new configuration and layout, therefore, even well designed heat exchangers in a particular configuration are subject to change in effectiveness. To enhance the effectiveness of the sensible heat exchangers, one may look for a variety of solutions in the given situation. One of the solutions may be increasing the surface area of heat transfer, which increases the size of the heat exchanger, whereas, the other solution may be increasing the flow rates of the fluids involved, which results in more pressure drops of the fluids. The first option needs more space, whereas, the second may not be permitted by virtue of design implications. In the recent past, heat pipe heat exchangers (HPHE) have been used in various thermal systems for improving their effectiveness [1-3]. Most of the studies on these exchangers are limited to forced convection but a little work has been reported in the natural convection conditions. Therefore, the present work aims at conducting research on heat pipe heat exchangers under natural convection conditions.

The aim of the present investigation is to develop an analytical model for predicting the thermal performance of a heat pipe heat exchanger with evaporator exposed to forced convection & condenser to natural convective conditions, and validation of the same with experimental results. The complete design of a heat exchanger involves thermal aspects and mechanical design [4]. The present work has considered only thermal aspects. The heat exchanger thermal design problems are further categorized as **rating** and **sizing** problems. The rating or performance problem involves analysis for predicting

the thermal performance of a known configuration, while the sizing problem involves the design of a new configuration for a specified thermal performance. The objectives set forth in the present investigation have been achieved by considering rating problem only.

The scope of the present investigation includes:

(i) To develop an analytical model for thermal performance evaluation of a HPHE with condenser exposed to natural convection conditions,

(ii) Conduct experimental studies on different operating parameters of heat pipe and HPHE under natural convective conditions, and

(iii) Validation of analytical results with typical experimental data.

The prediction of heat transfer rate and pressure drop has been carried out by standard procedures and by selecting suitable correlations [1,3]. Data available from typical experiments carried out on a heat pipe as well as on heat pipe heat exchanger for given configuration have been used for validating the analytical model developed. It is hoped that the studies carried out will help the thermal system manufacturers in optimizing their designs for obtaining maximum heat transport rate at minimum cost.

CHAPTER 2

LITERATURE REVIEW

2.1 Introduction

This chapter presents an overview of research work carried out in the area of fundamental studies on heat pipe and its applications, general empirical correlations under forced & natural convection, modeling of heat pipe heat exchangers (HPHE), experimental studies, and applications of HPHE. This survey has been carried out with the following objectives:

a) to identify some of the important design aspects of heat pipe heat exchangers, and
b) to identify the correlations for heat transfer, which can be used in the present study.

2.2 Fundamental Studies

The fundamental design studies of heat pipe have been reviewed by various authors [2,3]. Chi [3] has presented a design methodology for heat pipes, which includes a) selection of heat pipe container materials, working fluid, and wick structures, b) computation of operating limits, and c) computation of overall thermal conductance. The authors have discussed in detail various types of heat pipes and their manufacturing techniques.

The overall **thermal resistance** of a heat pipe determines its thermal performance. Theoretical & experimental studies on thermal resistances of heat pipes have been reported by various authors [1-3, 5]. Chi [3] and Peterson [5] have presented relationships for estimating various thermal resistances for a cylindrical heat pipe. In radial direction, these resistances occur at the interface of heat source & external heat pipe wall, in heat pipe wall, liquid-wick interface, liquid-vapor interface at evaporator & condenser, and the external condenser section of heat pipe & heat sink or surrounding. In axial direction, the thermal resistances occur in pipe wall depending on design (smooth tube, grooved tube, liquid saturated wick at wall, etc.), in liquid & liquid saturated wick, and vapor core between evaporator & condenser. In many of the applications, the combination of resistances occurring between heat source & evaporator and condenser & heat sink are of the same order as the overall thermal resistance of a heat pipe [5].

Romestant et al. [6] have carried out an experimental work on a copper water heat pipe. They have reported that the evaporator conductance decreases at low heat flux due to the increase of liquid film thickness. The conduction through the liquid requires more temperature gradient for the same heat flux. When the temperature of wall reaches the boiling point of working fluid, the conductance was found to be increased. The condenser conductance increases with increase in temperature due to recession of non-condensable gas plug.

Hwan Moon et al. [7] have reported an experimental study on a micro heat pipe with triangular cross section. The pipe was made of stainless steel with water as working fluid. The performance measurements were conducted in the horizontal condition. They have found that the thermal resistance decreases from 3.5 °C/W to 1.5 °C/W as the operating temperature increases from 45 °C to 80 °C.

Kim et al. [8] have reported cooling characteristics of a miniature heat pipe with woven wire mesh. Experiments were performed to determine the heat transfer characteristics of the heat pipe having a diameter of 3 or 4 mm, which can be used for cooling of electronic components. The thermal resistance was highest when velocity of cooling air was zero and it decreased as the velocity of cooling air increased at the condenser end. The thermal resistance was reduced as the thermal load was increased.

It has been reported that the **tilt angle** is a critical parameter in the thermal performance of heat pipe [9-15].

Tathgir et al. [9] have reported an experimental study of a carbon steel heat pipe of length 630 mm, outside diameter 25.4 mm, and thickness 3.05 mm with an annular wick of brass mesh using water as working fluid. The study was conducted by varying power input (20 W to 250 W), mass of working fluid (4.5 gm to 10.5 gm), and tilt angle of heat pipe (0^{o} to 35^{o}). The best performance was observed at 8.5 gm mass of working fluid. The optimum tilt angle was found to be 15^{o} from the horizontal.

Negishi et al. [10] have conducted an experimental study on thermosyphon made of copper in which distilled water was used as the working fluid. The influences of the

liquid charge ratio and the tilt angle on the heat-transfer performance were studied. The best performance was reported at a tilt angle of 30° from the horizontal.

Terdtoon et al. [11] have conducted an experimental investigation of a plastic thermosyphon using R-113 as a working fluid. The thermosyphon with an outside diameter of 21.6 mm and an aspect ratio of 30 was employed with a selected filling ratio of 50 %. The inclination angle from the horizontal was varied as 5°, 10°, 20°, 30°, 40°, 50°, 60°, 70°, 80°, and 90°. It has been found that the Q/Q_{90} of the thermosyphon reached the highest value of 1.18 at an angle of 60°.

Shiraishi et al. [12] have experimentally investigated critical heat transfer rate in an inclined two-phase thermosyphon by taking into account of the ratio of evaporator length to diameter, fill charge, working fluid property, and operating pressure. New dimensionless parameter such as modified Kutateladze number (Ku*) was introduced to correlate the data of the maximum critical heat transfer rate (Q_{cmax}) based on the critical heat transfer rate at the vertical position (Q_{c90}). It has been found that Q_{cmax}/Q_{c90} can be correlated well with Ku*.

Terdtoon et al. [13] have investigated the effect of **aspect ratio** (ratio of evaporator length to diameter, L_e/d_o) and Bond number on the heat transfer characteristics of a thermosyphon. The aspect ratio is varied over the range of 5, 10, 20, 30, and 40 with variation of inclination angle being 0°, 10°, 20°, 30°, 40°, 50°, 60°, 70°, 80°, and 90° measured from the horizontal. The results show that the ratio of the highest heat transfer rate of the inclined thermosyphon to that of the vertical one gradually decreases in the range of $L_e/d_o < 10$, but it is nearly constant at $L_e/d_o > 10$. The aspect ratio does not affect the angle at which the highest heat transfer rate occurs.

Abhat & Nguyenchi [14] have reported an experimental work on a copper/water heat pipe with screen wick. The heat transport rate of the heat pipe has been evaluated at different operating temperatures (20 - 100 °C), tilt angles (0° - 30° from the horizontal) and working fluid inventory (7.4 ml & 9.6 ml). The best thermal performance of the heat pipe has been obtained at a tilt angle of 30°.

Wilkins & Al-left [15] have reported the performance characteristics of a gravity-assisted heat pipe made of aluminum with internal grooves as the wick and Freon-113 as the working fluid. The effects of the length of the pipe, the input power, and the tilt angle on the axial heat transfer rate and the performance limits have been examined. Experimental results showed that gravity-assisted heat pipes exhibit efficient heat transfer.

Mathematical model & computer simulation codes have been developed by various authors [16-18] to predict the thermal performance of a heat pipe under forced/natural convective conditions and some of the models have been validated with experiments.

Maziuk et al. [16] have developed a computer programme to predict the thermal performance parameters of a heat pipe, e.g., Q_{max}, R_{HP}, temperature profile along the pipe surface, and heat transfer coefficients in the evaporator & condenser zones. Experiments were carried out on a flat miniature heat pipe with a copper sintered powder wick saturated with water and the results were compared with the numerical simulation, which were approximately matching. It has been found that the heat transfer coefficients in the evaporator and condenser of the flat heat pipe depend on the various parameters such as, capillary permeability, capillary pressure, and temperature distribution along the heat pipe.

Lee et al. [17] have developed a computer simulation code using lumped network method for predicting the performance of a heat pipe cooling system for electronic component such as multichip module under different operating conditions. To assess the validity of simulation study, the simulation results have been compared with the experimental results. The code correctly predicts the characteristics of the cooling system. It has been found that the increase in the air velocity increases the heat transportation capacity of the cooling system.

Lee & Rhi [18] have reported that the **overall heat transfer coefficient** of a two-phase closed thermosyphon depends on many variables such as, type of working fluid, saturation temperature of working fluid, evaporator-condenser length ratio, air flow velocity in the condenser section, and heat flux. They have computed overall heat transfer coefficient with various correlations of h_{ev} (boiling) and h_{cond} (condensation) of Rohsenow and compared with their experiments. They have suggested modification in

heat transfer coefficients for boiling and condensation as

$$h_j = C_j x_j^{mj}, \text{ where } j = \text{evaporator or condenser} \quad (2.1)$$

where x_j is the original correlation. The constant C_{ev} & C_{cond} and exponents m_{ev} & m_{cond} were determined from the experimental data.

Howard & Peterson [19] have conducted a combined experimental and analytical investigation to evaluate a heat pipe convective cooling device consisting of sixteen small copper/water heat pipes mounted vertically in a 4 x 4 array for electronics application. The analytical portion of the study focuses on determination of the maximum heat transport capacity and the thermal resistances of the individual heat pipes. In the experimental testing, two different modules were tested. The first module uses ten circular aluminum fins mounted on the condenser end of each heat pipe to enhance heat rejection, while the second contained only sixteen copper/water heat pipes without fins. The effects of flow velocity, input power, and base plate temperature on the overall thermal resistance and the heat rejection capacity were determined, as well as the pressure drop resulting from each module.

Thermal energy can be transferred from the surface of heat pipe to the surrounding environment by forced or natural convection. In **forced convection**, heat transfer is due to flow of fluid from external source such as by a fan or a pump over the heated surface.

Fand [20] has reported heat transfer coefficient from liquid to cylinder in cross flow as follows:

$$Nu = (0.35 + 0.56\, Re^{0.52})Pr^{0.3} \quad (2.2)$$

This relation is valid for $10^{-1} < Re < 10^5$, provided excessive free-stream is not encountered.

Dobson & Kröger [21] have conducted extensive experiments to determine evaporator heat transfer coefficient and maximum heat transfer rate of an ammonia charged inclined two phase thermosyphon. The experimental thermosyphon consisted of a 6.2 m long stainless steel tube of 31.9 mm inside diameter. The thermosyphon was tested at different evaporator to condenser length ratios, liquid charge fill ratios, inclination angles of 30° to 90° from the horizontal, cooling temperature between 10 °C to 20 °C, and heating

temperature up to 80 °C. The heat transfer coefficient between heating water and the outside surface of the thermosyphon for a 400 mm long water jacket was experimentally determined as

$$h_h = 4.55\ Re^{0.733}\ Pr^{0.362} \qquad (2.3)$$

Tilting the thermosyphon increases the maximum possible evaporator heat transfer flux but with a decreased evaporator heat transfer coefficient.

The average heat transfer coefficients inside the evaporator and condenser sections are described by the classical Nusselt analysis [1]. Abhat & Seban [22] reported heat transport measurements in vertical tubes using water, ethanol, and acetone as the working fluids. The experiments were conducted for smooth surfaces, immersed wicks, and evaporating wicks. The authors conclude that up to heat fluxes of 1,50,000 W/m^2, the heat transfer coefficient for a screen or felt wicked tube is similar to that of the bare tube and also not very different from that for the evaporating surface. Davis & Chaffey [23] conducted experiments on grooved heat pipe with water as working fluid. The vapour temperature varied from 40 °C to 120 °C. The mean heat transfer coefficients on the evaporator and condenser were found to be 17,755 W/(m^2-°C) and 17,983 W/(m^2-°C), respectively.

Zukauskas [24] has reported empirical correlation among Nusselt number, Reynolds number, and Prandtl number for flow over cylinder for calculating average heat transfer coefficient.

$$Nu = C\ Re^m Pr^n \left(\frac{Pr}{Pr_s}\right)^{1/4} \quad \text{for } 0.7 < Pr < 500 \text{ and } 1 < Re < 10 \qquad (2.4)$$

where, 'C' and 'm' are constant.

n = 0.37 for Pr ≤10 and n = 0.36 for Pr > 10. The values of 'C' and 'm' are given in Table 2.1.

Table 2.1: Values of 'C' and 'm' for Zukauskas' equation for flow normal to singular circular cylinder

Sl. No.	Range of Reynolds number	C	m
1.	1- 40	0.75	0.4
2.	40 - 100	0.51	0.5
3.	1000 - 2 x 10^5	0.26	0.6
4.	2 x 10^5 - 10^6	0.076	0.7

Zukauskas has also proposed correlation for calculating average heat transfer coefficient in tube bundle having more than 20 rows.

$$Nu = C\,Re^m\,Pr^n\left(\frac{Pr}{Pr_s}\right)^{1/4} \quad \text{for } 0.7 < Pr < 500 \text{ and } 1 < Re < 10^6 \text{ and } N_L \geq 20 \qquad (2.5)$$

The values of 'C' and 'm' are given in Table 2.2.

Table 2.2: Values of 'C' and 'm' for Zukauskas' equation for flow over staggered tube bank arrangement

Sl. No.	Range of Reynolds number	Staggered		Aligned	
		C	m	C	m
1.	10 - 100	0.90	0.4	0.8	0.4
2.	100 - 1000	0.51	0.5	0.51	0.5
3.	1000 - 2 x 10^5	$S_T/S_L < 2$: $0.35(S_T/S_L)^{1/5}$ $S_T/S_L > 2$: 0.4	0.6	$S_T/S_L > 0.7$: 0.27	0.63
4.	2 x 10^5 - 10^6	0.076	0.7	0.021	0.84

In tube bundle, the Reynolds number is defined as

$$Re = \frac{v_{max} \times D_h}{(\mu/\rho)} \qquad (2.6)$$

If the number of tube rows in tube bundle is less than 20, a correction factor is required, which is empirically related as

$$Nu|_{N_L<20} = C_1 Nu|_{N_L>20}$$

where C_1 is given in Table 2.3.

Table 2.3: Correction factor C_1 for $N_L < 20$ ($Re > 10^3$)

Sl. No.	N_L	1	2	3	4	5	7	10	13	16
1.	Aligned	0.70	0.80	0.86	0.90	0.92	0.95	0.97	0.98	0.99
2.	Staggered	0.64	0.76	0.84	0.89	0.92	0.95	0.97	0.98	0.99

Zukauskas has further reported that the pressure drop across the staggered tube bank is computed by

$$\Delta P = N_L \left(\frac{\mu_s}{\mu}\right)^{0.14} \left(\frac{\rho v_{max}^2}{2}\right) f \tag{2.7}$$

$$f = [\, C_2 + \frac{C_3}{(S_T/d_O - 1)^n} \,] \, Re^{-m} \tag{2.8}$$

The values of C_2, C_3, n and m are given in Table 2.4.

Table 2.4: Coefficients of pressure drop for tube bank

Sl. No.	Tube arrangement	C_2	C_3	n	m
1.	Staggered bank	1.0	0.470	1.08	0.16
2.	Aligned bank	0.176	$0.34(S_L/d_o)$	$0.43 + 1.13/S_T$	0.15

Churchill & Bernstein [25] have proposed a correlation for Nusselt number, which covers wide range of Prandtl number and Reynolds number under forced convection:

$$Nu = 0.33 + \frac{0.62\, Re^{1/2}\, Pr^{1/3}}{\left[1+\left(\frac{0.4}{Pr}\right)^{2/3}\right]^{1/4}} \left[1+\left(\frac{Re}{282000}\right)^{5/8}\right]^{4/5} \quad \text{for all } RePr > 0.2 \tag{2.9}$$

Fundamental studies on **natural convection** have been reported by various authors [26, 27]. Free convection exists due to the locally induced buoyancy. The buoyant free convective terms are described in terms of the Grashof number, which governs free convective flow & heat transfer and it incorporates the effect of coefficient of thermal

expansion. Buoyancy induced free convection may be laminar or turbulent. The laminar-turbulent transition depends on the relative magnitude of the buoyant and resisting viscous forces as expressed through Rayleigh number, which is the product of Grashoff number and Prandtl number. The transition occurs at critical Rayleigh number of $Ra_x \approx 10^9$. Where Ra_x represents the local Rayleigh number in which, L, the distance traveled by fluid particle in the boundary layer, is used as the characteristic length.

$$Ra_x = \frac{g\beta(T_s - T_a)\,L^3\rho^2\,Pr}{\mu^2} = \frac{g\beta(T_s - T_a)\,L^3\,Pr}{\nu^2} \qquad (2.10)$$

Churchill & Chu [28] reported correlation for free convection over the vertical plane surface for entire range of Ra_L

$$Nu_L = \left\{0.825 + \frac{0.387\,Ra_L^{1/6}}{\left[1+(0.492/Pr)^{9/16}\right]^{8/27}}\right\}^2 \quad \text{for } 10^{-1} < Ra_L < 10^{12} \qquad (2.11)$$

Nusselt number for laminar flow is determined by

$$Nu_L = 0.68 + \frac{0.670\,Ra_L^{1/4}}{\left[1+(0.492/Pr)^{9/16}\right]^{4/9}} \quad \text{for } 0 < Ra_L < 10^9 \qquad (2.12)$$

Sparrow & Gregg [29] have reported that the correlation for vertical plate may be applied to the vertical cylinder, if the boundary layer thickness 'δ' is much less than the cylinder diameter 'd_o' and it satisfies the following condition:

$$\frac{d_o}{L} \geq \frac{35}{Gr_L^{1/4}}$$

The availability of correlation for inclined plate under natural convection is limited. Fujii & Imura [30] investigated natural convection from a plate with arbitrary inclination. They proposed the following correlation for inclined surface:

$$Nu = 0.14[(GrPr)^{1/3} - (Gr_{cr}Pr)^{1/3}] + 0.56(Gr_{cr}Pr\cos\theta)^{1/4} \qquad (2.13)$$

where, $10^5 < GrPr \cos\theta < 10^{11}$, $15^o < \theta < 75^o$ for uniform heat flux facing downward
$Gr_{cr} = 5x\ 10^9$, $2x\ 10^9$, 10^8, and 10^6 for $\theta = 15^o$, 30^o, 60^o, and 70^o respectively from the vertical.

Yildiz & Yüncü [31] have experimentally investigated heat transfer characteristics of an annular fin-array mounted on a horizontal cylinder of 24.9 mm diameter in atmospheric conditions. They have reported that the convection heat transfer rate from the fin arrays depends on fin diameter, fin spacing, and base-to-ambient temperature difference. Experimental results show that the optimum fin spacing may be taken as 8 mm (approximately) for practical engineering applications.

Faghri [1] reported that the heat transfer capacity of heat pipe is limited by the condenser heat transport limit. The heat transfer coefficient is low when heat pipe dissipates heat to the ambient by natural convection.

2.3 Applications of Heat Pipe

Heat pipe has diverse applications in cooling of electrical transformers, electronic components, electrical motors, and piston of internal combustion engine, aircraft temperature control, HPHE, etc.

Zelko & Polasek [32] have reported the application of heat pipe for cooling of power semiconductor elements such as diodes and thyristors under natural and forced convection. A series of aluminium or copper fins have been attached to the condenser part of the heat pipe, which provide more heat rejection to the heat sink. Based on their extensive research, they have found that the pitch of the fins varies from **2 to 3 mm** in the case of forced air convection, and from **6 to 8 mm** in the case of natural convection.

Murase et al. [33] have reported the use of multiple parallel heat pipes to cool high power thyristors. Several heat pipes were mounted in a single heater block with a single set of heat rejecting fins. The grooved heat pipes were made of copper having an outside diameter of 15.9 mm and a length of 1200 mm with water as working fluid. The aluminum fins were placed at a pitch of **8 mm** to be suitable for natural convection. It

has been found that a black coating enhanced the effects of radiation at different vapour temperatures ranging from 50 °C to 100 °C.

Krishnamoorthy & Pillai [34] have carried out research work on application of heat pipes for cooling of transformer, which provide additional cooling to enable the distribution transformer to work safely on high overloads. Heat pipes, made of tubular copper container with copper wire mesh as wick and distilled water as the working fluid, have been used at the top of transformer tank. An array of annular fins made of aluminum has been provided on the condenser section to enhance the rate of heat transfer to air. They also developed an analytical model to predict the temperature profile of evaporator and condenser section. They have found that the theoretically predicted and experimentally observed axial temperature profiles of the heat pipes are reasonably in good agreement. Four heat pipes with a dissipating capacity of 75 W each have been used in a 100 kVA transformer to achieve 10 % overloading by dissipating 300 W under natural convection. Saaski & Franklin [35] have reported the use of heat pipe for better cooling of an oil cooled distribution transformer. The heat pipes were placed at the top oil zone. The transformer top oil temperature was reduced by 10 °C, which enhanced the transformer life. Waldon & Bennett [36] have patented a heat pipe, which can be used for cooling of distribution transformer.

Polasek [37] reported experimental work on cooling of an electric motor by incorporating a rotating heat pipe in the hollow shaft. He found that the power output was increased by 15 % with the heat pipe without any further rise in winding temperature. Groll et al. [38] have used copper water axial grooved heat pipe for cooling of stator and the circumferential grooved heat pipe for cooling of rotor. It has been observed that the application of heat pipe contributed 75 % of the heat dissipation. Bradford & Highgate [39] have also reported the use of copper water heat pipes in stator and rotor for cooling of an electric motor. The temperature of rotor and stator has been reduced using heat pipes. Heat pipe cooled motor enhanced the rating of motor and reduced the frame size. Ponnappan & Leland [40] have presented test results of a stainless steel water rotating heat pipe intended to regulate the temperature of an electrical machine directly mounted on the main shaft of a gas turbine engine. Yerkes & Beam [41] have tested artery-heat pipes and thermosyphon for thermal control of electric motors, compressors, and generators in aircraft experiencing transverse accelerations.

Heat pipes have been developed for cooling engine components in a conventional aircraft. Gottschlich & Meininger [42] have described the cooling of gas turbine engine vanes using heat pipes. Silverstein et al. [43] have reported the use of heat pipes to cool the vanes of gas turbine engines. Cao & Wang [44] have presented their study on a **reciprocating heat pipe** for piston cooling of an internal combustion engine.

2.4 Mathematical Modeling of Heat Pipe Heat Exchanger

The complete design of a heat exchanger [4] involves the following:

a) Thermal analysis,
b) Mechanical design, and
c) Design for manufacture

The thermal analysis is primarily concerned with the determination of the heat transfer surface area required to transfer heat at a specified rate for given flow rates and temperatures of the fluids. In the present study, the thermal aspect of HPHE has been analyzed.

The mathematical modeling of HPHE involves representation of various thermal resistances & pressure drop in a form of set of system equations to compute heat transfer rate & pressure drop for given input boundary conditions. A number of analytical studies have been carried out by various authors to predict the thermal performance of HPHE using mathematical model.

Tan & Liu [45] have developed an analytical model for analysis of the thermal performance of a heat-pipe heat exchanger based on the effectiveness-NTU method. The predicted thermal performance using this model is compared with results obtained by previous investigators, and a good agreement has been reported.

Hsieh [46] has employed a finite difference method based on the conductance model to analyze the overall heat transfer rate of HPHE. He developed a simplified but relatively generalized method to predict the thermal performance of the heat-pipe heat exchanger for any staggered type alignment. The model has been tested based on the results from

previous investigators, which provide thermal design data for a heat-pipe heat exchanger configuration applicable to waste heat recovery systems.

Hsieh & Huang [47] have presented a numerical calculation of thermal performance and pressure drop for heat pipe heat exchangers (counter flow as well as parallel flow) with aligned tube rows. The results show that counter flow exhibits a better heat transfer rate and lower pressure drop than parallel flow. Further, Hsieh & Huang [48] have presented a numerical analysis for comparison of thermal performance and pressure drop for heat pipe heat exchangers with aligned/staggered tube rows. In this study, the variation of the number of rows and columns from 1 to 6 for 36 arrangements is presented and discussed. From the results, an optimum arrangement of heat-pipe heat exchangers has been found out.

Peretz & Horbaniuc [49] have reported different optimization methods to design a heat pipe heat exchanger with continuous planar fins and a staggered triangular pitch. The optimization techniques helped in determining equilateral triangular pitch of tubes, density of continuous planar fins, ratio of evaporator to condenser lengths, heat capacities ratio of hot & cold fluid so as to obtain a maximum heat flow per unit weight, and maximum heat transfer effectiveness.

Tan et al. [50] have formulated an equation to determine the optimum position of the partition separating a heat pipe into evaporator and condenser regions in a HPHE by minimizing the total thermal resistance of the heat path. The optimum position of the partition plate for various operating conditions was found and analyzed. The results indicated that the optimal position of the partition plate of a heat-pipe heat exchanger is not necessarily at the middle of the heat exchanger. It depends upon the relative magnitude of the flow rates of the hot and cold fluids. The optimal partition position is quite near the middle when the difference in flow rate of the two fluids is small. When the difference is large, the position of the partition plate should be optimized.

Swanson [51] has developed a mathematical model of a countercurrent plate fin heat pipe heat exchanger for waste heat recovery. The model computes the optimal heat exchange areas in the evaporator and condenser as well as the corresponding temperature

distribution of heat pipe, the plate temperature distribution, and individual heat pipe energy transfer rates. The results show that the distribution of heat exchange area between the ducts is solely dependent on the ratio of the average overall heat transfer coefficients. The ratio of the heat capacity flow rates influences only the total minimum heat exchange area and does not affect the distribution of heat exchange area between the ducts. These expressions were used to determine the minimum total external surface area and corresponding distribution of heat pipe temperatures for an air preheater recovering waste heat from a boiler exhaust stream.

Azad et al. [52] have presented a design study of water to air gravity assisted heat pipe heat exchanger. The characteristics of the heat exchanger have been studied analytically to predict the performance of the heat exchanger. The variations of overall effectiveness of exchanger with evaporator & condenser capacity rate ratio, and Reynolds number for different values of condenser capacity rate have been plotted. Further, they have presented overall effectiveness as a function of outlet air temperature from the exchanger to a solar dryer with and without a heat recovery unit.

Azad & Gibbs [53] have presented a theoretical study of an air to water heat pipe heat exchanger. In this study, the variations of heat exchanger effectiveness with ratio of cold to hot flow-stream capacity rate for 8, 10, and 12 rows are presented. They report that the overall effectiveness increases by decreasing Reynolds Number on evaporator side and increasing the face velocity on condenser side. The heat transfer effectiveness increases by increasing number of fins per meter on air side.

Peretz & Bendescu [54] have reported the influence of the heat pipe heat exchanger's geometry on its heat transfer effectiveness. The authors have analysed the variation of heat transfer effectiveness (HTE) of a series of heat pipe heat exchangers differing in the number of rows, depth, frontal face area, and fin density. They have found that the frontal face area has little influence on heat transfer effectiveness.

Azad & Geoola [55] have presented a theoretical approach to design the gravity assisted heat pipe heat exchanger (GAHPHE). Based on this analysis, the variations of overall effectiveness of GAHPHE with conductance ratio of evaporator and condenser for different values of tube spacing normal to the direction of flow, number of fins per

meter, fin thickness, and evaporator & condenser length are plotted. In order to obtain an optimum design for GAHPHE, the variations of overall effectiveness with conductance ratio for different values of modified number of transfer units covering broad design range are presented.

Azad et al. [56] have investigated multi-stage heat pipe heat recovery system. The system contains several units, each individual unit is a heat pipe heat exchanger and they operate independently. The different combinations of multi-stage heat pipe heat exchangers include flow in series in the condenser and parallel in the evaporator section of the unit or in condenser sections the flows are in parallel and series in the evaporator section. They found that the system effectiveness in multi-stage heat pipe heat exchanger system is lower than the single stage but it has some advantages, which include easy cleaning, individually replaceable stages, ease of transportation, and possibility of addition of stage.

Shah & Giovannelli [57] have reported an overall design methodology for design of a heat pipe heat exchanger. The authors discussed about the operating principle, various operating limits, and characteristics of heat pipes & heat pipe heat exchanger. They also discussed design considerations of heat pipe. All quantitative information needed for design of a heat pipe heat exchanger are summarized, which include heat transfer and fluid flow friction characteristics for bare and finned tube banks, fin efficiency, geometrical properties, and pressure drop analysis.

2.5 Studies on Heat Pipe Heat Exchanger

The following experimental studies have been reported for validation of the analytical models developed by various authors for thermal performance evaluation of HPHE.

Liu et al. [58] presented a model to calculate the heat transfer coefficient of each tube row of a heat pipe heat exchanger under forced convection. It was reported that the difference between theoretical and experimental temperatures of both hot and cold fluids in their respective first and second rows were in good agreement. While calculating the heat transfer rate and temperature distribution of each individual row, an arithmetic mean convective heat transfer coefficient was used. Using the values of f_N for the staggered

arrangement, and assuming that the heat transfer areas for each row are equal, the relationship between h_1, h_2.....h_N and $\bar{h}$ could be calculated. For the first row (heat exchanger contains only one row of tubes) $f_1 = 0.68$, thus $h_1 = 0.68\ \bar{h}$, considering the first two rows as a single heat exchanger, h_2 was found as $h_2 = 0.82\ \bar{h}$, likewise, $h_3 = 0.99\ \bar{h}$.

The results agreed well with Gnielinski's [59] statement that from the first to about fifth row the heat transfer coefficient increases and then remains constant. The present model could predict the air temperature better than the model using average heat transfer coefficient for all the rows.

Feldman & Lu [60] have experimentally studied the effects of various evaporator lengths, the number of heat pipe rows, heat pipe diameter, heat pipe bundle geometry, and fin spacing. The effectiveness of the HPHE increases as the length, the number of heat pipes, and the number of rows increase. The effectiveness of the staggered HPHE is more than in-line bundles, which is due to increased coverage of fluid streams by the staggered-tube bundles.

Gamal et al. [61] have carried out an experimental investigation on heat transfer analysis of a heat pipe heat exchanger for nuclear heating supply system. They developed a physical model to vary the length ratio between condenser and evaporator section. Water is chosen as working fluid for the gravity heat pipe. They discussed about counter-current flow limitation and revealed that the counter-current flow limitation increases as the tube diameter is increased.

Wakiyama et al. [62] have studied the effect of HPHE operating both horizontally and vertically with the same fluid stream. They found that the HPHE using vertical heat pipes has a higher effectiveness than similar horizontal unit. The increase in thermal effectiveness is more significant at high and low temperature streams due to the decreased thermal resistance in heat pipe operating vertically over horizontally because of gravity effects on condensate return.

Wen et al. [63] have compared the construction and performance of a heat pipe air preheater with conventional preheater. They revealed that fouling, corrosion and leakage can be reduced in heat pipe air preheater. They suggested some measures to reduce corrosion, which include increasing the wall temperature of heat pipes on the flue gas side by adjusting heat exchange area, and using the effective soot blower with moving tubes.

Dube et al. [64] have designed, constructed, and tested air-to-air thermosyphon heat exchangers under medium temperature (below 300 °C). These heat exchangers used continuous plate finned copper tubes and plate finned steel tubes respectively. Water was chosen as the working fluid with a fill ratio of 60 % of the evaporator length. Both copper finned and steel finned tube heat exchangers were tested by varying air face velocity between 2 to 6 m/s. The effectiveness of the rectangular plate finned copper tube heat exchanger was about 10 % more than that of the rectangular plate finned steel tube heat exchanger.

Wadowski et al. [65] have carried out an experimental study on the performance of an air-to-air thermosyphon based heat exchanger, utilizing R-22 as the working fluid, to investigate its behavior under different operating conditions. The results describe the influence of various parameters such as: input and output air stream mass flow rates, stream temperatures, and exhaust stream moisture content on the effectiveness of the heat exchangers. A minimum temperature difference between the two air streams is required to initiate operation of the heat exchanger. When full operating power is reached, the effectiveness is independent of temperature difference of the two air streams. It has been found that the performance of the heat exchanger does not improve with change of air stream density and with condensation.

Terdtoon et al. [66] have designed and evaluated a thermosyphon type economizer for a package boiler with 78 stainless steel-water thermosyphons in a 7 row x 12 tube arrangement. The diameter of thermosyphon is 25.7 mm with evaporator, adiabatic, and condenser sections of length 700 mm, 50 mm, and 250 mm, respectively. At the evaporator section, hot flue gases pass and pretreated water passes through condenser. A test run was conducted to determine the thermal characteristics, e.g., heat transfer rate,

thermal resistance, and thermal effectiveness. From the experimental results, the thermal effectiveness of the thermosyphon economizer was found to be 0.58.

2.6 Applications of Heat Pipe Heat Exchanger

HPHE has been used in waste heat recovery, dehumidification, heating, ventilation, and air conditioning applications.

Hill & Lau [67] have studied heat pipe heat exchangers associated with air-conditioning systems in four different climatic conditions. The heat pipe heat exchangers were used to save refrigeration energy by reducing the humidity of the refrigerated spaces.

Wasim [68] has reported use of a heat pipe heat exchanger for indirect evaporative cooling as well as heat recovery for fresh air preheating. He evaluated the thermal performance of a heat exchanger consisting of 48 thermosyphons arranged in six rows in staggered manner. The thermosyphons were made of 16.4 mm copper pipes with R-22 as working fluid. Evaporative cooling was achieved by spraying the condenser sections of the thermosyphons.

Danielewicz [69] has reported use of a two-phase thermosyphon heat exchanger for heat recovery in HVAC systems. The heat exchanger was made of copper pipes of 16 mm diameter with R-12 as working fluid. It had 10 rows with a dimension of 500 x 360 x 1250 mm. The highest efficiency of the heat exchanger was obtained when air fluxes of hot air & cold were equal. The efficiency of heat exchanger varied from 35 % to 60 % by changing the velocity of external air at condenser end.

Khantha & Terdtoon [70] have reported use of a heat pipe air preheater for waste heat recovery from power plant and its application in Gypsum drying. The air preheater has dimension of 0.33 x 0.3 x 1.0 m with 76 copper water heat pipes in a 8 row x 10 tube staggered arrangement. The outside diameter of heat pipe is 15.9 mm with evaporator and condenser section length of 0.5 m each. The air preheater used continuous plate fins with 12 fins per inch. From the experimental results, it was found that at flue gas inlet temperature of 170 ^{o}C & the flue gas flow rate of 5400 m^3/h, and the cold air flow rate of

2700 m^3/h & inlet temperature of 30 °C, the heated air outlet temperature was 134 °C. The heat transfer rate was 73.4 kW, the effectiveness was 0.71, the pressure drop was 27 Pa, and the internal rate of return was 28 %.

2.7 Thermo-Physical Properties of Fluids

Bhatt & Vora [71] have given the thermo-physical properties of air and water, such as density, specific heat, thermal conductivity, and viscosity as a function of temperature, which can be used in calculating heat transfer coefficient.

2.8 Fouling

Somerscales [72] and TEMA Standards [73] reported on different types of fouling such as crystallization fouling (precipitation and solidification fouling), particulate fouling, chemical reaction fouling, corrosion fouling, and biological fouling (microbial and macrobial fouling). The fouling deposits on the heat transfer surface, which increases resistance to heat transfer and fluid flow. The data on normal fouling factors for various types of waters, oils, industrial liquids, and gases have also been provided.

2.9 Conclusions

For manufacturing heat pipe heat exchangers, the design of individual heat pipe is very important. The configuration of the individual heat pipe is decided based on several factors, such as the operating temperature range of the HPHE, the orientation of the evaporator with respect to the condenser, and the possibility of corrosion and erosion of the heat pipe wall by the high or low temperature fluid streams [1].

The literature review indicates that a good amount of work has been carried out on fundamental studies of heat pipes, which includes different types of transport limitations, selection of working fluid, material of construction of wick & wall of heat pipe, and thermal resistances. These are critical parameters, which determine the performance of a heat pipe. For low temperature applications in the range of 30 °C to 200 °C, copper-water heat pipe has been extensively used, which may be because of its better thermal performance and cost effectiveness. The heat transport capacity of grooved heat pipe is more as compared to the copper-water wicked heat pipe, which may be due to less

resistance in condensate return and uniform distribution of working fluid in grooves, but its manufacturing procedure is relatively more complicated [3].

The thermal performance of a heat pipe is determined by its thermal resistance. It has been reported that the internal thermal resistance of a heat pipe is very low but the thermal resistances at the external surface of evaporator and condenser are high, which limit the rate of heat transfer. In many cases, it may be approximately equal to the overall thermal resistance of heat pipe. The external thermal resistance at condenser decreases as the operating temperature at condenser increases or by increasing the velocity of cooling fluid. The thermal resistance at condenser under natural convection is very high as compared to other thermal resistances. In natural convection, fins are used to increase the heat transfer area and in turn augment the rate of heat transfer. The pitch of fins is usually around 6 to 8 mm in the case of natural convection, whereas 2 to 3 mm in the case of forced convection.

It has been found that the tilt angle of heat pipe influences the rate of heat transport. The thermal performance of a heat pipe is low when the heat flux is applied to the evaporator lying above the condenser (top heating mode). The thermal performance improves, as the location of condenser changes from bottom cooling mode to top cooling mode. In many of the cases, the best performance of heat pipe is reported at tilt angles varying between 15^{o} to 60^{o} from the horizontal.

Various mathematical models (numerical as well as lumped network) have been developed to predict the temperature profile, peak heat transfer (dry out), heat transfer coefficient in evaporator & condenser, vapor flow, pressure distribution, start up behaviour, and transient response of heat pipe. The effects of aspect ratio and the number of layers of wick screen on the thermal performance of heat pipe have been studied. It has been found that the highest heat transfer rate of an inclined thermosyphon is obtained when aspect ratio (L_e/d_o) is greater than or equal to 10. Further, some of the analytical correlations have been validated by experimental work.

The design aspects of HPHE have been classified into three categories, i.e., namely thermal, mechanical, and manufacturing. The present review is restricted to thermal

design only. Most of the research works on heat pipe heat exchangers have been reported to calculate heat transfer coefficient of each tube row, overall thermal performance, optimum length of evaporator & condenser, and pressure drop across tube bundle under forced convection. The effects of pitch, flow pattern (countercurrent and co-current), number of tube rows, and fin density on the thermal performance of HPHE have been reported under forced convection. It has been reported that the staggered arrangement of heat pipes with counter flow gives better thermal performance as compared to that of the in-line arrangement. A very limited amount of work has been reported on cooling of heat pipe heat exchangers under natural convection. Some empirical correlations of Nusselt number for single cylinder as well as for tube bundle under forced convection and that of a vertical cylinder under natural convection have been reviewed.

The application range of heat pipe is very wide, which includes cooling of electronic components, transformer, motor, engine, and turbine, aircraft temperature control, HPHE, etc. Thermosyphons and wicked heat pipe heat exchangers have been used in waste heat recovery from air-conditioning and flue gases of oil fired furnaces.

With the present correlations available for computation of thermal resistance under forced and natural convection, it has been planned to develop suitable analytical model, which can estimate overall heat transfer coefficient of heat pipe heat exchangers with condenser exposed to natural convection, followed by validation of the analytical model with experimental result.

CHAPTER 3

DESIGN CONSIDERATIONS AND ANALYTICAL MODEL

3.1 Introduction

This chapter presents the design considerations of the heat pipe along with the analytical model developed for thermal performance evaluation of the heat pipe heat exchanger under natural convection.

3.2 Design Considerations of Heat Pipe

The various design considerations for the design of a heat pipe are: selection of working fluid, container & wick materials, wick design, and computation of heat transport limits. The required operating temperature for a particular application is a guiding factor in deciding these parameters. Since the present investigation aims at low temperature applications, such as cooling of transformer oil and cutting fluids, therefore, the operating temperature range of 40 °C to 70 °C has been considered. The stepwise design considerations are presented below.

3.2.1 Selection of Working Fluid

The working fluid is selected based on the cost, availability, compatibility with wick & container materials, and operating vapour temperature range. The other prime considerations for selection of working fluid are wettability, good thermal stability, high latent heat, high surface tension, low liquid & vapour viscosities and vapour pressure not too high or low at the operating temperature range. In the low temperature range of 30 °C to 200 °C, water has better heat transport & conductance properties as compared to other working fluids, like, ammonia, pentane, acetone, methanol, heptane, ethanol, etc., and is cheaply available. Based upon these considerations, distilled water is chosen as the working fluid. The amount of working fluid required should be sufficient to saturate the wick and fill the core volume in the vapour phase. The heat pipe should neither be underfilled nor overfilled. An underfill may result in degradation of performance and an overfill may result in condenser blockage. The fluid inventory required for a wicked heat pipe is calculated by the following equation [3]:

$$m = A_v L_t \rho_v + A_w L_t \varepsilon_o \rho_l \qquad (3.1)$$

3.2.2 Selection of Container

The selection of container depends on its compatibility with working fluid, high thermal conductivity, ease of fabrication, and strength to weight ratio. Literature indicates that copper, nickel, and titanium are compatible with water. Copper has superior thermal conductance property as well as cost advantage including the ease of fabrication, therefore, it has been selected as the material for the heat pipe container.

Heat pipes can be made of different cross-sectional shapes. The circular cross sections are most common configuration and can withstand high stresses [3]. Copper pipe with 25.4 mm outer diameter and 22 mm inner diameter having a length of 800 mm has been selected for fabrication of the heat pipe. The evaporator length of the heat pipe has been considered as 330 mm to maintain the aspect ratio (L_e/d_o) greater than 10 as suggested by Terdtoon et al. [13]. The adiabatic & condenser lengths are kept as 70 mm & 400 mm, respectively.

3.2.3 Selection of Wick

The various selection criteria of wick include its compatibility with working fluid, cost of fabrication, permeability, pore size, self priming, etc. The wrapped wire screen and the composite screen wicks are most commonly used because of their simplicity in construction. The temperature drop is more in screen wick. For good temperature characteristics, axial grooves or screen covered grooves may be used, but unit cost of small quantity production of grooved pipes is high. The mesh number of most commonly used wrapped screen wicks varies in the range of 50 to 300. The wick with wire mesh numbers greater than 300 tends to have insufficient rigidity, while the wick with wire mesh number less than 50 tends to have insufficient capability in developing capillary pressure. A very small pore size is needed, where pumping is required against gravity [3]. The gravity assisted heat pipes permit maximum liquid flow rate for mesh with pore size such as 100 or 150 [2].

Based on the above considerations, phosphorus bronze wire screen has been selected as wick material because of its easy availability and compatibility with water. Two layers of bronze screen (125 No.) have been considered for fabrication of wick having a thickness

of 0.34 mm. Literature reports that the optimum ratio of r_v/r_o should be approximately equal to $\sqrt{2/3}$ [74], which in the present case is nearer to $\sqrt{2/3}$ with an error of 2.7 %.

3.2.4 Selection of Fins

Fins are used to enhance the heat transfer rate by increasing the surface area across which the convection occurs. The fin material should have a large thermal conductivity to minimize temperature variations from its base to tip. The different types of fin configuration include straight fin, annular fin, and pin fin, etc. The selection of fin depends upon space, weight, ease of manufacturing, and cost of fabrication. Annular fins are easy to fabricate for a cylindrical heat pipe. The literature suggests the use of three to four fins per inch under natural convective conditions [32]. Keeping this consideration in view, the condenser section of each heat pipe has been provided with 41 annular aluminum fins of 50.8 mm diameter at a pitch of 9.0 mm.

3.3 Heat Transport Limitations

The different heat transport limitations of the heat pipe have been calculated at different evaporator surface temperatures. The computed heat transport limits are presented in Table A-3 (Appendix – A). It has been found that the capillary limit is the smallest as compared to the other limits. The overall heat transport limit for the heat pipe is 30.9 W at 40 °C under horizontal condition, which will increase in the thermosyphon mode as well as with increase in operating vapour temperature.

3.4 HPHE Configuration

The arrangement of heat pipes influences thermal performance of HPHE. The staggered arrangement of heat pipes gives better performance as compared to inline arrangement [60]. It is desirable to arrange the pitch of heat pipe (centre to centre distance) such that it is not less than 1.25 times the outer diameter of tubes. There are different possible pitch angles, viz., 30°, 45°, 60°, and 90°. To achieve compactness, 30° & 60°, pitch angles are preferred but 60° pitch angle is rarely used, and 30° pitch angle is the preferred one [75]. A higher value of pitch to diameter ratio (outer diameter of fin) 1.7 has been considered with 30° pitch angle for arranging the heat pipes in the HPHE, keeping in view of the present study under natural convection. Based on the above considerations, it has been

decided to construct the HPHE having a longitudinal pitch of 43 mm and transverse pitch of 150 mm with 4 rows and 9 columns, each column having two heat pipes.

3.5 Development of Analytical Model

An analytical model is required to be developed to study the thermal performance of the HPHE under natural convection conditions. The mathematical formulation of the analytical model has been done based on the computation of various thermal resistances [1, 57]. The different heat transfer correlations available in the literature have been used to compute the overall heat transfer coefficient, rate of heat transfer and pressure drop across evaporator system of the HPHE. The steps followed for development of the model are as follows:

3.5.1 Analytical Considerations & Assumptions

The analytical considerations for analysing the HPHE are:

- Laminar flow regime has been assumed in the evaporator side
- A temperature range of 40 °C to 70 °C is assumed for the heating (hot) fluid in the evaporator section for low temperature applications
- The thermodynamic properties of heating water and ambient air have been evaluated at the mean temperature of fluids
- Uniform flow rate of heating fluid in the evaporator section
- Constant temperature of heating fluid over any cross section of its path in the evaporator section of the HPHE
- Uniform surface temperature of evaporator and condenser
- Bond efficiency between the heat pipe and fins was considered to be 100 per cent

3.5.2 Step Wise Procedure

The model development involves thermal analysis of three sections of the HPHE, which are as follows:

- Hot fluid (or evaporator) side
- Internal surface of heat pipe
- Cold fluid (or condenser) side

3.5.2.1 Inputs Required

The following are the input parameters:

- Outer & inner diameter of heat pipe and its vapor core diameter, m
- Lengths of evaporator, adiabatic, and condenser sections, m
- Number of fins, its dimensions, and pitch on condenser side
- Heat pipe working fluid and its thermo-physical properties at its operating temperature
- Heat pipe wick parameters
- Thermal conductivities of materials at the operating temperature, W/(m-K)
- Number of heat pipes
- Longitudinal and transverse pitch of HPHE, m
- Flow rate of hot fluid, m^3/sec
- Inlet temperature of hot fluid, °C
- Fluid (hot & cold) thermo-physical properties at its bulk mean temperature
- Ambient temperature, °C
- Fouling factors of hot and cold fluids, m^2-K/W

3.5.2.2 Computed Parameters

The following parameters have been computed:

1. Hot fluid side

- Mass velocity, kg/(m^2-sec)
- Average temperature, °C
- Hydraulic diameter, m
- Frontal area, free flow area, heat transfer area, etc., m^2
- Reynolds number
- Individual heat transfer coefficient, W/(m^2-K)
- Evaporator surface temperature, °C
- Fanning friction factor
- Pressure drop in the evaporator section, Pa

2 Internal surface of heat pipe

- Resistances offered by individual components such as pipe wall, saturated wick, and vapor thermal resistance, m^2-K/W
- Total thermal resistance offered by the heat pipe, m^2-K/W
- Internal heat transfer coefficient, W/(m^2-K)
- Condenser surface temperature, °C

3 Cold fluid side under natural convection

- Film temperature, °C
- Thermo-physical properties of air at film temperature
- Characteristic length of condenser, m
- Grashof number
- Rayleigh number
- Nusselt number
- Individual heat transfer coefficient, W/(m^2-K)

4. Overall resistance offered by the above mentioned three zones of the heat pipe heat exchanger besides fouling factors, m^2-K/W

5. Overall heat transfer coefficient, W/(m^2-K)

6. Rate of heat transfer, W

7. Pressure drop, Pa

3.5.3 Mathematical Formulation

To determine the over all heat transfer coefficient, the HPHE has been modelled as a thermal resistance network [57]. The individual heat transfer coefficients have been computed on the external surface of evaporator, internal surface of the heat pipe, and the external surface of condenser. The methodology adopted for calculation of overall heat transfer coefficient, rate of heat transfer, and pressure drop across evaporator system of the HPHE is described below:

3.5.3.1 Evaporator Side

The following parameters have been computed for determining the heat transfer coefficient on the external surface of the evaporator tube bank:

1. Frontal area, $A_{frontal} = L_e \times L_3$ (3.2)

2. Free flow area, $A_{free} = \left(\frac{X_t - d_o}{X_t}\right) L_e L_3$ (3.3)

3. Evaporator heat transfer area, $A_e = \pi d_o L_e$ (3.4)

4. Hydraulic diameter, $D_h = \frac{4 \times A_{free} \times L_2}{A_e}$ (3.5)

5. Free flow area/frontal area, $\sigma_A = \frac{A_{free}}{A_{frontal}}$ (3.6)

6. Mass flow rate, $\dot{m} = V_f \times \rho$ (3.7)

7. Linear velocity, $v = \frac{\dot{m}}{\rho A_{free}}$ (3.8)

8. Mass velocity , $G = v \times \rho$ (3.9)

9. Maximum velocity, $v_{max} = v \times \frac{X_t}{(X_t - d_o)}$ (3.10)

10. Reynolds number

$$Re = \frac{v_{max} \times D_h}{(\mu / \rho)} \quad (3.11)$$

11. Nusselt number

The Nusselt number of heating fluid flowing through the heat pipe is computed by using the following correlation [20]:

$$Nu = (0.35 + 0.56\, Re^{0.52})\, Pr^{0.3} \quad (3.12)$$

where 'Pr' is Prandtl number

The Nusselt number of heating fluid flowing through heat pipes (tube bank) in cross flow is computed by using the following generalized correlation [24]:

$$Nu = C\, Re^{n}\, Pr^{0.36} \quad (3.13)$$

where 'C' and 'n' are available in literature for different values of $\frac{X_t}{d_o}$ and $\frac{X_l}{d_o}$.

12. Individual heat transfer coefficient

$$h_h = \frac{Nu\, k_l}{D_h} \tag{3.14}$$

The heat transfer coefficient on the external surface of evaporator has also been computed by using the following correlation [21]:

$$h_h = 4.55\, Re^{0.733}\, Pr^{0.362} \tag{3.15}$$

13. Evaporator surface temperature

$$T_{p,e} = T_m - \frac{Q}{h_h A_e N} \tag{3.16}$$

3.5.3.2 Internal Heat Transfer Coefficient of Heat Pipe

1. The internal heat transfer coefficient of a heat pipe is reciprocal of sum of its thermal resistances [3].

$$U_{HP,p} = \frac{1}{R_{p,e} + R_{w,e} + R_v + R_{w,c} + R_{p,c}} \tag{3.17}$$

where

$$R_{p,e} = \frac{r_o\, t_p}{2 L_e k_p}$$

$$R_{w,e} = \frac{r_o^2\, t_w}{2 L_e r_i k_{e,e}}$$

$$k_{e,e} = \frac{k_l\left[k_l + k_w - (1-\varepsilon_o)(k_l - k_w)\right]}{\left[k_l + k_w + (1-\varepsilon_o)(k_l - k_w)\right]}$$

$$k_{e,c} = k_{e,c}$$

$$R_v = \frac{\pi r_o^2 F_v (\frac{L_e}{6} + L_a + \frac{L_c}{6}) T_v}{\rho_v \lambda J}$$

$$R_{w,c} = \frac{r_o^2 t_w}{2 L_c r_i k_{e,c}}$$

$$R_{p,c} = \frac{r_o t_p}{2 L_c k_p}$$

2. Condenser surface temperature

$$T_c = T_{p,e} - \frac{Q}{U_{HP,p} A_p N} \tag{3.18}$$

3.5.3.3 Condenser Side

The following parameters have been computed for determining the external heat transfer coefficient of condenser section of the heat pipe [26, 27]:

1. Film temperature, T_f, °C

$$T_f = \frac{(\text{Wall temparature} + \text{Ambient temperature})}{2} \tag{3.19}$$

2. Thermo-physical properties of air such as volumetric expansion coefficient, kinematic viscosity, thermal conductivity, and Prandtl number are calculated at film temperature

3. Grashof number, Gr_L

$$Gr_L = \frac{g \beta (T_c - T_a) L^3}{\nu^2} \tag{3.20}$$

Characteristic length of finned surface is calculated by following its basic definition.

$$\text{Characteristic length, } L = S + 2^* A_f/P_f \tag{3.21}$$

For inclined position L is taken as L cosθ, where θ is the inclination angle from vertical.

4. Rayleigh number, Ra

$$Ra = Gr_L Pr \tag{3.22}$$

5. Flow conditions

   - For, $Ra < 10^9$, the flow is laminar
   - For, $Ra > 10^9$, the flow is turbulent

6. Nusselt number, Nu

$$Nu = f(Gr_L Pr) \tag{3.23}$$

The following empirical relations have been used for calculating Nusselt number as proposed by Churchill & Chu [28] for vertical plate:

* For entire range of Ra

$$Nu_{plate} = \left\{ 0.825 + \frac{0.387 Ra^{1/6}}{\left[1 + (0.492/Pr)^{9/16}\right]^{8/27}} \right\}^2 \tag{3.24}$$

for $10^{-1} < Ra < 10^{12}$

* For laminar flow

$$Nu_{plate} = 0.68 + \frac{0.670 Ra^{1/4}}{\left[1 + (0.492/Pr)^{9/16}\right]^{4/9}} \quad \text{for } 0 < Ra < 10^9 \tag{3.25}$$

Corrected Nusselt number for cylinder = $Nu_{plate}(1 + 1.43\,\zeta^{0.9})$ (3.26)

Where, $\zeta = (L/d_o) G_{r,L}^{-1/4}$

7. Individual heat transfer coefficient on condenser side, h_c

$$h_c = \frac{Nu\, k_{air}}{L} \tag{3.27}$$

3.5.3.4 Overall Heat Transfer Coefficient

The overall heat transfer coefficient of the HPHE has been computed as follows:

$$\frac{1}{UA} = \frac{1}{U_c A_c} = \frac{1}{U_h A_h} = \frac{1}{(hA)_c} + R_{f,c} + R_{HP} + R_{f,h} + \frac{1}{(hA)_h} \qquad (3.28)$$

3.5.3.5 Heat Transfer Rate

The heat transported by HPHE includes heat loss by convection as well as heat loss by radiation

$$Q_T = Q_C + Q_R \qquad (3.29)$$

1. Heat transfer by convection

The heat transfer by convection has been computed as follows:

$$Q_C = h_c N (A_o + A_f \eta_f) (T_c - T_a) \qquad (3.30)$$

2. Heat transfer by radiation

The heat transfer by radiation has been computed as follows:

$$Q_R = \sigma N (A_o + A_f \eta_f) \varepsilon F (T_c^4 - T_a^4) \qquad (3.31)$$

3.5.3.6 Pressure Drop across Evaporator Section

The total pressure drop in the evaporator section of the HPHE consists of skin or core friction, expansion of fluid due to temperature difference, and entry & exit losses at the evaporator inlet & outlet. The skin friction is computed based on fanning friction factor.

$$\Delta P = 4 f \frac{G^2 L_2}{2\rho_m D_h} + G^2 \left(\frac{1}{\rho_{out}} - \frac{1}{\rho_{in}} \right) \qquad [57] \qquad (3.32)$$

where $f = 9.465\, Re^{-0316} \left(\frac{X_t}{d_o} \right)^{-0.937}$ [1]

Pressure loss at the entry of the evaporator, in meters of water $= \frac{v_{max}^2}{2g}$ (3.33)

Pressure loss at the exit of the evaporator, in meters of water $= \frac{v_{cp}^2}{2g}$ (3.34)

3.6 Computer Program

Using the correlations given in the previous sections, computer programmes have been developed for carrying out the thermal performance analysis of the HPHE. The first programme computes operating limits of the heat pipe and the second programme evaluates thermal performance of the heat pipe heat exchanger under natural convection. The salient features of these programmes are described along with simplified flow diagrams.

3.6.1 Operating Limits of Heat Pipe

The flowchart of the program for computation of operating limits of the heat pipe is shown in Figure 3.1. The program takes input data related to evaporator surface temperature, dimensions of the heat pipe, e.g., tube outer & inner diameter, evaporator, adiabatic & condenser length, wick detail such as wire mesh number, wick thickness, and thermal conductivities of materials of the heat pipe.

This program has a subroutine, called WATPROP, in which the properties of water are calculated based on the evaporator surface temperature. The programme computes cross section area of wick & vapour core, maximum effective pumping pressure, capillary radius, effective thermal conductivity of saturated wick, wick permeability, vapour & liquid frictional coefficient, amount of working fluid, maximum capillary heat transport factor, vapour constant, and critical pressure for nucleation. Based on these parameters, capillary limit, sonic limit, entrainment limit, boiling limit, and viscous limit are computed. By using this computer program, the operating limits of the heat pipe can be calculated at different evaporator surface temperatures as well as for different internal dimensions of wicked heat pipes.

3.6.2 Thermal Performance Evaluation

The flowchart of the program for thermal performance evaluation of the HPHE is shown in Figure 3.2. The program takes input data related to fluid operating parameters such as flow rates and inlet temperature of the heating fluid at evaporator section, dimensions & wick detail of the heat pipe, number of heat pipes, longitudinal & transverse pitch, number of rows & columns, number of fins & its dimensions, thermal conductivities of materials of wick & heat pipe wall, and fouling factors.

The program assumes outlet temperature of the heating fluid discharged from the evaporator section and it computes heat load, surface geometry properties such as free flow area, heat transfer area, and hydraulic diameters. This program has three subroutines, called WATPROP, AIRPROP, and METPROP, in which the properties of water, air, and thermal conductivity of the heat pipe container & fin material are calculated based on the average operating temperature. In the evaporator section, the program computes mass flow rate of fluid, Reynolds number, and individual heat transfer coefficient on the external surface of evaporator. The evaporator heat transfer coefficient is used to compute evaporator surface temperature. Based on the evaporator surface temperature, it computes thermal resistance of the heat pipe wall at evaporator & condenser, thermal resistance of the wick structure at the evaporator & condenser, and thermal resistance due to vapour flow. The internal heat transfer coefficient of the heat pipe has been calculated by taking into account of all these thermal resistances. The internal heat transfer coefficient is used to calculate the condenser surface temperature by considering the evaporator external surface temperature and the heat transport rate. On the condenser side, film temperature is computed and air properties are calculated at this temperature. Further, Grashof number, Rayleigh number, Nusselt number, heat transfer coefficient on the condenser side, and fin efficiency are calculated. Individual heat transfer coefficient at the external surface of evaporator, internal surface of heat pipe, and external surface of condenser along with fouling factors are used to determine the overall heat transfer coefficient of the HPHE. Using condenser heat transfer coefficient, heat loss by convection is calculated. For computing total heat loss, heat loss by radiation is also computed and it is added to the convection heat loss. Finally, it computes outlet temperature based on the total heat transfer and compares the computed outlet temperature with the assumed outlet temperature. If the difference between assumed outlet temperature and calculated outlet temperature is less than 0.005 K, i.e., $(T_{ass} - T_{cal}) < 0.005$ K, it calculates the rate of heat transfer, else iterations continue, till the convergence is achieved. It also computes fanning friction factor and pressure drop across evaporator section of the HPHE. By using this computer program, heat transfer rate and pressure drop across the evaporator system of the HPHE are evaluated as a function of operating parameters, such as, flow rate and temperature of the heating fluid at the evaporator inlet.

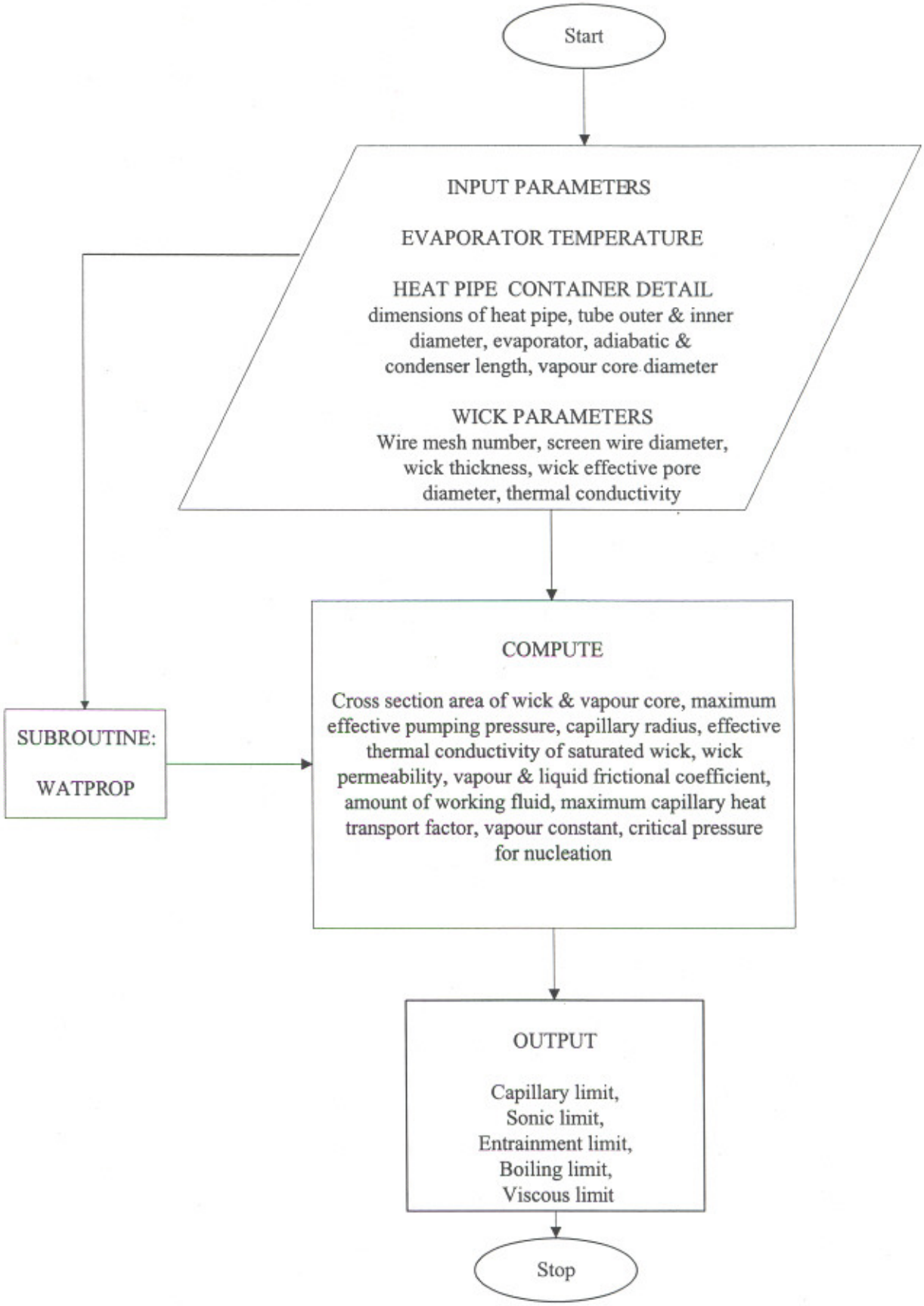

Figure 3.1: A flowchart for computation of transport limits of the heat pipe

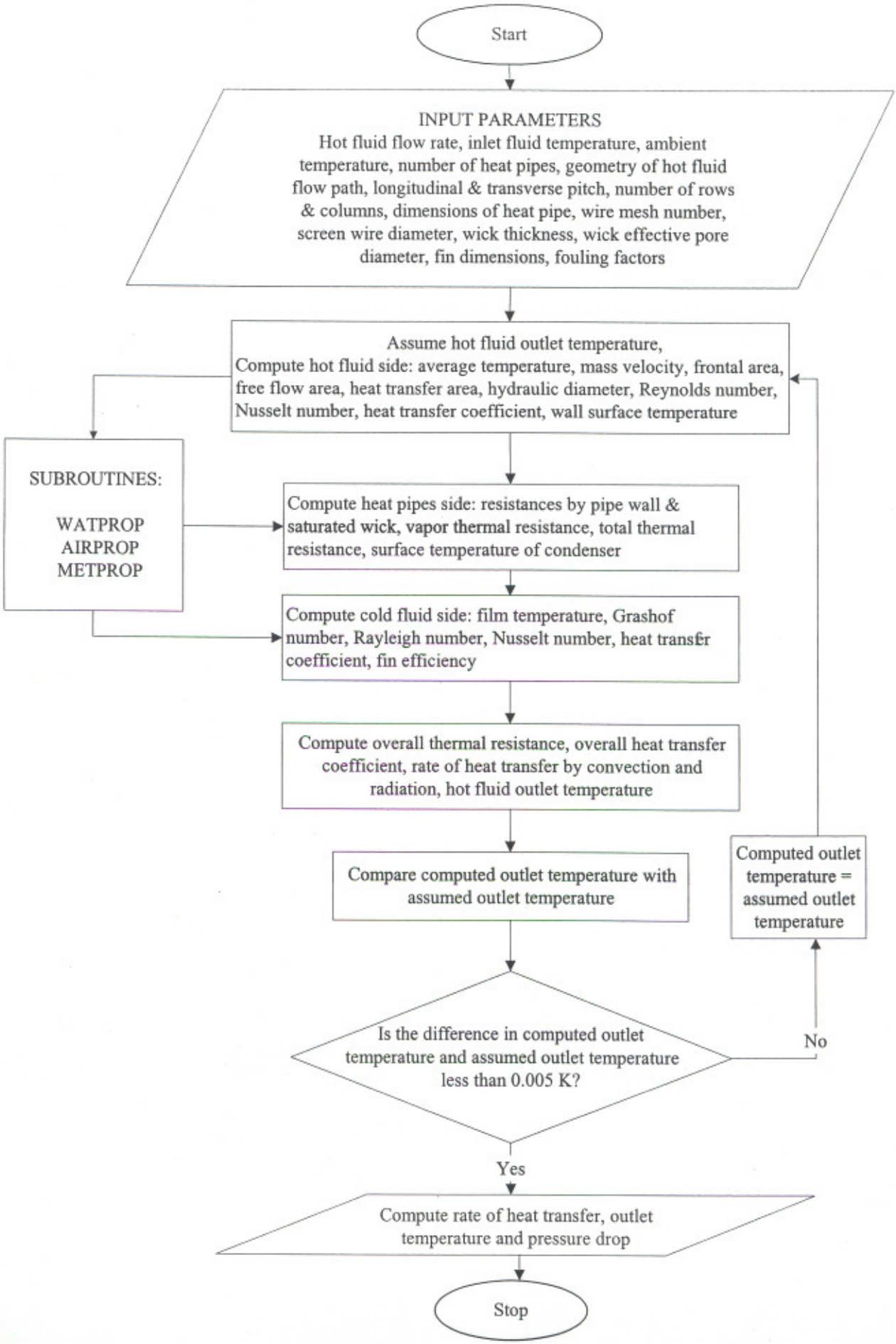

Figure 3.2: A flow chart for thermal performance evaluation of the HPHE

CHAPTER 4

EXPERIMENTATION

4.1 Introduction

This chapter presents manufacturing of the heat pipe & the heat pipe heat exchanger (HPHE) and the detail of the test rigs developed for thermal performance evaluation of the same under natural convective conditions & validation of the analytical model.

4.2 Manufacturing of Heat Pipe

The geometrical dimensions and materials of construction of the heat pipe based upon various design aspects, as given in the Chapter 3, have been considered for its manufacturing. First of all cleaning operation was performed for the heat pipe container and wick material. Mechanical brushing was done to dislodge the solid particle from the inner surface of copper pipe and rinsed with alkaline solution to remove dirt and oily substances. The cleaned pipe was rinsed with diluted sulphuric acid (4-7 %) and followed by washing with distilled water. The pipe was dried in an oven at 105 °C. The wick was wrapped on a mandrel and inserted in the pipe. The pipe with wick was rinsed with acetone 2-3 times and again allowed to dry in the oven. The pipe then had been evacuated using a vacuum pumping system. The mass spectrometer was used for leak detection in the evacuated pipe. After completion of leak test, the working fluid was charged to the evacuated pipe with the help of a graduated burette having a least count of 0.1 ml. The evacuated pipe was then crimped and sealed at the end of fill tube. The condenser section of the heat pipe was fixed with 41 annular aluminium fins (50.8 x 0.3 mm) mechanically at a pitch of 9.0 mm.

4.3 Test Rig for Heat Pipe

The test rig has been designed in a manner such that the performance of the heat pipe can be evaluated at different tilt angles under natural convection conditions. A schematic diagram of the test set-up is shown in Figure 4.1. The evaporator, adiabatic and condenser lengths are 330 mm, 70 mm, and 400 mm, respectively. The evaporator section of the heat pipe is enclosed in a cylindrical jacket made of galvanized iron pipe having 75 mm diameter and 450 mm length. The evaporator jacket is insulated with glass

wool and housed in a wooden box. The condenser is exposed to ambient environment, which removes heat by natural convection. Hot water, heated through an electrical heater in a tank, has been used as a heating source to the evaporator section of the heat pipe. The power input to the heater has been controlled by a variac and measured by power analyser. The hot water has been circulated with the help of a pump through the cylindrical jacket, which has provision for inlet and outlet of hot water. A calibrated rotameter has been used for measuring the flow rate of hot water. A personal computer based data acquisition system has been used to monitor the temperature profile of the heat pipe at various locations on the external surface of evaporator & condenser as well as at the inlet & outlet of the evaporator jacket. Heat flux sensors have been placed on the surface of wooden box to measure the heat flux through the wooden box and its surface temperature at different locations to estimate the heat loss. The test set up of the heat pipe under vertical & tilt conditions are shown in Plate 4.1 and Plate 4.2, respectively.

4.3.1 Instrumentation

The equipments used in manufacturing of the heat pipe and setting up of the test rig are provided in Appendix B-1.

4.3.2 Experimental Procedure

For studying the performance of the heat pipe under natural convective conditions, several test runs were carried out under steady state at a constant heating fluid flow rate of 1.6×10^{-5} m^3/s in the evaporator section at various operating parameters, such as the tilt angle of the heat pipe from the horizontal was varied and kept at 15°, 20°, 25°, 30°, 35°, and 90°. The temperature of heating fluid was varied at the inlet of the evaporator jacket and kept constant at 40 °C, 50 °C, 60 °C, and 70 °C. At given operating temperature, the temperature variation of heating fluid at evaporator inlet was controlled within the range of ± 0.5 °C and the average heating fluid temperature was found to be 40.9 °C, 49.5 °C, 60 °C, and 70.3 °C. The ambient temperature variation was in the range of 11.8 °C to 14 °C. The heat input to the heat pipe is equal to the amount of heat removed from the heating fluid passing through the evaporator jacket and is calculated with the help of equation 4.1.

$$Q_{in} = \dot{m}\ c_p (T_i - T_o) \quad (4.1)$$

Heat transfer coefficient at the surface of wooden box was determined based on the heat flux measured by heat flux sensors using digital micro voltmeter and the temperature recorded by using a personal computer based data acquisition system. The heat loss through the wooden box was then computed as follows:

$$Q_w = h_w \times A_{sw} \times (T_{sw} - T_a) \quad (4.2)$$

The heat transported by the heat pipe was calculated as the difference between heat input to the evaporator section and heat loss from the wooden box.

4.4 Experimentation on Heat Pipe Heat Exchanger

4.4.1 Manufacturing

The HPHE was fabricated by using 18 heat pipes (specifications mentioned in section 3.2) and a 3 mm thick mild steel box having a dimension of 440 x 340 x 450 mm. The top plate of the box was made of 6 mm thick plate, where galvanized iron sockets were welded for holding the heat pipes. The evaporator, adiabatic, and condenser lengths of the heat pipe were kept as 330 mm, 70 mm, and 400 mm, respectively. The heat pipes were arranged in a staggered manner on the top plate with four rows and nine columns, each column having two heat pipes. The longitudinal and the transverse pitch of the heat pipes in the HPHE were kept at 43 mm and 150 mm, respectively. The top plate was fitted tightly to evaporator tank with gasket to avoid leakage of heating fluid.

4.4.2 Test Rig

Another test rig was developed to evaluate the thermal performance of the heat pipe heat exchanger under natural convective conditions. A schematic diagram of the same is shown in Figure 4.2. It consists of a heating tank, HPHE, measurement unit comprising of a personal computer based temperature datalogger, rotameter & power analyzer, and a variac for controlling the power input to the heater. The equipments used for this experiment are listed in Appendix B-II. The evaporator section of the HPHE was housed in a mild steel box and the condenser portion was exposed to ambient conditions. The HPHE tank was insulated and tightly fitted in a wooden box. The mild steel box of dimensions (400 x 400 x 400 mm) was fitted with two electric heaters of 3.0 kW each

for using it as a heating tank. The inlet and outlet connections were provided diagonally in the heating tank and the HPHE tank to increase the residence time of heating fluid for better mixing. Hot water was used as a heating medium for the evaporator section. The centrifugal pump was used to circulate the heating fluid (hot water) from heating tank to the HPHE. The calibrated rotameter was used to measure the flow rate of heating fluid. The power supply to the electrical heater was varied by using variac and monitored by a power analyzer. For temperature measurement of heating fluid at inlet & outlet of the HPHE evaporator section as well as at the external surface of the condenser section, thermocouples (T- type) were provided. The temperatures of different locations as well as the temperature of external wooden surface and the top plate of the HPHE were recorded by using a PC based data acquisition system. Microfoil heat flux sensors were used to measure the heat flux from the wooden box for heat loss estimation. The set-up of the HPHE under vertical condition as well as under tilt conditions are shown in Plate 4.3 and Plate 4.4, respectively.

4.4.3 Experimental Studies

The thermal performance of the HPHE was studied under natural convective conditions by conducting several test runs under various operating conditions given as under:

(i) **Tilt angle:** The tilt angle from the horizontal was varied at 15°, 20°, 25°, 30°, and 90°.

(ii) **Fluid inlet temperature:** The temperature of heating fluid at the inlet of the evaporator section was varied at 40 °C, 50 °C, 60 °C, and 70 °C. At a given operating temperature, the temperature variation of the heating fluid at the evaporator inlet was controlled within the range of ± 0.5 °C.

(iii) **Fluid flow rate:** The heating fluid flow rate in the evaporator section of the HPHE was varied in the range of 320 lph to 630 lph (8.88×10^{-5} m^3/s to 1.75×10^{-4} m^3/s), viz., 320 lph, 385 lph, 450 lph, 510 lph, 570 lph, and 630 lph.

The ambient temperature variation was recorded and found in the range of 18 °C to 22 °C. The temperature readings at various locations of the heat pipe were recorded after achieving the steady state condition. The pressure drop across evaporator system was measured by using an inverted U tube manometer. The heat transfer rate of the HPHE

was calculated using the same methodology as adopted in the calculation of a single heat pipe. The heat input to the HPHE was measured by the amount of heat removed from the hot water passing through the evaporator section as stated in the above paragraph. The heat transport rate of the HPHE was calculated by subtracting the heat losses from the total heat input to the evaporator tank.

Therefore, heat transport rate (Q) of the HPHE is given as:

Q = Heat input to the HPHE – heat losses from wooden box surface and top plate

A sample calculation of heat transport rate of the HPHE is given in Appendix B-III.

4.5 Experimental Error

The temperature data acquisition system and thermocouples have been calibrated against a precision mercury thermometer at ice point & water boiling point and the variations have been observed within the range of ± 0.1 °C. The errors in flow measurement and heat transport rate are of the order of 1.8 % and 4.1%, respectively [76, 77]. The error calculation of each parameter is given in Appendix - B-III.

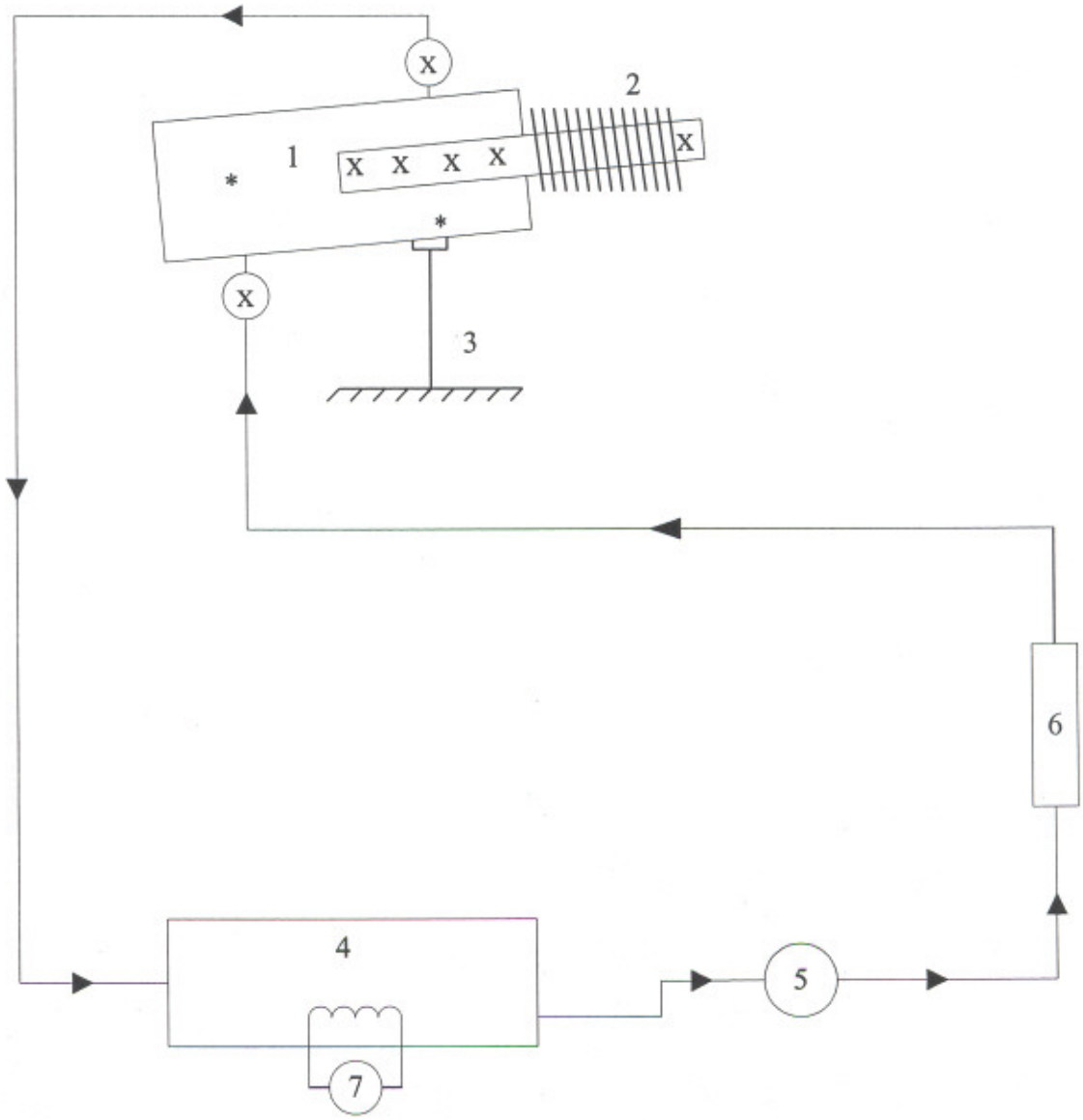

1. Evaporative section
2. Condenser section
3. Tilting arrangement
4. Heating tank
5. Pump
6. Rotameter
7. Electric heater with variac & power analyser

x Thermocouple

* Heat flux sensor

Figure 4.1: A schematic diagram of test rig for single heat pipe

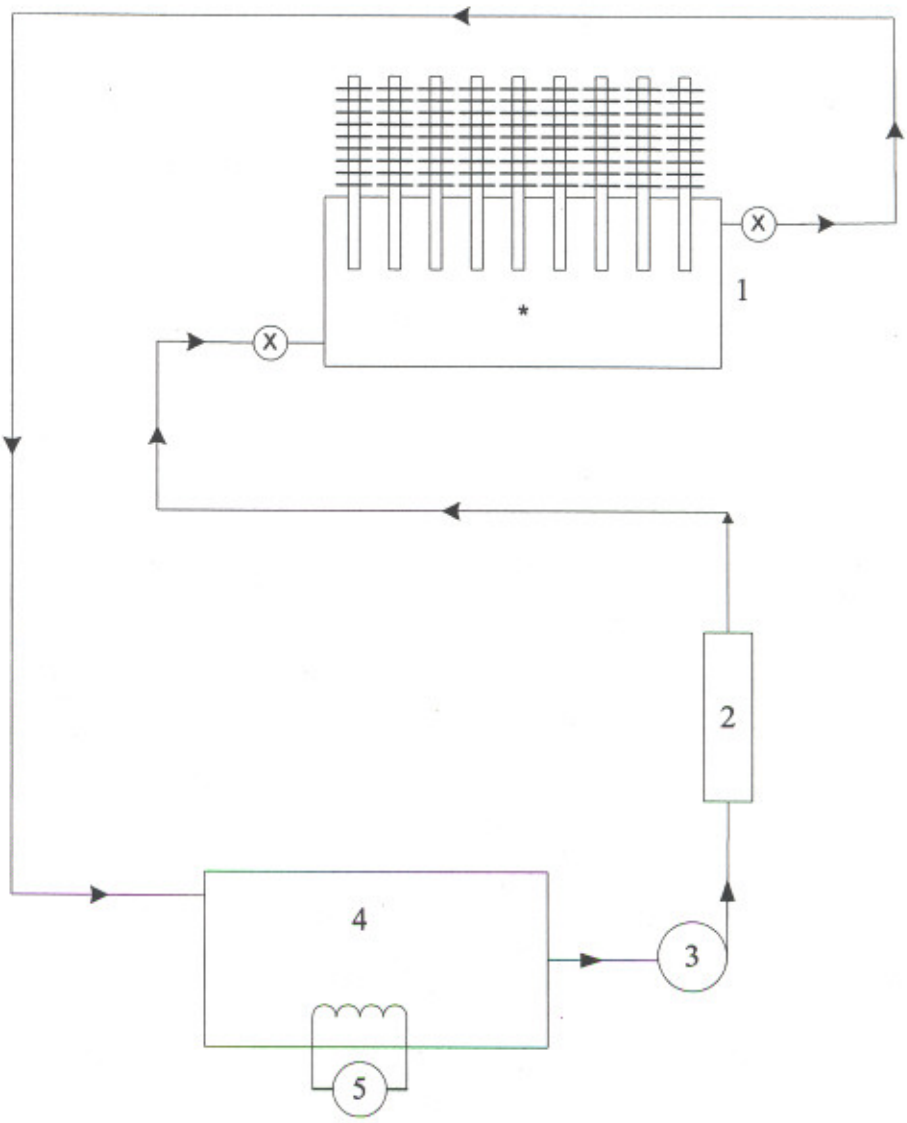

1. Heat pipe heat exchanger
2. Rotameter
3. Pump
4. Heating tank
5. Electrical heater with variac & power analyser

x Thermocouple * Heat flux sensor

Figure 4.2: A schematic diagram of test rig for heat pipe heat exchanger

Plate 4.1: A test set up of single heat pipe under vertical condition

Plate 4.2: A test set up of single heat pipe under inclined condition

Thapar Institute of Engg: & Tech
PATIALA-147001
CENTRAL LIBRARY
92082 27 MAY 2005

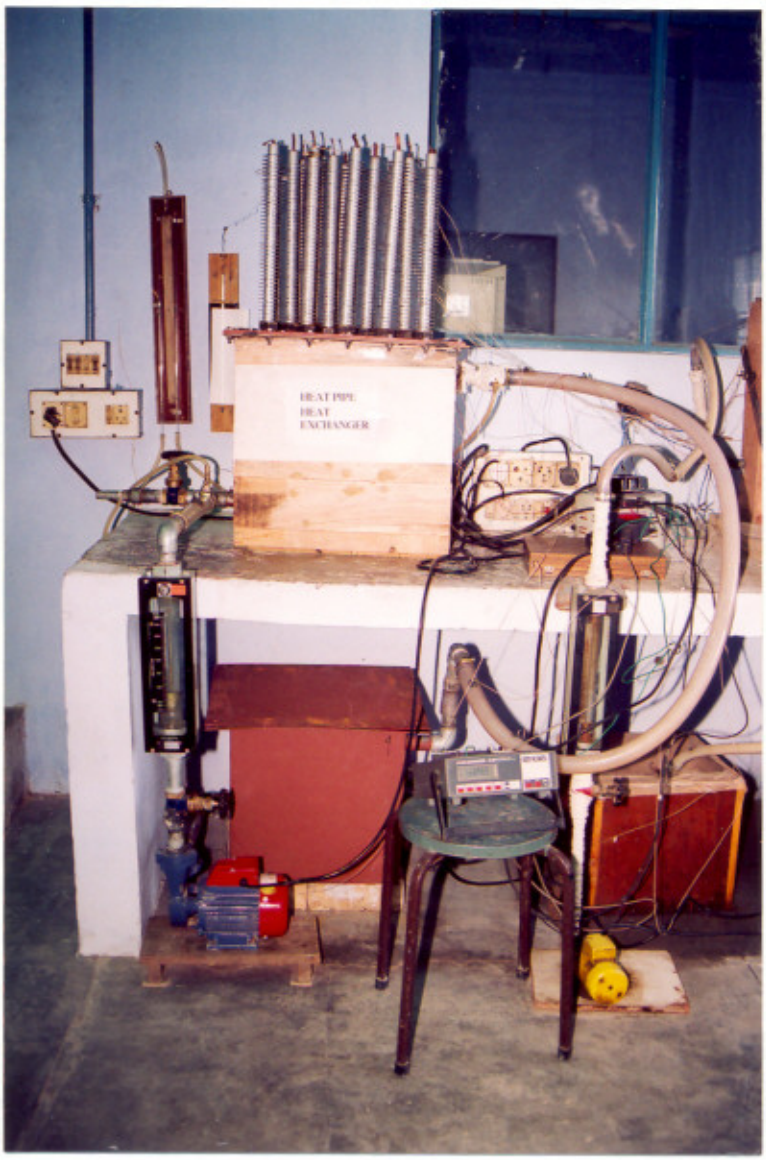

Plate 4.3: A test set up of HPHE under vertical condition

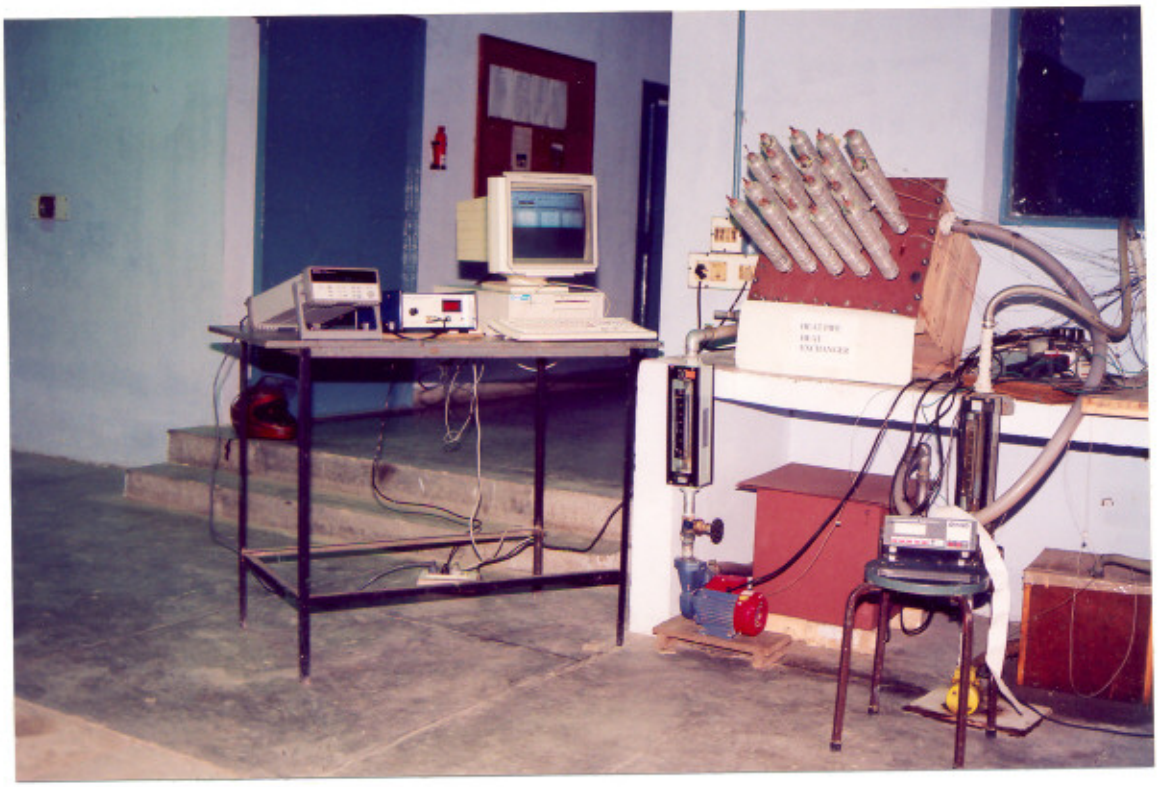

Plate 4.4: A test set up of HPHE under inclined condition

CHAPTER 5

RESULTS AND DISCUSSIONS

5.1 Introduction

This chapter presents experimental results of the heat pipe and the HPHE under natural convective conditions. Individual heat transfer coefficients predicted by the analytical model at the external surface of evaporator & condenser and inside the heat pipe have been compared with experimental results. Further, the heat transport rate of the HPHE and the pressure drop across its evaporator system predicted by the analytical model have also been compared with experimental results of the HPHE.

5.2 Experimental Results of the Heat Pipe

The experiments have been conducted on a single heat pipe to evaluate its thermal performance characteristics, which involves determination of heat transport rate & individual heat transfer coefficients of the heat pipe, and temperature distribution analysis on its external surface. The typical experiments have been carried out in the temperature range of 40 °C to 70 °C.

5.2.1 Heat Transport Rate

The heat transport rate of the heat pipe at different heating fluid temperatures and tilt angles is presented in Table 5.1. It has been observed that the heat transport rate of the heat pipe has been influenced by tilt angle and heating fluid temperature. The heat transport rate of the heat pipe at constant heating fluid temperature increases as the tilt angle increases from 15° to 25°. It starts decreasing beyond 25°. At constant tilt angle, it increases as the heating fluid temperature increases from 40 °C to 70 °C at the inlet of evaporator jacket, which may be due to increase in evaporator & condenser surface temperature, which results in higher convective heat transfer coefficient of condenser at higher temperature. The maximum heat transport rate of the heat pipe (79.9 W) has been observed at 25° tilt angle & 70.3 °C heating fluid inlet temperature and that of minimum (23 W) at 15 ° & 40.9 °C. The best thermal performance of the heat pipe at 25° may be attributed to the optimum rate of evaporation & condensation, and condensate return to the evaporator, which results in its lowest overall internal thermal resistance.

Table 5.1: Effect of tilt angle on the thermal performance of the heat pipe at different heating fluid temperatures

Sl. No.	Tilt angle (Degree)	Heat transport rate (W)			
		Heating fluid temperature			
		40.9 °C	49.5 °C	60.0 °C	70.3 °C
1.	15	23.0	34.9	50.3	60.2
2.	20	25.5	35.3	58.8	73.7
3.	25	33.6	45.6	66.3	79.9
4.	30	32.3	39.9	63.2	77.7
5.	35	32.6	40.5	58.2	76.2
6.	90	33.1	42.4	60.5	68.4

To compare the thermal performance of the heat pipe at different tilt angles, a dimensionless parameter Q/Q_{90} (ratio of rate of heat transport at any angle with respect to rate of heat transport at 90°) has been computed [11]. The effect of tilt angle on Q/Q_{90} is presented in Table 5.2 and also shown in Figure 5.1. As the tilt angle of the heat pipe increases from 15° to 25°, the Q/Q_{90} increases up to 1.16 at 70.3 °C and decreases beyond 25° tilt angle.

Table 5.2: Effect of tilt angle on the heat transport ratio of the heat pipe at different heating fluid temperatures

Sl. No.	Tilt angle (Degree)	Heat transport ratio (Q/Q_{90})			
		Heating fluid temperature			
		40.9 °C	49.5 °C	60.0 °C	70.3 °C
1.	15	0.69	0.82	0.83	0.88
2.	20	0.77	0.83	0.97	1.07
3.	25	1.01	1.07	1.09	1.16
4.	30	0.97	0.94	1.04	1.13
5.	35	0.98	0.95	0.96	1.11
6.	90	1.0	1.0	1.0	1.0

Q/Q_{90} increases with increase in the temperature of heating fluid. The effect of tilt angle on the thermal performance of the heat pipe has been established in the present investigation and the same is also reported by various authors [9-15], which reveal that the thermal performance of a heat pipe under inclined position is better as compared to the vertical position.

5.2.2 Heat Transfer Coefficients

Individual heat transfer coefficients of the heat pipe have been computed at the external surface of evaporator, inside the heat pipe, and at the external surface of the condenser.

5.2.2.1 External Side of Evaporator

The heat transfer coefficient on the external side of evaporator determines the rate at which heat is transported from heating fluid to the evaporator section of the heat pipe. The experimental heat transfer coefficient has been determined based upon the heat transported by the heat pipe and the difference between average heating fluid temperature and the average external surface temperature of the evaporator. The evaporator heat transfer coefficient at different heating fluid temperatures and tilt angles is presented in Table 5.3 and the same is also shown in Figure 5.2.

Table 5.3: Effect of tilt angle on the evaporator heat transfer coefficient of the heat pipe at different heating fluid temperatures

Sl. No.	Tilt angle (Degree)	Evaporator external heat transfer coefficient ($W/(m^2-K)$)			
		Heating fluid temperature			
		40.9 °C	49.5 °C	60.0 °C	70.3 °C
1.	15	309	400	486	696
2.	20	350	419	627	628
3.	25	593	574	624	672
4.	30	358	407	590	548
5.	35	298	368	453	567
6.	90	399	447	466	540

It is observed that the heat transfer coefficient increases as the heating fluid temperature increases, however, a few exceptions have been observed in some cases, which may be due to slight variation in ambient temperature and experimental error to some extent. The heat transfer coefficient is more at lower tilt angles in the range of 15° to 25° at 70.3 °C heating fluid temperature, because the heat transport rate is more at these angles. This study shows that the evaporator heat transfer coefficient is influenced by tilt angle as well as by heating fluid temperature.

5.2.2.2 Internal Side

The internal heat transfer coefficient determines the rate at which the heat is transported from evaporator to condenser. The internal heat transfer coefficient of the heat pipe at different heating fluid temperatures and tilt angles is presented in Table 5.4 as well as in Figure 5.3. The figure shows that it increases as the heating fluid temperature increases except in a few cases, as explained in the section 5.2.2.1. The maximum internal heat transfer coefficient of the heat pipe has been observed at 90° tilt angle, due to less temperature drop between evaporator & condenser.

Table 5.4: Effect of tilt angle on the internal heat transfer coefficient of the heat pipe at different heating fluid temperatures

Sl. No.	Tilt angle (Degree)	Internal heat transfer coefficient of the heat pipe based on cross section area (W/(m^2-K))			
		Heating fluid temperature			
		40.9 °C	49.5 °C	60.0 °C	70.3 °C
1.	15	10,261	14,139	13,054	14,480
2.	20	13,260	17,386	16,759	20,882
3.	25	19,877	25,658	23,164	27,878
4.	30	17,849	20,489	23,307	30,453
5.	35	17,584	23,195	26,741	28,807
6.	90	24,824	30,916	36,550	41,327

The internal heat transfer coefficient also determines the external surface temperature of condenser. The observed condenser temperature at different heating fluid temperatures and tilt angles is presented in Table 5.5 and also shown in Figure 5.4. It has been

observed that the condenser surface temperature is influenced by tilt angle and heating fluid temperature. The condenser temperature increases as the heating fluid temperature increases. The maximum condenser temperature is observed at 90° tilt angle.

Table 5.5: Effect of tilt angle on the condenser surface temperature of the heat pipe at different heating fluid temperatures

Sl. No.	Tilt angle (Degree)	External surface temperature of condenser (°C)			
		Heating fluid temperature			
		40.9 °C	49.5 °C	60.0 °C	70.3 °C
1.	15	33.3	40.0	46.5	55.5
2.	20	33.6	40.5	47.0	57.1
3.	25	33.6	40.5	47.6	57.0
4.	30	33.6	39.8	48.2	56.2
5.	35	32.5	41.1	49.0	56.9
6.	90	34.7	43.6	50.1	61.7

5.2.2.3 External Side of Condenser

The condenser external side heat transfer coefficient plays a major role, as it determines the rate at which the heat is transferred from condenser surface to surrounding. In most of the heat transfer applications, the condenser heat transfer coefficient is a limiting factor [1,5]. The condenser side heat transfer coefficient of the heat pipe at different heating fluid temperatures and tilt angles is presented in Table 5.6. The effect of tilt angle on the condenser side heat transfer coefficient is shown in Figure 5.5. In most of the cases, the condenser side individual heat transfer coefficients are found to be maximum at 60 °C heating fluid temperature. The heat transfer coefficient is higher at 25° tilt angle as compared to other tilt angles because the rate of heat transport is higher at this angle, however some deviations have been observed in a few cases. Although the condenser temperature is higher at 90° tilt angle, the condenser heat transfer coefficient is low, which is due to less amount of heat transferred at this angle. A number of experimental studies have been conducted under natural convection for the heat pipe at 25° tilt angle by varying heating fluid temperatures at evaporator inlet, thereby varying condenser temperature & Rayleigh number. The effect of Rayleigh number on Nusselt

number for the heat pipe at different heating fluid temperature is shown in Figure 5.6, which shows that the Nusselt number increases marginally with the increase in Rayleigh number under natural convection. A comparison of individual heat transfer coefficients at the external surface of evaporator & condenser as well as inside the heat pipe has been presented in Table 5.7 at 25° tilt angle. It has been observed that the condenser heat transfer coefficient under natural convection is the lowest as compared to evaporator and internal heat transfer coefficient of the heat pipe, which is due to the highest thermal resistance between condenser & the ambient, thereby limiting the rate of heat transport of the heat pipe. The similar trend has been observed at other tilt angles as well.

Table 5.6: Effect of tilt angle on the condenser heat transfer coefficient of the heat pipe at different heating fluid temperatures

Sl. No.	Tilt angle (Degree)	Heat transfer coefficient at the external surface of condenser ($W/(m^2-K)$)			
		Heating fluid temperature			
		40.9 °C	49.5 °C	60.0 °C	70.3 °C
1.	15	6.8	8.2	9.5	9.2
2.	20	7.4	8.1	10.9	10.8
3.	25	9.7	10.2	12.1	11.8
4.	30	9.7	9.1	11.4	11.6
5.	35	9.8	8.9	10.2	12.4
6.	90	9.0	8.5	10.1	9.1

Table 5.7: A comparison of individual heat transfer coefficients of the heat pipe at different heating fluid temperatures

Sl. No.	Heating fluid temperature (°C)	Evaporator heat transfer coefficient ($W/(m^2-K)$)	Internal heat transfer coefficient ($W/(m^2-K)$)	Condenser side heat transfer coefficient ($W/(m^2-K)$)
1.	40.9	592	19,877	9.7
2.	49.5	573	25,658	10.2
3.	60.0	624	23,164	12.1
4.	70.3	671	27,878	11.8

5.2.2.4 Overall Heat Transfer Coefficient

The overall heat transfer coefficient of the heat pipe at different heating fluid temperatures and tilt angles is presented in Table 5.8 and also shown in Figure 5.7. For tilt angles varying from 15° to 25°, the overall heat transfer coefficient increases as the heating fluid temperature increases, however, this trend has been not observed after 60 °C heating fluid temperature. It indicates that the rate of increase in heat transport decreases beyond this temperature, which may be attributed to the fact that the rate of increase in capillary limit decreases after 60 °C as shown in Table A-3 and Figure A.1. The maximum overall heat transfer coefficient is obtained at 60 °C heating fluid temperature and 25° tilt angle. There are some deviations in the normal trends due to slight variation in condenser environment, which do not remain uniform in natural convection conditions. This study shows that tilt angle and heating fluid temperature play a major role in heat transport of the heat pipe.

Table 5.8: Effect of tilt angle on the overall heat transfer coefficient of the heat pipe at different heating fluid temperatures

Sl. No.	Tilt angle (Degree)	Overall heat transfer coefficient of the heat pipe (W/(m^2-K))			
		Heating fluid temperature			
		40.9 °C	49.5 °C	60.0 °C	70.3 °C
1.	15	6.6	8.0	9.3	9.0
2.	20	7.7	7.7	10.7	10.6
3.	25	9.6	10.0	11.8	11.5
4.	30	9.1	8.9	11.1	11.4
5.	35	9.5	8.7	10.0	11.0
6.	90	8.8	8.4	9.9	8.9

5.2.3 Temperature Distribution

The axial temperature distribution on the external surface of the heat pipe at different tilt angles, viz., 15°, 20°, 25°, 30°, 35°, and 90° has been recorded by varying heating fluid temperature at the inlet of evaporator section, viz., 40.9 °C , 49.5 °C , 60 °C, and 70.3 °C. The external surface temperatures of the heat pipe at different tilt angles and heating

fluid temperatures are presented in Tables 5.9 to 5.12. The graphs for temperature distribution of the heat pipe along its axial length are also shown in Figures 5.8 to 5.11. The pattern of temperature profile has close resemblance with the results published by Peterson [5].

Table 5.9: Effect of tilt angle on the external surface temperature distribution of the heat pipe at 40.9 °C heating fluid temperature

Sl. No.	Tilt angle (Degree)	External surface temperature of the heat pipe along its axial length from evaporator end (°C)							
		10 mm	65 mm	120 mm	175 mm	230 mm	285 mm	340 mm	790 mm
1.	15	39.9	39.7	39.5	38.4	38.5	38.1	37.6	31.9
2.	20	39.9	39.2	38.5	38.3	38.5	38.2	37.9	32.2
3.	25	38.8	38.6	38.3	38.3	38.4	38.1	37.9	32.3
4.	30	39.2	38.9	38.5	38.4	38.7	38.2	37.5	32.3
5.	35	38.4	38.1	37.8	37.7	37.7	36.5	36.4	31.3
6.	90	38.7	38.7	38.8	38.9	39.0	38.7	38.1	33.9

Table 5.10: Effect of tilt angle on the external surface temperature distribution of the heat pipe at 49.5 °C heating fluid temperature

Sl. No.	Tilt angle (Degree)	External surface temperature of the heat pipe along its axial length from evaporator end (°C)							
		10 mm	65 mm	120 mm	175 mm	230 mm	285 mm	340 mm	790 mm
1.	15	48.2	47.6	47.0	45.3	45.4	45.0	44.2	38.2
2.	20	47.1	46.3	45.6	45.5	45.9	45.4	44.9	39.0
3.	25	45.8	45.6	45.4	45.4	45.8	45.4	44.9	39.0
4.	30	45.3	45.4	45.4	45.5	45.8	46.0	45.0	38.3
5.	35	45.9	46.0	46.1	46.2	46.3	45.2	44.9	39.8
6.	90	47.2	47.3	47.5	47.4	47.7	47.3	46.5	42.6

Table 5.11: Effect of tilt angle on the external surface temperature distribution of the heat pipe at 60 °C heating fluid temperature

Sl. No.	Tilt angle (Degree)	External surface temperature of the heat pipe along its axial length from evaporator end (°C)							
		10 mm	65 mm	120 mm	175 mm	230 mm	285 mm	340 mm	790 mm
1.	15	58.4	58.2	58.1	56.2	54.1	53.5	51.7	44.5
2.	20	57.9	57.4	57.0	54.8	54.2	53.2	52.4	45.3
3.	25	57.4	56.5	55.5	54.4	54.2	53.8	52.6	46.0
4.	30	57.7	56.8	55.9	54.1	54.4	54.5	53.0	46.6
5.	35	55.3	55.1	54.9	54.7	54.9	54.5	53.0	47.7
6.	90	55.4	55.4	55.4	55.6	55.7	54.5	53.9	49.8

Table 5.12: Effect of tilt angle on the external surface temperature distribution of the heat pipe at 70.3 °C heating fluid temperature

Sl. No.	Tilt angle (Degree)	External surface temperature of the heat pipe along its axial length from evaporator end (°C)							
		10 mm	65 mm	120 mm	175 mm	230 mm	285 mm	340 mm	790 mm
1.	15	68.6	68.5	68.3	66.0	63.4	64.2	61.7	53.5
2.	20	69.1	67.0	65.0	64.6	65.1	63.7	62.1	55.5
3.	25	67.4	66.1	64.8	63.4	63.5	63.5	62.3	55.2
4.	30	66.0	64.2	62.5	62.1	62.4	62.3	61.3	55.0
5.	35	65.7	64.6	63.4	63.0	63.6	63.2	60.9	55.6
6.	90	65.9	66.0	66.1	66.1	66.1	65.3	64.2	60.8

The temperature profile in the evaporator section is nearly uniform. It decreases smoothly & linearly. The temperature drop across the ends of the evaporator section has been found to be small. The temperature drop between heating fluid and evaporator external surface is low, which is due to higher evaporator outside heat transfer coefficient and high heat carrying capacity of heating fluid, i.e., water, whereas in the condenser section, the temperature drop is high along the external surface of the heat pipe due to low outside heat transfer coefficient as well as low heat carrying capacity of cooling fluid, i.e., ambient air. The temperature drop across the external end of evaporator and condenser at different heating fluid temperatures and tilt angles is presented in Table 5.13 and the same is shown in Figure 5.12.

Table 5.13: Effect of tilt angle on the temperature drop across the external end of evaporator and condenser at different heating fluid temperatures

Sl. No.	Tilt angle (Degree)	Temperature drop across evaporator and condenser end at different heating fluid temperatures (°C)			
		40.9 °C	49.5 °C	60.0 °C	70.3 °C
1.	15	8.7	9.7	13.7	15.1
2.	20	7.9	8.0	12.6	13.6
3.	25	6.5	7.2	11.5	12.1
4.	30	6.8	7.0	11.0	11.5
5.	35	7.1	6.1	7.6	10.2
6.	90	4.7	4.6	5.7	5.2

The temperature drop across evaporator and condenser end at constant heating fluid temperature decreases as tilt angle of the heat pipe increases from 15° to 90° and it is minimum at 90°. At constant tilt angle, the temperature drop increases as the heating fluid temperature increases from 40 °C to 70 °C, which indicates that more amount of heat is transported at higher heating fluid temperatures. The maximum temperature drop across the end of evaporator and condenser is found to be 15.1 °C at 15° tilt angle and 70.29 °C heating fluid temperature, but heat transport rate is not maximum at this tilt angle. This shows that the heat transport rate of a heat pipe depends on several operating parameters, like tilt angle, heating fluid temperature, etc.

5.3 Validation of the Analytical Model for a Single Heat Pipe

The analytical model has been investigated for a single heat pipe by selecting the appropriate geometrical parameters and heat transfer correlations available from the literature, which also has been extended to the HPHE analysis in further studies. The analytical model computes the heat transfer coefficients on the external surface of evaporator & condenser, inside the heat pipe, and the overall heat transfer coefficient.

To validate the analytical model for single heat pipe, some typical values of individual heat transfer coefficients obtained from experimental results of the heat pipe at 25° tilt angle have been compared with the analytical model. The observations revealed are described in the following paragraphs.

5.3.1 Evaporator External Surface Heat Transfer Coefficient

The evaporator external surface heat transfer coefficient has been computed by using the correlation for flow across a cylinder by Fand [20] as well as the correlation proposed by Dobson & Kröger [21] for an inclined thermosyphon housed in a cylindrical jacket. The evaporator surface temperature has been computed based on the evaporator heat transfer coefficient and the heat transport rate. A comparison of evaporator heat transfer coefficient and surface temperature, determined by Fand's correlation, Dobson & Kröger's correlation, and experimental values is presented in Table 5.14. The comparisons are also shown in Figures 5.13 & 5.14. It has been observed that the evaporator heat transfer coefficient predicted by Fand's correlation is approximately 3 times less as compared to the experimental value due to which the predicted evaporator surface temperature using this correlation is less (approximately 15 %) as compared to the experimental value. The evaporator heat transfer coefficient and the evaporator surface temperature predicted by Dobson & Kröger's correlation have close agreement with experimental values. From the present investigation, it has been established that the correlation proposed by Dobson & Kröger is more appropriate as compared to Fand's correlation in the present model.

Table 5.14: A comparison of external evaporator heat transfer coefficient and surface temperature predicted by different correlations with experimental values at different heating fluid temperatures

Sl. No.	Heating fluid temperature (°C)	Reynolds number	Fand's correlation		Dobson & Kröger's correlation		Experimental value	
			Evaporator heat transfer coefficient ($W/(m^2-K)$)	Evaporator external surface temperature (°C)	Evaporator heat transfer coefficient, ($W/(m^2-K)$)	Evaporator external surface temperature (°C)	Evaporator heat transfer coefficient ($W/(m^2-K)$)	Evaporator external surface temperature (°C)
1.	40.9	408	193	33.2	622	37.8	592	38.3
2.	49.5	488	201	39.7	676	45.5	574	45.5
3.	60.0	574	212	47.8	716	55.1	624	54.9
4.	70.3	660	221	55.6	755	64.4	672	64.4

5.3.2 Internal Heat Transfer Coefficient of Heat Pipe

The internal heat transfer coefficient of the heat pipe has been calculated based upon the various internal thermal resistances of a heat pipe as reported by Chi [3]. These thermal resistances include the thermal resistances of the heat pipe wall at the evaporator & condenser sections, thermal resistances of the liquid saturated wick at the evaporator & condenser surfaces inside the heat pipe, and the thermal resistance of vapour flow. A comparison of the internal heat transfer coefficient & the external condenser surface temperature predicted by the analytical model and obtained experimentally is presented in Table 5.15 and the same are shown in Figures 5.15 & 5.16.

Table 5.15: A comparison of predicted internal heat transfer coefficient and condenser temperature of the heat pipe with experimental result at different heating fluid temperatures

Sl. No.	Heating fluid temperature (^{o}C)	Internal heat transfer coefficient (W/(m^2-K))		External condenser surface temperature (^{o}C)	
		Predicted	Experimental	Predicted	Experimental
1.	40.9	92,470	19,877	36.8	33.7
2.	49.5	93,880	25,659	44.3	40.5
3.	60.0	95,400	23,164	53.2	47.6
4.	70.3	96,800	27,879	62.5	56.9

It has been observed that the experimental values of heat transfer coefficients at different heating fluid temperatures are 3.4 to 4.6 times less as compared to that of the theoretically predicted values. The deviation in theoretically predicted heat transfer coefficient and experimental value is higher at lower temperatures (below 50 ^{o}C), which decreases at higher temperatures (60 ^{o}C & above). The predicted internal heat transfer coefficient is higher, therefore, the predicted condenser temperature is on the higher side (3.1-5.6 ^{o}C) as compared to the experimental value. It has been found from the analytical model that the thermal resistance of the wick structure at the condenser end is the highest, which governs the internal heat transfer coefficient of the heat pipe to a greater extent. The lower experimental value of internal heat transfer coefficient may be due to higher thermal resistances of wick structure of the heat pipe and imperfect contact of wick to the heat pipe

container wall, which has resulted in more temperature drop across evaporator & condenser end.

5.3.3 Condenser External Surface Heat Transfer Coefficient

The correlations proposed by Churchill & Chu for vertical plate (laminar range as well as for all range of Rayleigh number) have been used to predict the heat transfer coefficient on the condenser side of the heat pipe with appropriate correction factor and the characteristic length [28]. A comparison of heat transfer coefficient predicted by the analytical model and the experimental value is presented in Table 5.16 and the same is also shown in Figure 5.17.

Table 5.16: A comparison between predicted and experimental condenser side heat transfer coefficient of the heat pipe at different heating fluid temperatures

Sl. No.	Heating fluid inlet temperature (°C)	Condenser heat transfer coefficient ($W/(m^2-K)$)		
		Churchill & Chu (laminar)	Churchill & Chu (all range)	Experimental value
1.	40.9	11.5	10.9	9.7
2.	49.5	12.2	11.4	10.2
3.	60.0	12.7	11.9	12.1
4.	70.3	13.1	12.3	11.8

It has been found that the heat transfer coefficient predicted by using Churchill & Chu's correlation for laminar range is on higher side (5 to 18 %) as compared to the experimental value even though the Grashof number lies in laminar flow regime. The heat transfer coefficient predicted by using Churchill and Chu's correlation for all range is close (-1 to 12 %) to the experimental value. The predicted heat transfer coefficient is little higher as compared to the experimental value except at 60 °C heating fluid temperature, which is due to fact that the model predicts higher value of internal heat transfer coefficient and in turn the predicted condenser temperature is more.

5.3.4 Overall Heat Transfer Coefficient

The overall heat transfer coefficient has been computed by using the correlation proposed by Dobson & Kröger for evaporator heat transfer coefficient, Chi for internal heat transfer coefficient and Churchill and Chu (for all range) for condenser heat transfer coefficient. A

comparison of overall heat transfer coefficient predicted by the analytical model & obtained from the experimental results is presented in Table 5.17, and the same is plotted in Figure 5.18. The overall heat transfer coefficient predicted by the analytical model is in good agreement with experimental value as the value of internal heat transfer coefficient is very high and it contributes practically nothing to the overall heat transfer coefficient, which is mostly governed by condenser and to a much less degree by evaporator heat transfer coefficient.

Table 5.17: A comparison between predicted and experimental overall heat transfer coefficient of the heat pipe at different heating fluid temperatures

Sl. No.	Heating fluid temperature (°C)	Predicted heat transfer coefficient ($W/(m^2-K)$)	Experimental heat transfer coefficient ($W/(m^2-K)$)	Deviation with respect to experimental value (%)
1.	40.9	10.3	9.6	7.6
2.	49.5	10.7	10.0	6.8
3.	60.0	11.2	11.8	-5.6
4.	70.3	11.5	11.6	-1

5.4 Experimental Studies on the Heat Pipe Heat Exchanger

The thermal performance of the HPHE has been evaluated based on the amount of heat transported by the HPHE under various operating conditions, viz., different flow rates of heating fluid, temperatures of heating fluid, and tilt angles of the HPHE.

The heat transport rate of the HPHE at various flow rates & temperatures of heating fluid as well as at different tilt angles is presented in Table 5.18. The effects of heating fluid flow rate in the evaporator section on the heat transport rate of the HPHE have also been shown in graphical plots from Figures 5.19 to 5.23. It has been observed that at a particular heating fluid temperature, the heat transport rate of the HPHE increases marginally with the increase in flow rate of heating fluid in the evaporator section, because the condenser temperature does not increase significantly. This effect has been observed at all the tilt angles, viz., 15°, 20°, 25°, 30°, and 90°. At constant flow rate of heating fluid, the heat transport rate increases as the heating fluid temperature increases from 40 °C to 70 °C. The effects of tilt angle on the heat transport rate of the HPHE are shown in Figures 5.24 to 5.29. It has been observed that as the tilt angle increases from 15° to 25°, the heat transport rate increases, and it starts decreasing beyond 25° tilt angle.

The minimum heat transport rate has been obtained at 90°, which may be due to the higher overall thermal resistance of the heat pipe at this position because of the highest resistance offered by the condenser [11]. The best thermal performance of the HPHE has been obtained at a tilt angle of 25°, which may be due to the best performance of the heat pipe at this orientation. In some cases, the heat transport rate of the HPHE at 20° is almost the same as that of at 15°, which may be due to slightly higher ambient temperature in the former case.

Table 5.18: Heat transport rate of the HPHE under natural convection at different tilt angles and various heating fluid temperatures

Sl. No.	Heating fluid temp. (°C)	Amb. temp. (°C)	Tilt angle (Deg.)	Heat transport rate at different fluid flow rates (W)					
				Fluid flow rate (lph)					
				320	385	450	510	570	630
1.	40	17.9	15	341	332	333	335	339	349
2.	50	19.3	15	555	573	578	591	613	645
3.	60	20.8	15	793	814	827	850	863	888
4.	70	21.0	15	905	930	943	953	961	991
5.	40	19.0	20	377	406	411	423	431	434
6.	50	20.8	20	558	577	579	598	613	649
7.	60	21.3	20	853	886	901	918	927	938
8.	70	22.0	20	1117	1150	1192	1192	1208	1252
9.	40	18.0	25	484	490	493	506	518	526
10.	50	20.0	25	656	683	719	749	781	807
11.	60	21.0	25	1038	1048	1060	1076	1090	1118
12.	70	22.0	25	1218	1272	1313	1338	1360	1373
13.	40	17.8	30	469	478	484	490	491	516
14.	50	19.6	30	680	690	710	727	747	776
15.	60	21.2	30	849	881	887	923	939	953
16.	70	21.7	30	1112	1146	1171	1179	1194	1230
17.	40	18.2	90	274	289	324	335	339	342
18.	50	21.0	90	394	402	413	415	421	422
19.	60	21.5	90	634	657	681	705	714	724
20.	70	22.7	90	751	778	828	857	916	963

5.5 Validation of the Analytical Model

To validate the analytical model for the HPHE, some typical experimental results for the heat transport rate obtained at 25° tilt angle have been compared with the results predicted by the analytical model and the same are presented in Table 5.19. The comparisons of the same are also shown in graphical plots from Figures 5.30 to 5.35. It

has been observed that the heat transport rate predicted by the analytical model is more than the experimental heat transport rate and its deviations at different heating fluid temperatures and flow rates are presented in Table 5.19.

Table 5.19: A comparison of experimental heat transport rate of the HPHE at 25° tilt angle with the analytical model at different heating fluid temperatures

Sl. No.	Amb. temp. (°C)	Fluid inlet temp. (°C)	Fluid flow rate (lph)	Experimental heat transport rate (W)	Computed heat transport rate (W)	Difference (W)	Dev. (%)
1.	18	40.9	320	484	597	113	23.2
2.	20	50.5	320	656	833	177	26.9
3.	21	60.2	320	1038	1117	79	7.6
4.	22	70.2	320	1218	1423	205	16.9
5.	18	40.7	385	490	603	113	22.9
6.	20	50.5	385	683	849	166	24.2
7.	21	60.6	385	1048	1154	106	10.1
8.	22	70.4	385	1272	1460	188	14.8
9.	18	40.5	450	493	605	112	22.7
10.	20	50.0	450	719	848	129	17.9
11.	21	60.9	450	1060	1182	122	11.5
12.	22	70.7	450	1313	1491	178	13.5
13.	18	40.4	510	506	609	103	20.4
14.	20	50.0	510	749	856	107	14.2
15.	21	60.8	510	1076	1188	112	10.4
16.	22	70.5	510	1338	1507	169	12.6
17.	18	40.4	570	518	614	96	18.6
18.	20	50.1	570	781	864	83	10.5
19.	21	60.5	570	1090	1190	100	9.2
20.	22	70.5	570	1360	1512	152	11.2
21.	18	40.7	630	526	627	101	19.1
22.	20	50.1	630	807	869	62	7.7
23.	21	60.5	630	1118	1196	78	6.9
24.	22	70.4	630	1373	1520	147	10.7

The higher heat transport rate of the HPHE predicted by the analytical model is due to the higher value of condenser temperature computed by the model. A comparison of condenser temperatures predicted by the analytical model and those obtained from the experiments is also presented in Table 5.20. It has been observed that the variation in predicted condenser temperature and the experimental value is in the range of 3.8 °C to 6.4 °C, which results in more temperature drop between condenser and ambient. The higher condenser temperature is due to higher value of internal heat transfer coefficient

predicted by the model and the same has been explained in the validation analysis of a single heat pipe. The variation is higher at lower heating fluid temperature, which may be due to higher prediction of condenser side heat transfer coefficient by the model at lower temperature. Literature reports that the calculated heat transfer coefficient may vary ± 25 % from the actual value in natural convection [27].

Table 5.20: A comparison of experimental condenser temperature of the HPHE at 25° tilt angle with the condenser temperature computed by the analytical model at different heating fluid temperatures

Sl. No.	Amb. temp. (°C)	Heating fluid temp. (°C)	Fluid flow rate (lph)	Experimental condenser temperature (°C)	Computed condenser temperature (°C)	Difference (°C)
1.	18	40.9	320	33.6	37.5	3.9
2.	20	50.5	320	41.4	45.9	4.5
3.	21	60.2	320	49.1	54.2	5.1
4.	22	70.2	320	57.0	62.8	5.8
5.	18	40.7	385	33.7	37.6	3.9
6.	20	50.5	385	41.9	46.3	4.4
7.	21	60.6	385	50.1	55.1	5.0
8.	22	70.4	385	58.1	63.7	5.6
9.	18	40.5	450	33.9	37.7	3.8
10.	20	50.0	450	41.5	46.3	4.8
11.	21	60.9	450	50.6	55.8	5.2
12.	22	70.7	450	58.6	64.4	5.8
13.	18	40.4	510	33.8	37.8	4.0
14.	20	50.0	510	41.0	46.5	5.5
15.	21	60.8	510	49.6	56.0	6.4
16.	22	70.5	510	58.8	64.8	6.0
17.	18	40.4	570	34.1	37.9	3.8
18.	20	50.1	570	41.5	46.7	5.2
19.	21	60.5	570	49.9	56.0	6.1
20.	22	70.5	570	59.2	64.9	5.7
21.	18	40.7	630	34.2	38.3	4.1
22.	20	50.1	630	41.7	46.8	5.1
23.	21	60.5	630	50.1	56.2	6.1
24.	22	70.41	630	59.4	65.1	5.7

The experimentally measured pressure drop across evaporator section of the HPHE and the pressure drop predicted by the analytical model are presented in Table 5.21 and the same are also shown in Figure 5.36. It has been observed that the pressure drop across inlet and outlet of evaporator section increases as the flow rate of heating fluid increases. The pressure drop across the tube bundle of the HPHE is very small in magnitude due to

large pitch of the heat pipe in longitudinal and lateral direction. The most of the pressure drop is due to sudden expansion of heating fluid at the inlet and sudden contraction of heating fluid at outlet. The variation in pressure drop monitored experimentally and computed by the analytical model is within the range of 2 to 13 %.

Table 5.21: A comparison of experimental pressure drop across evaporator section of the HPHE with the analytical model

Sl. No.	Fluid flow rate (lph)	Experimental pressure drop (Pa)	Computed pressure drop (Pa)	Difference (Pa)	Deviation, (%)
1.	320	16.8	15.4	1.4	8.8
2.	385	25.7	22.3	3.4	13.5
3.	450	33.6	30.4	3.2	9.5
4.	510	42.8	39.0	3.8	8.8
5.	570	50.8	48.8	2.0	3.9
6.	630	61.0	59.6	1.3	2.2

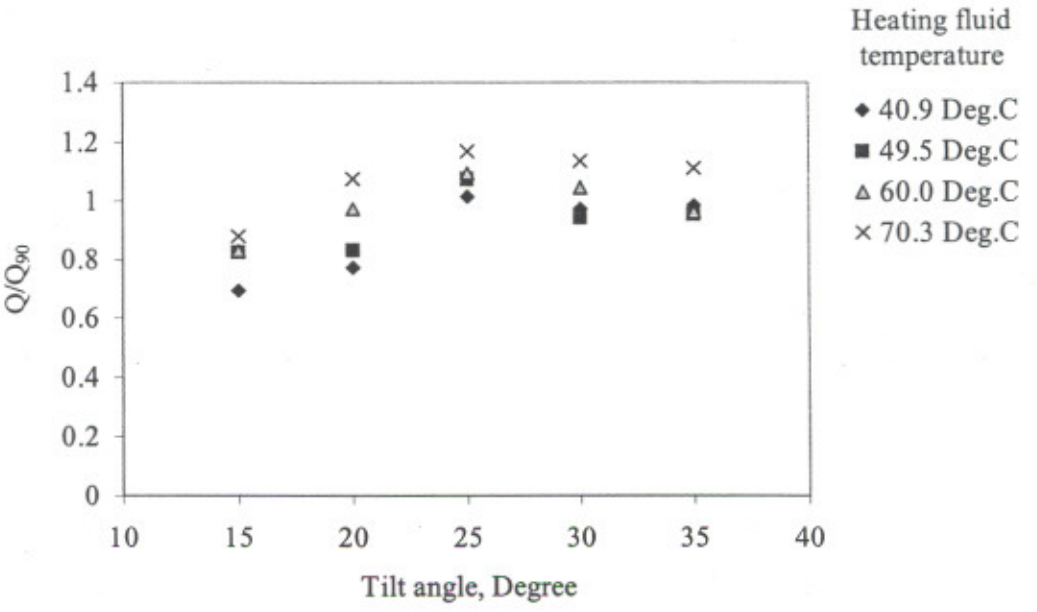

Figure 5.1: Effect of tilt angle on Q/Q_{90} of the heat pipe

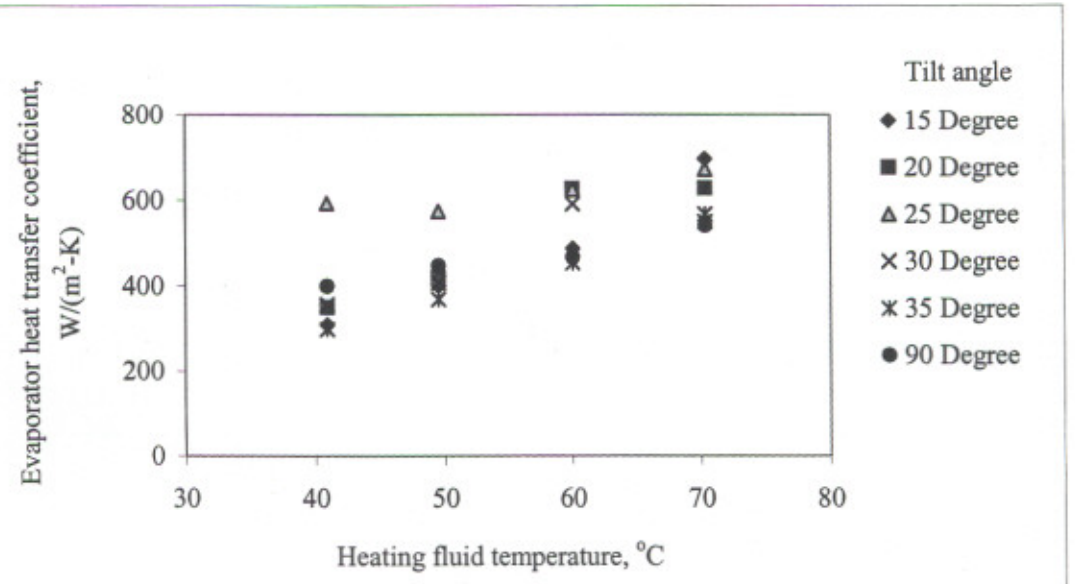

Figure 5.2: Effect of heating fluid temperature on the evaporator heat transfer coefficient of the heat pipe

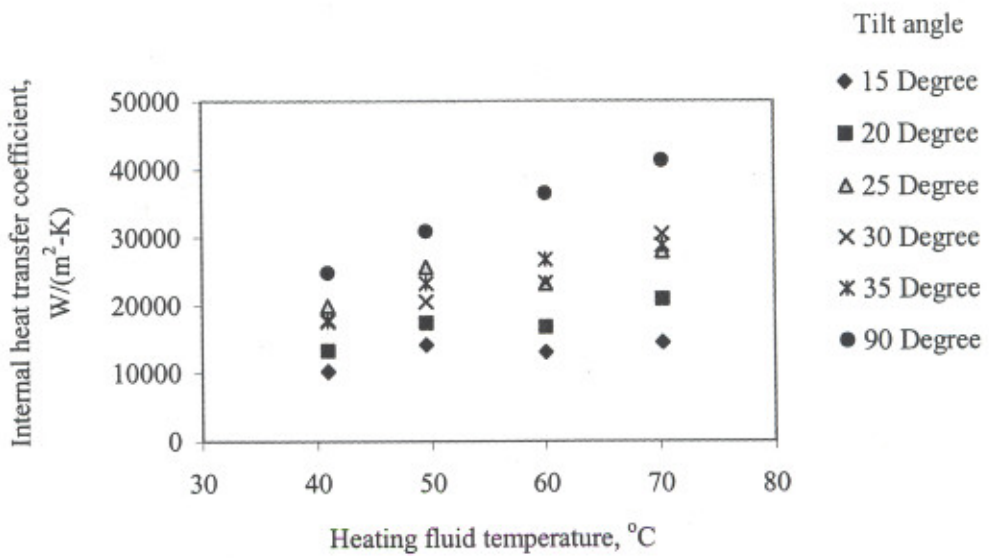

Figure 5.3: Effect of heating fluid temperature on the internal heat transfer coefficient of the heat pipe

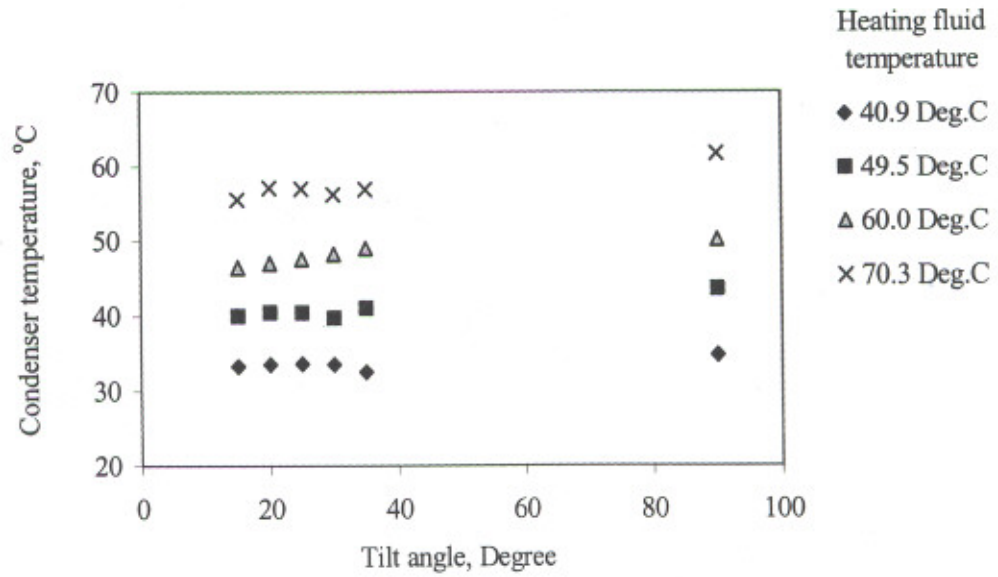

Figure 5.4: Effect of heating fluid temperature on the condenser temperature of the heat pipe

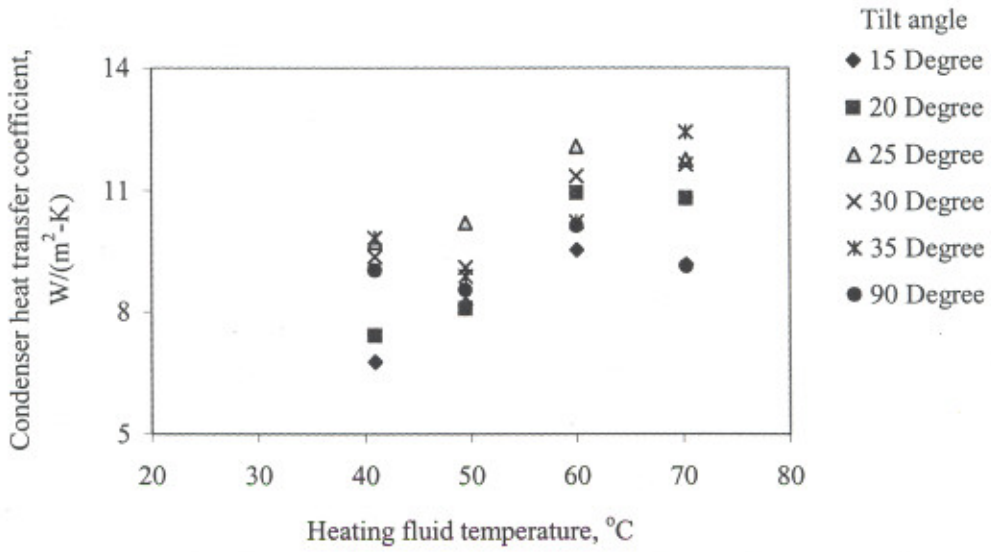

Figure 5.5: Effect of heating fluid temperature on the condenser heat transfer coefficient of the heat pipe

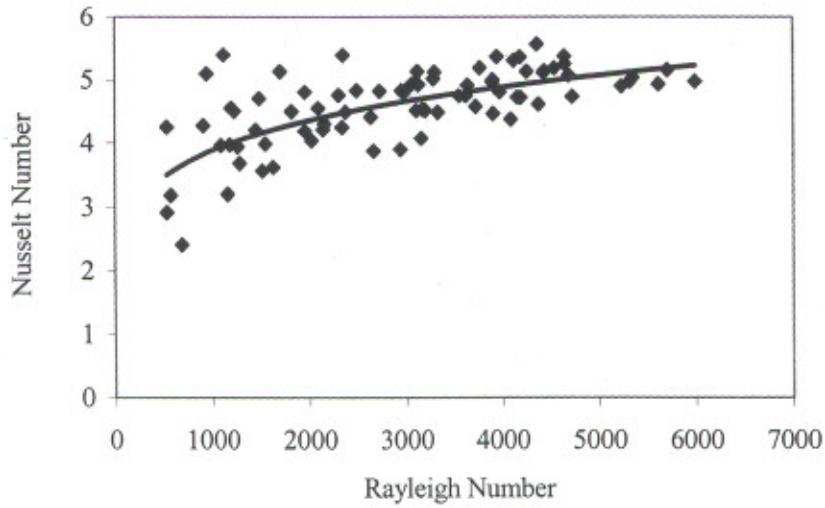

Figure 5.6: Effect of Rayleigh Number on Nusselt Number of the heat pipe at 25 Degree tilt angle

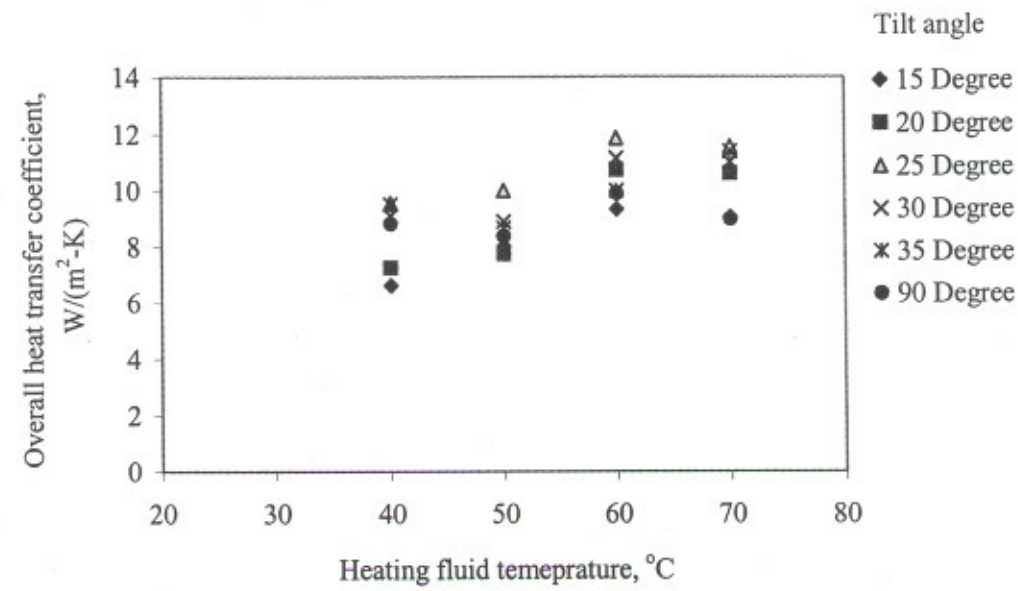

Figure 5.7: Effect of heating fluid temperature on the overall heat transfer coefficient of the heat pipe

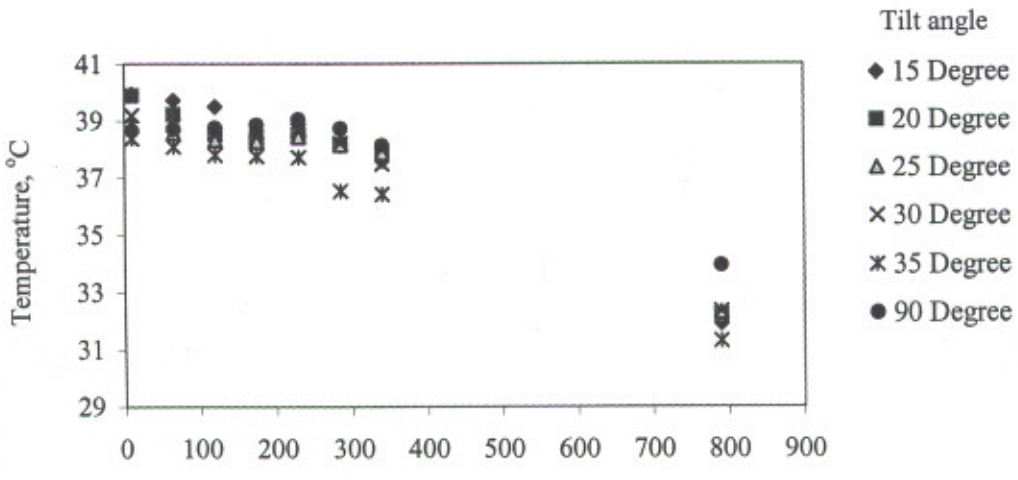

Figure 5.8: External surface temperature of the heat pipe at 40.9 °C heating fluid temperature

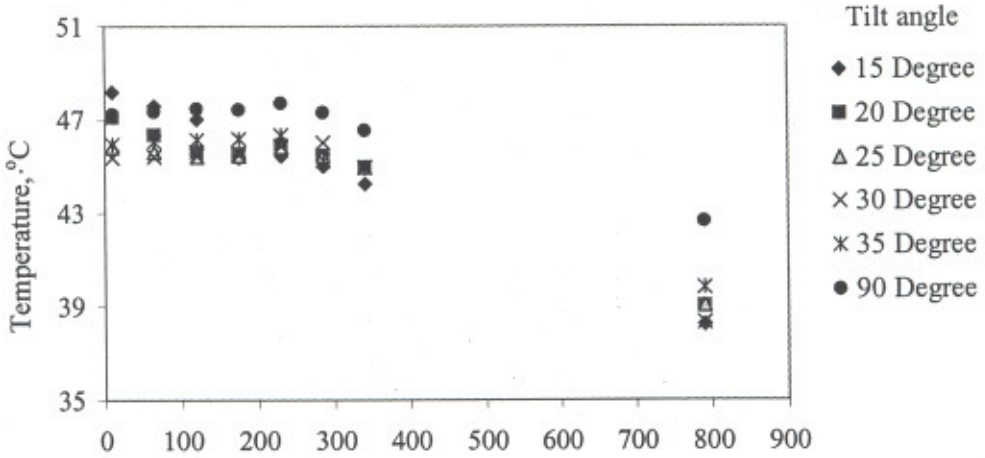

Figure 5.9: External surface temperature of the heat pipe at 49.5 °C heating fluid temperature

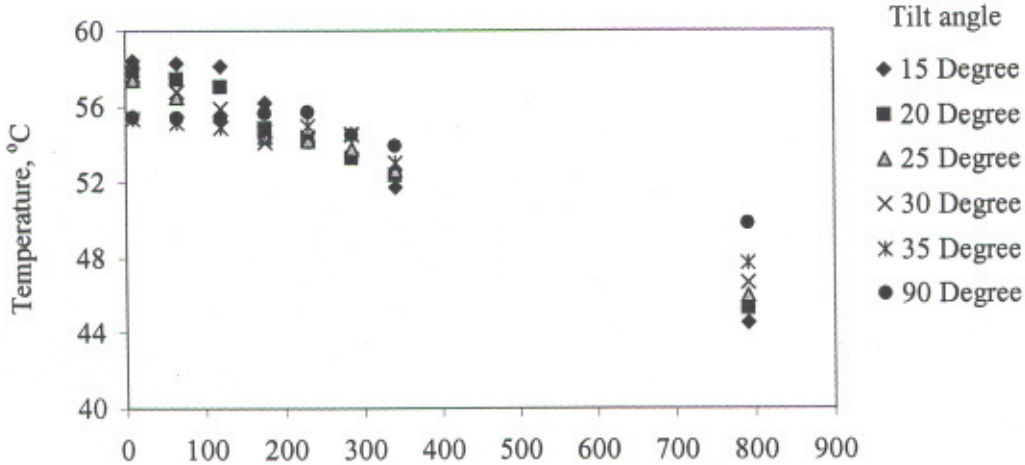

Figure 5.10: External surface temperature of the heat pipe at 60 °C heating fluid temperature

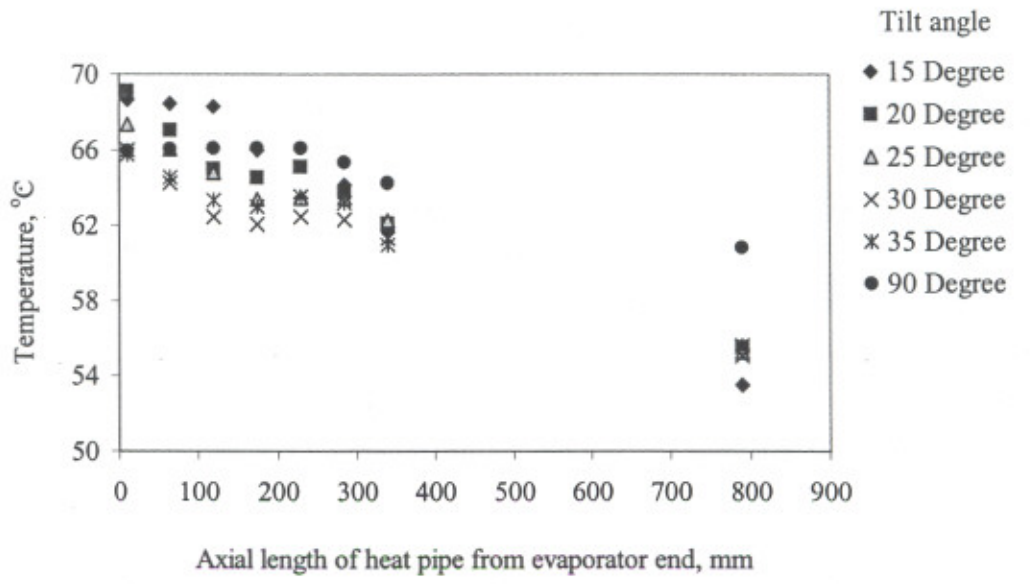

Figure 5.11: External surface temperature of the heat pipe at 70.3 °C heating fluid temperature

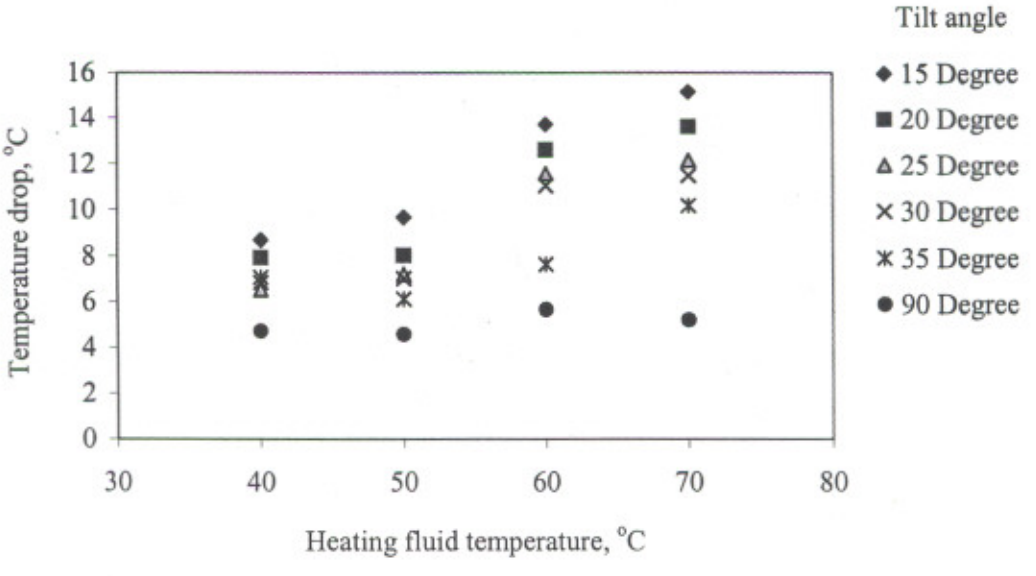

Figure 5.12: Effect of heating fluid temperature on temperature drop across evaporator and condenser end of the heat pipe

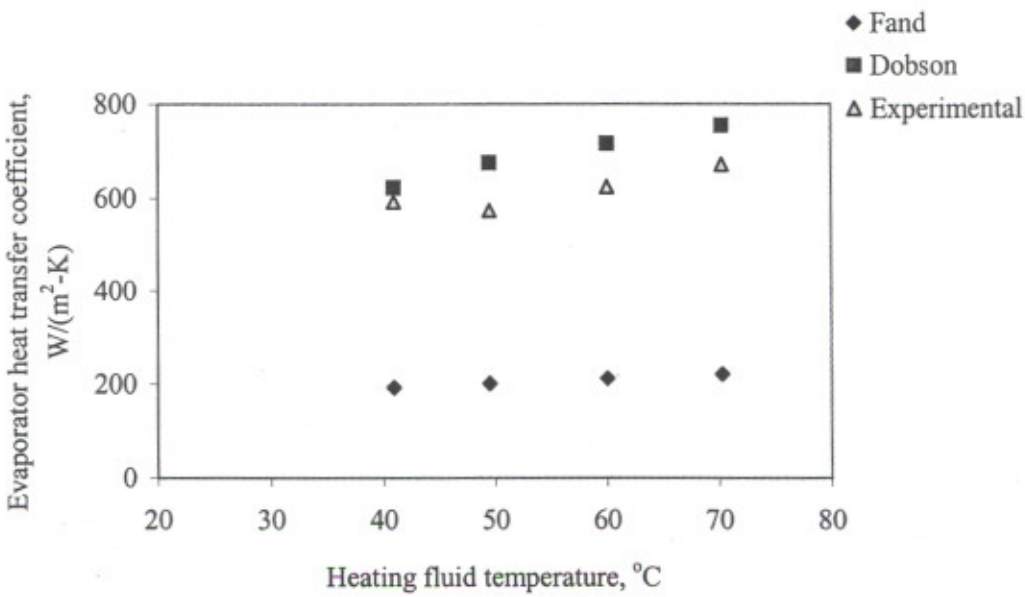

Figure 5.13: A comparison of the evaporator heat transfer coefficient obtained by the analytical model and experimental method

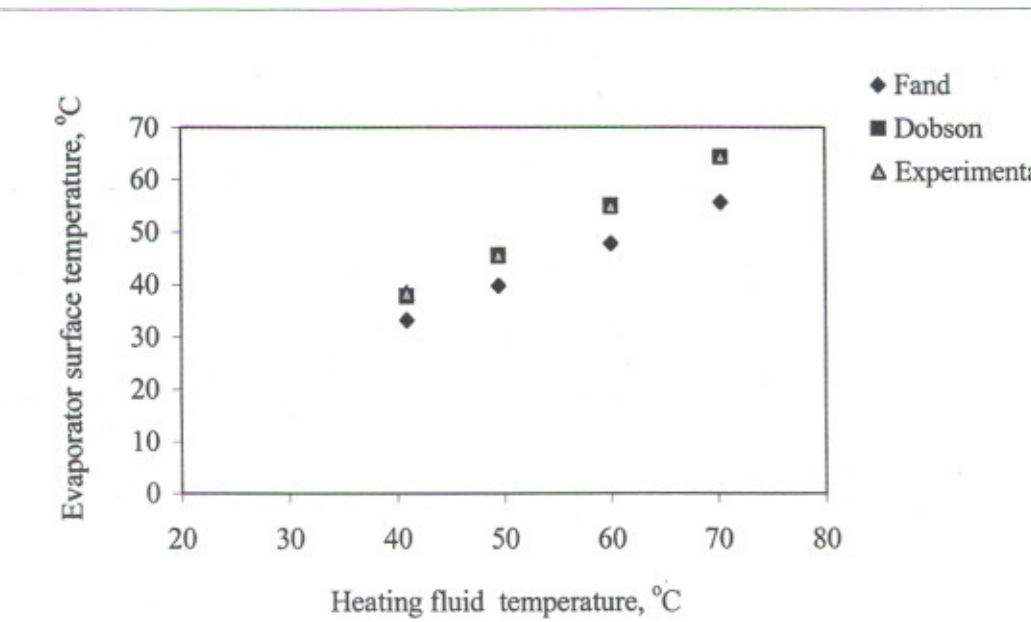

Figure 5.14: A comparison of the evaporator surface temperature predicted by the analytical model and measured experimentally

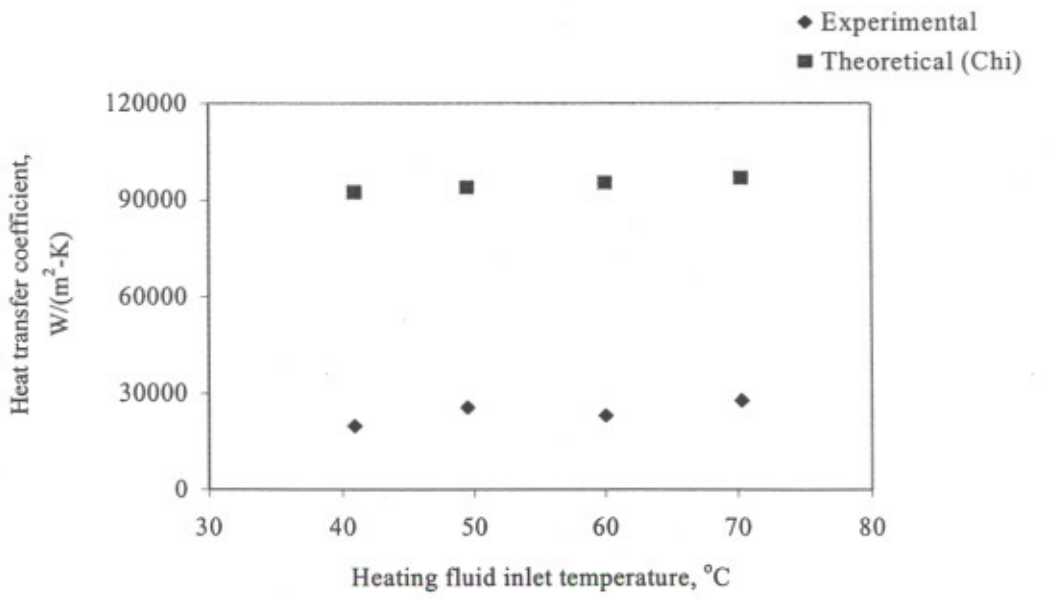

Figure 5.15: A comparison of the internal heat transfer coefficient obtained by analytical model and experimental method

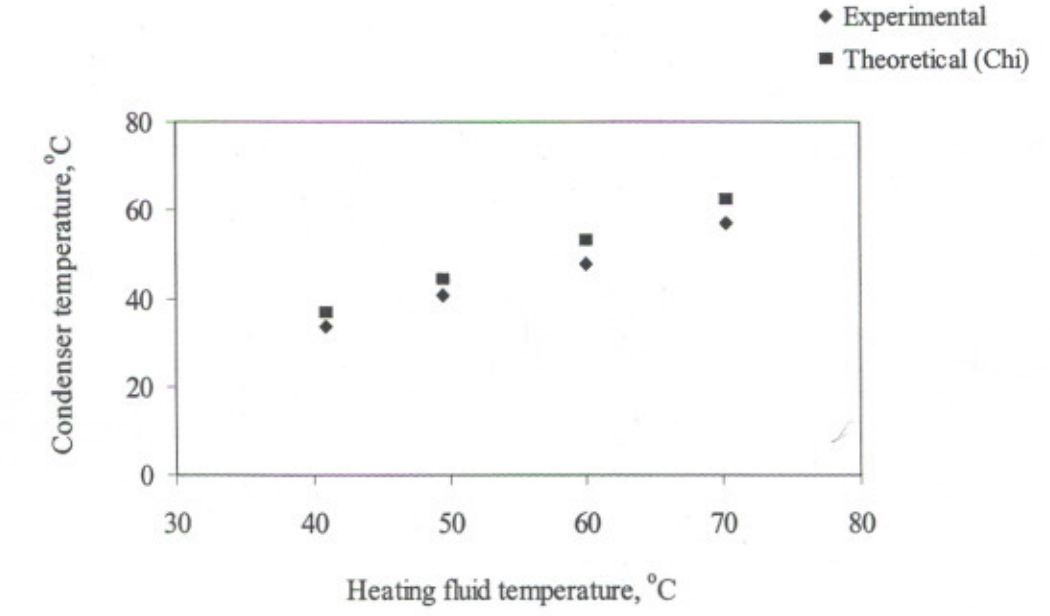

Figure 5.16: A comparison of the condenser temperature computed by the analytical model and measured experimentally

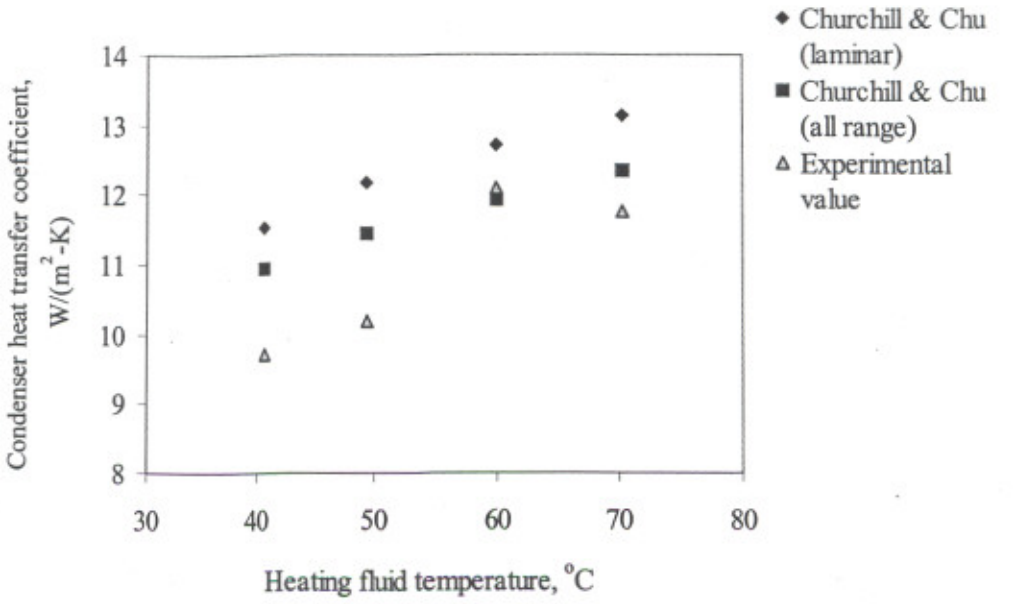

Figure 5.17: A comparison of the condenser heat transfer coefficient obtained by the analytical model and experimental method

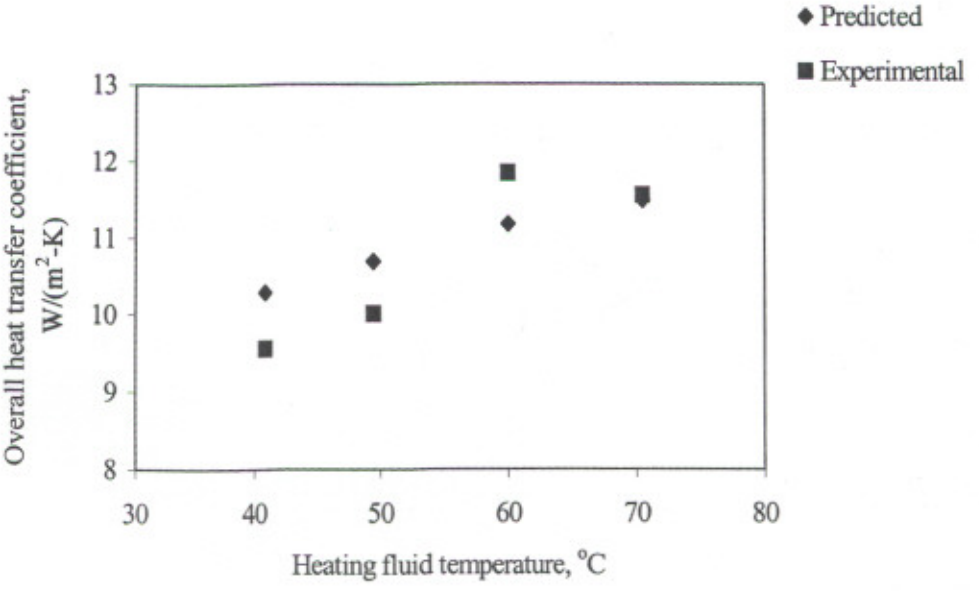

Figure 5.18: A comparison of the overall heat transfer coefficient obtained by the analytical model and experimental method

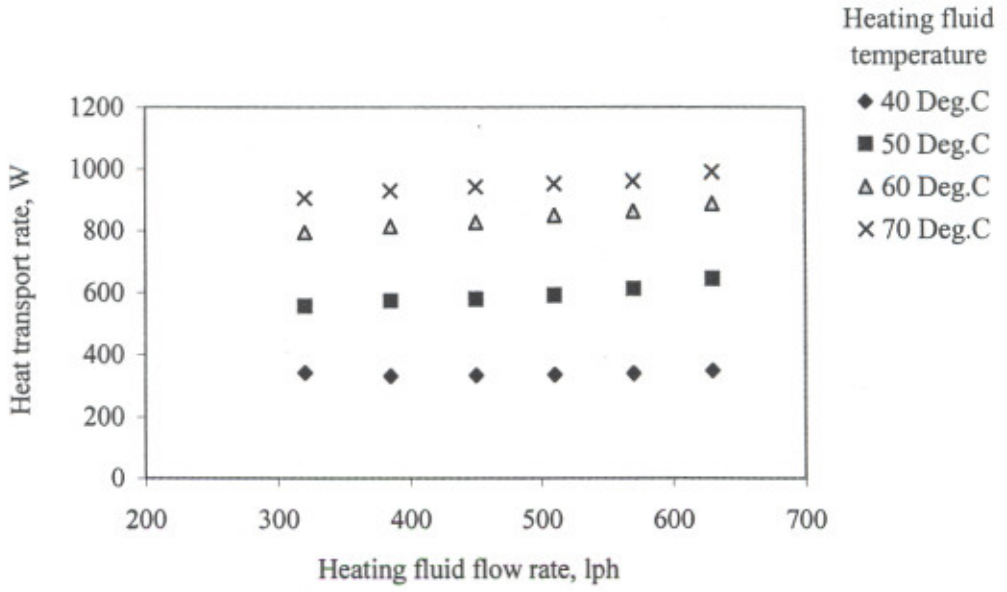

Figure 5.19: Effect of heating fluid flow rate on the heat transport rate of the HPHE at 15 Degree tilt angle

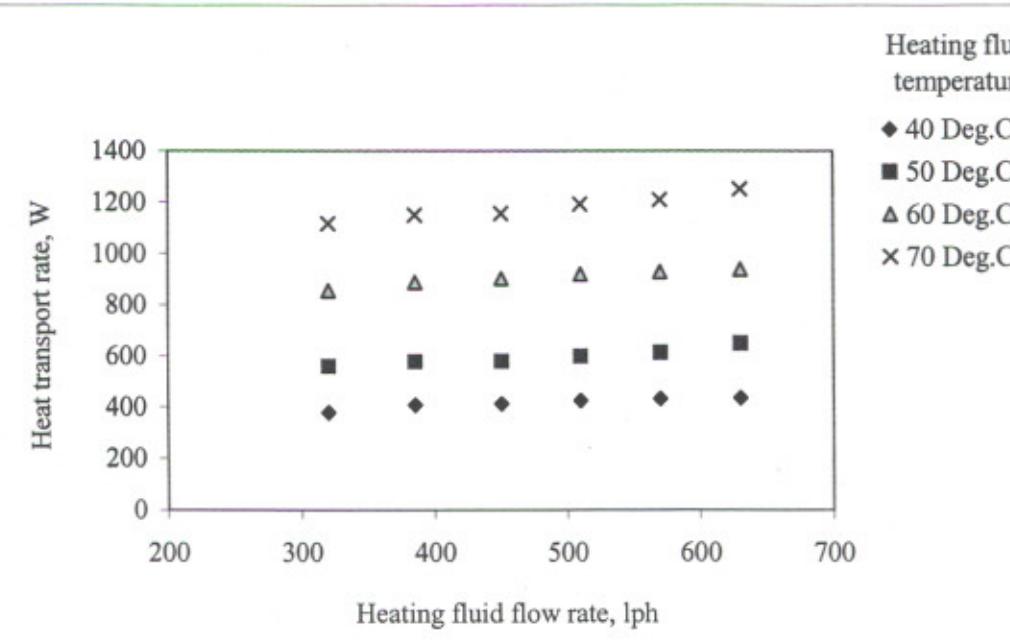

Figure 5.20: Effect of heating fluid flow rate on the heat transport rate of the HPHE at 20 Degree tilt angle

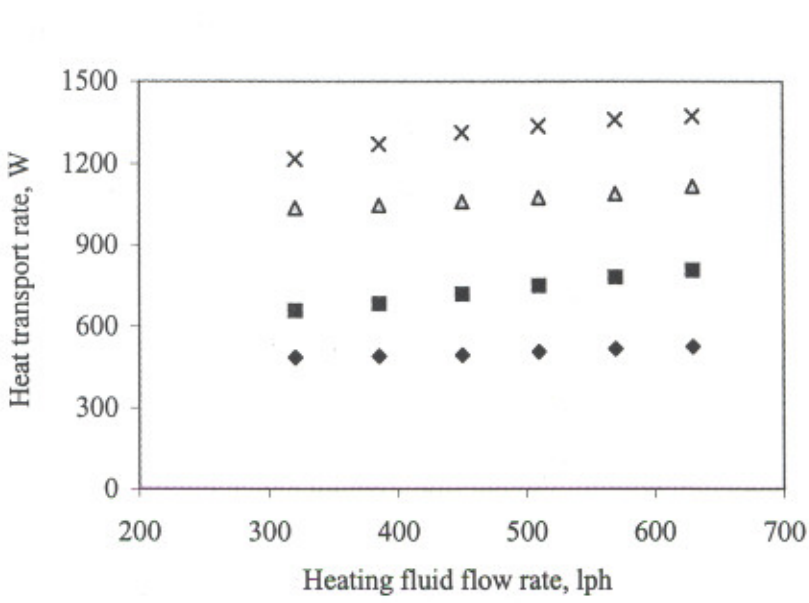

Figure 5.21: Effect of heating fluid flow rate on the heat transport rate of the HPHE at 25 Degree tilt angle

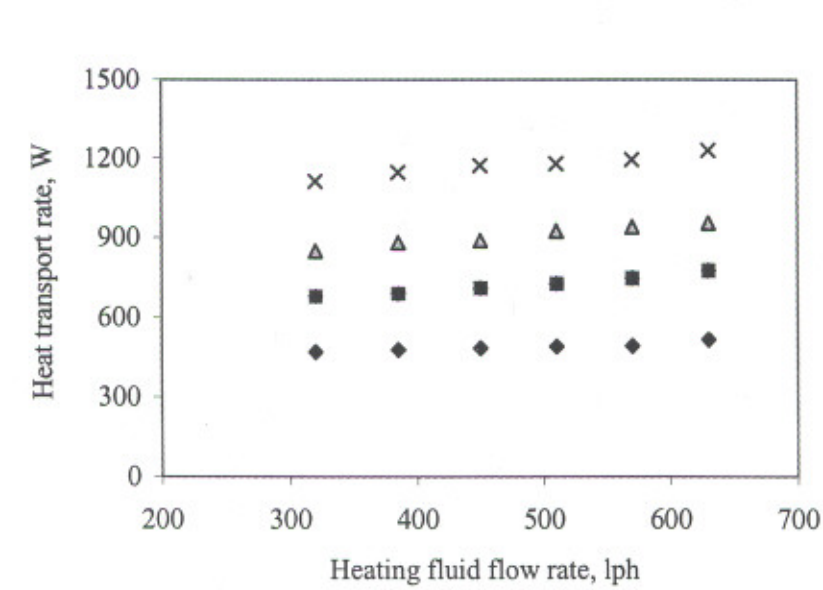

Figure 5.22: Effect of heating fluid flow rate on the heat transport rate of the HPHE at 30 Degree tilt angle

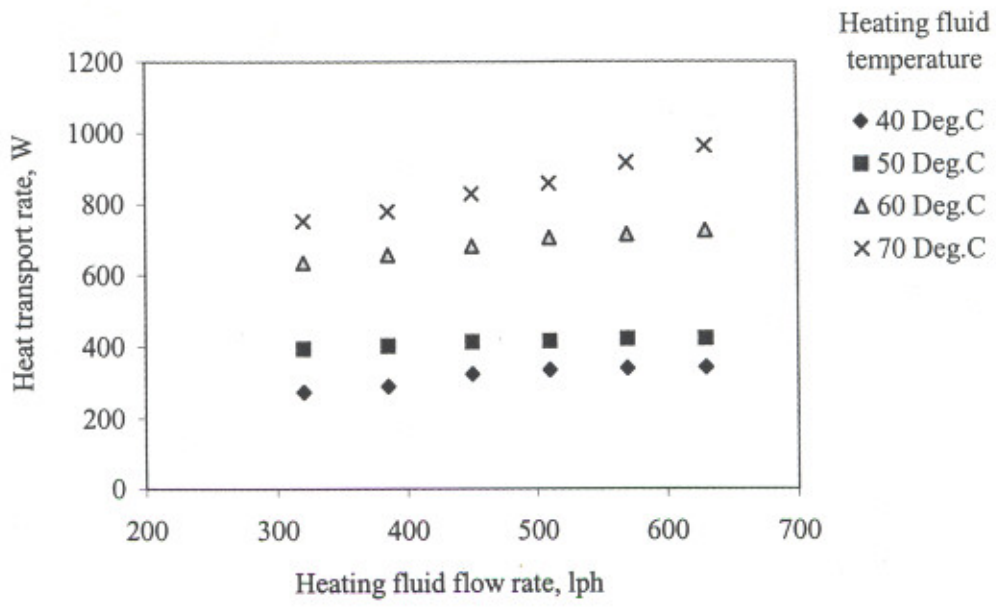

Figure 5.23: Effect of heating fluid flow rate on the heat transport rate of the HPHE at 90 Degree tilt angle

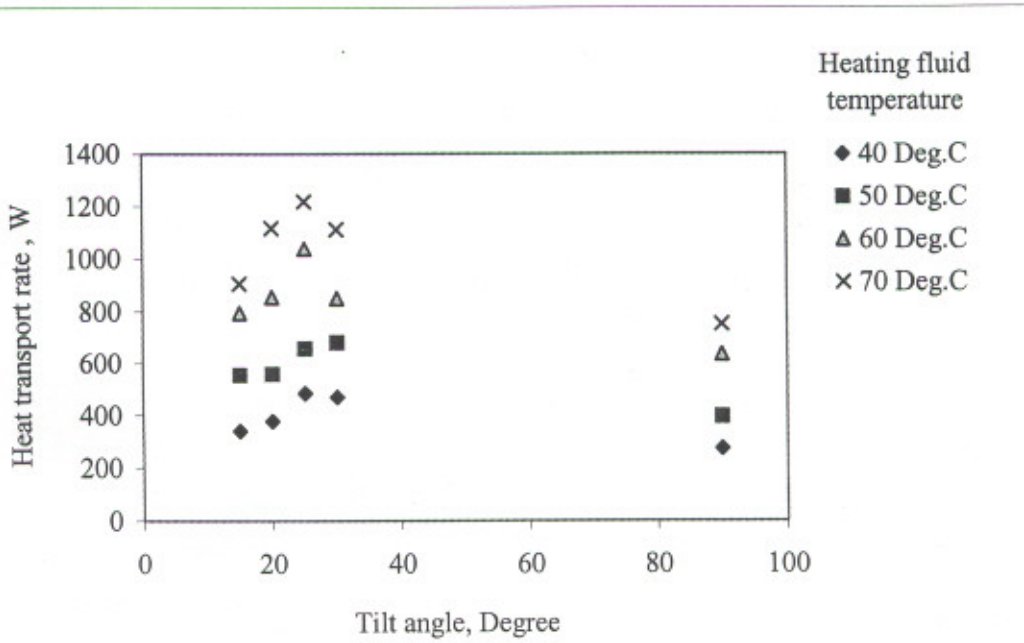

Figure 5.24: Effect of tilt angle on the heat transport rate of the HPHE at a flow rate of 320 lph

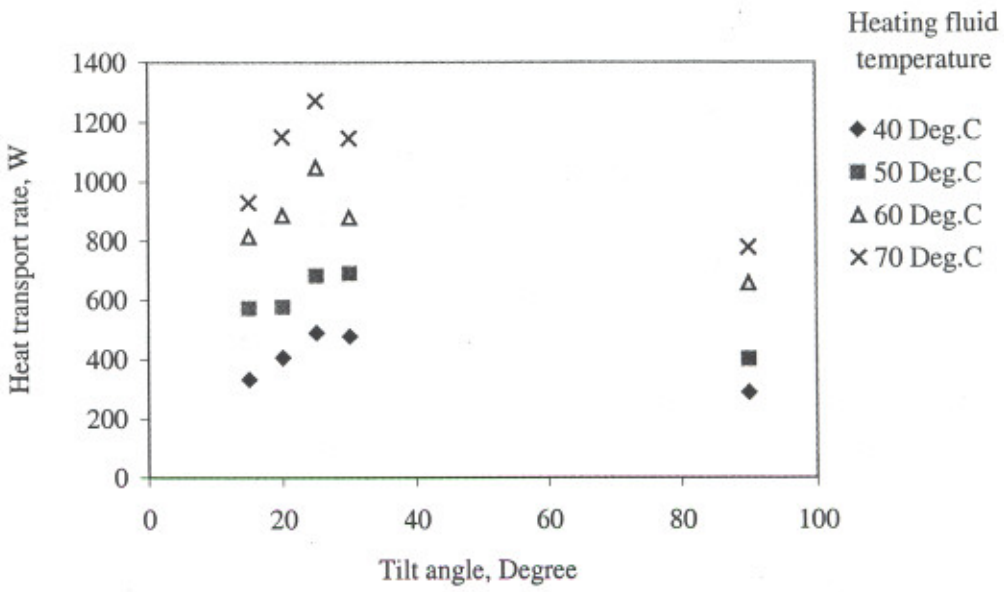

Figure 5.25: Effect of tilt angle on the heat transport rate of the HPHE at a flow rate of 385 lph

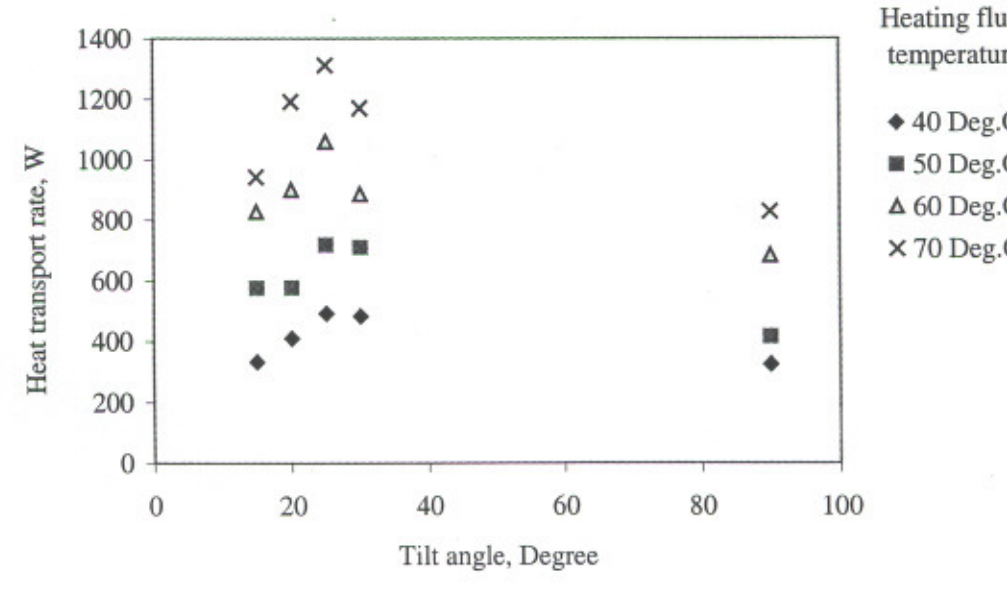

Figure 5.26: Effect of tilt angle on the heat transport rate of the HPHE at a flow rate of 450 lph

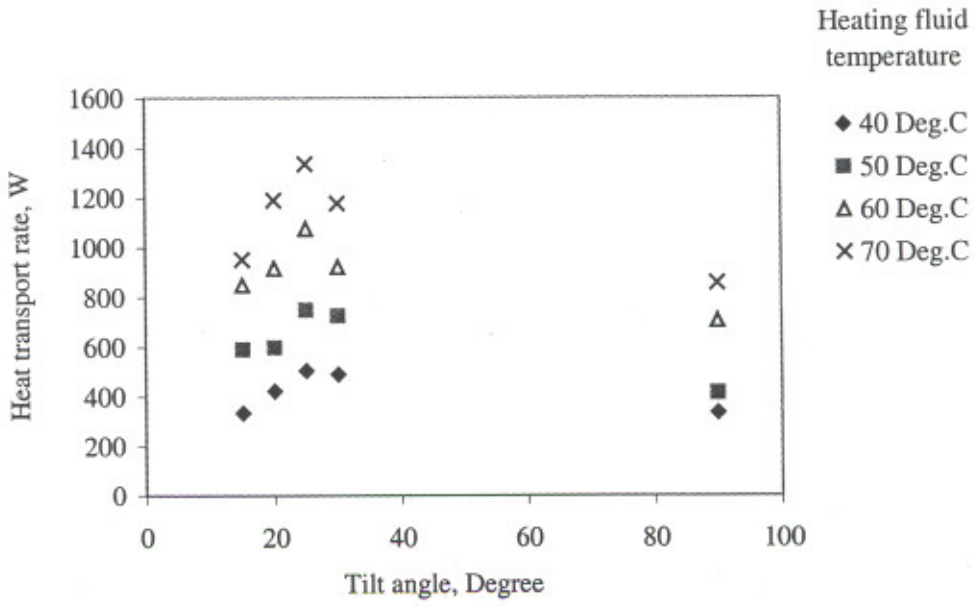

Figure 5.27: Effect of tilt angle on the heat transport rate of the HPHE at a flow rate of 510 lph

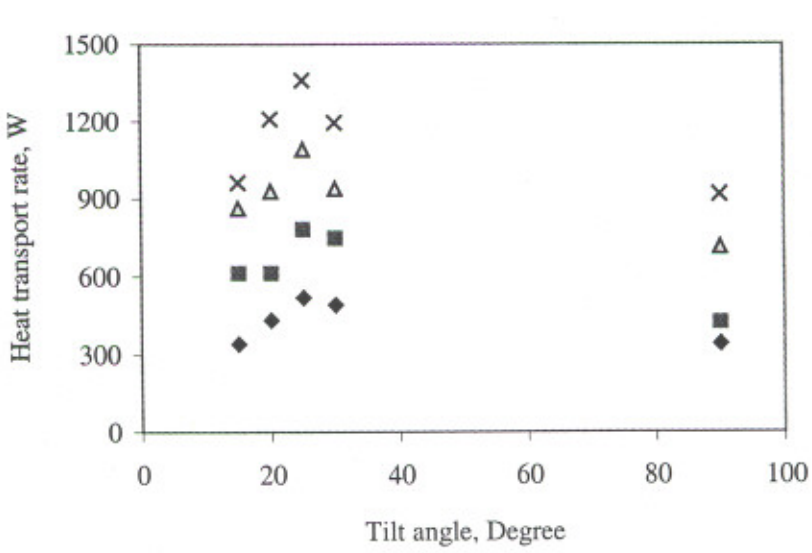

Figure 5.28: Effect of tilt angle on the heat transport rate of the HPHE at a flow rate of 570 lph

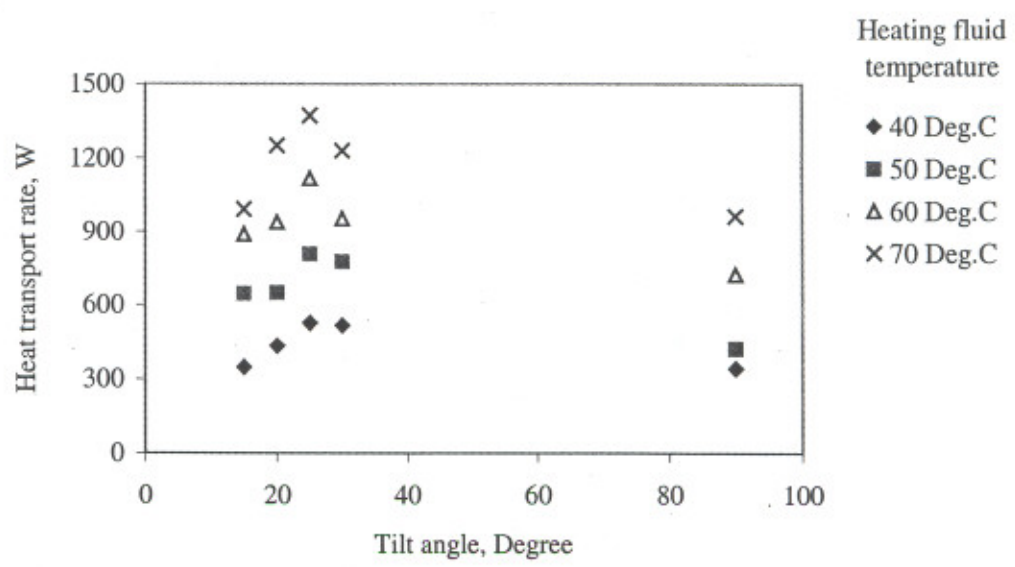

Figure 5.29: Effect of tilt angle on the heat transport rate of the HPHE at a flow rate of 630 lph

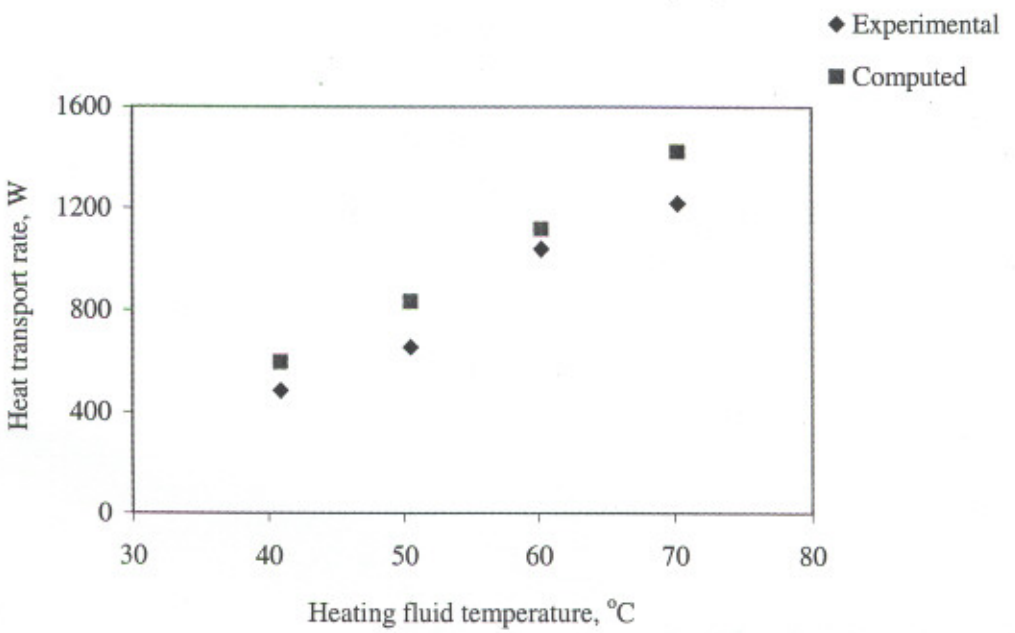

Figure 5.30: A comparison between computed and experimental heat transport rate of the HPHE at 320 lph

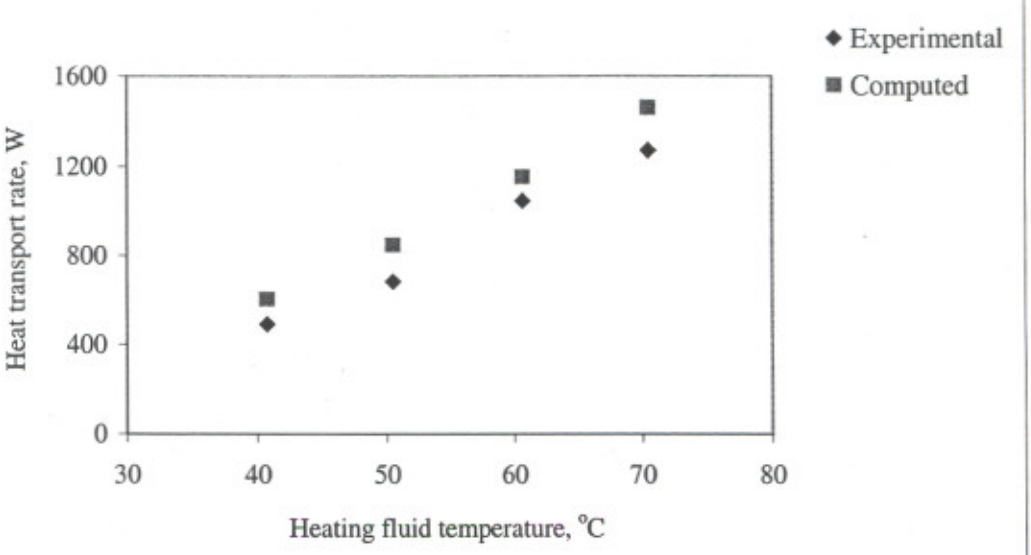

Figure 5.31: A comparison between computed and experimental heat transport rate of the HPHE at 385 lph

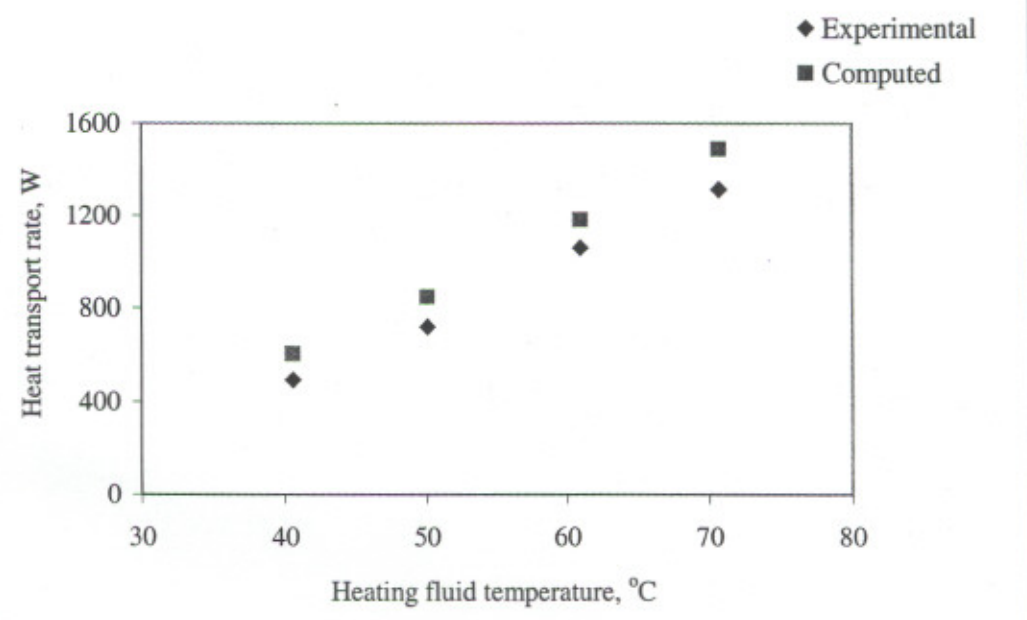

Figure 5.32: A comparison between computed and experimental heat transport rate of the HPHE at 450 lph

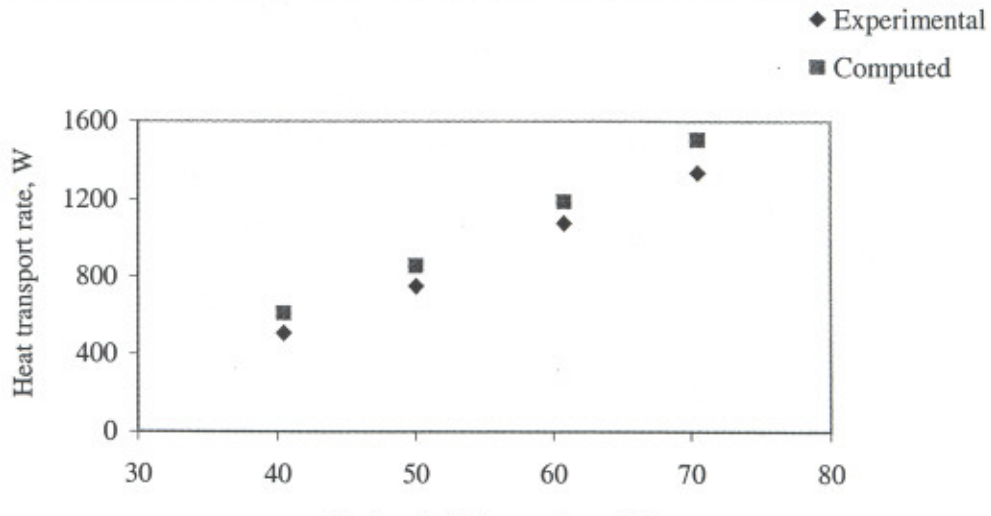

Figure 5.33: A comparison between computed and experimental heat transport rate of the HPHE at 510 lph

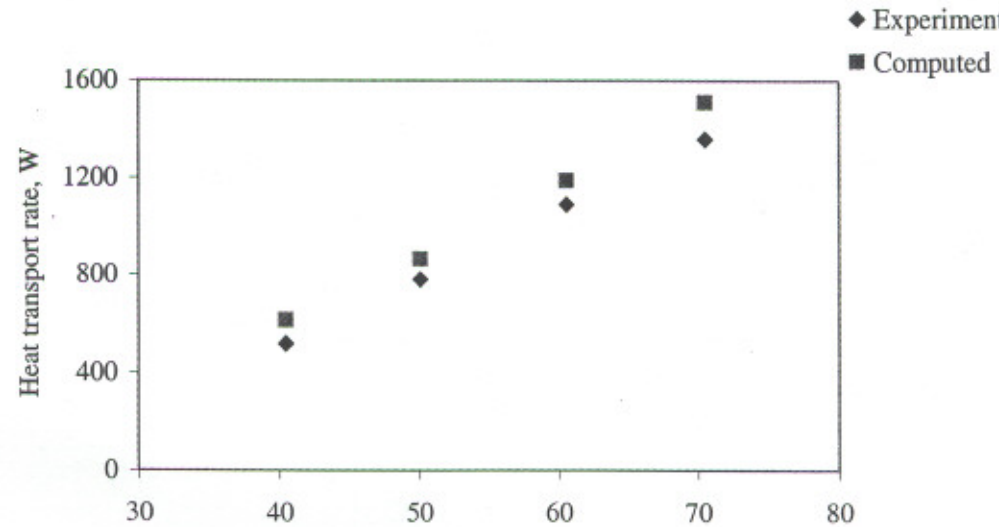

Figure 5.34: A comparison between computed and experimental heat transport rate of the HPHE at 570 lph

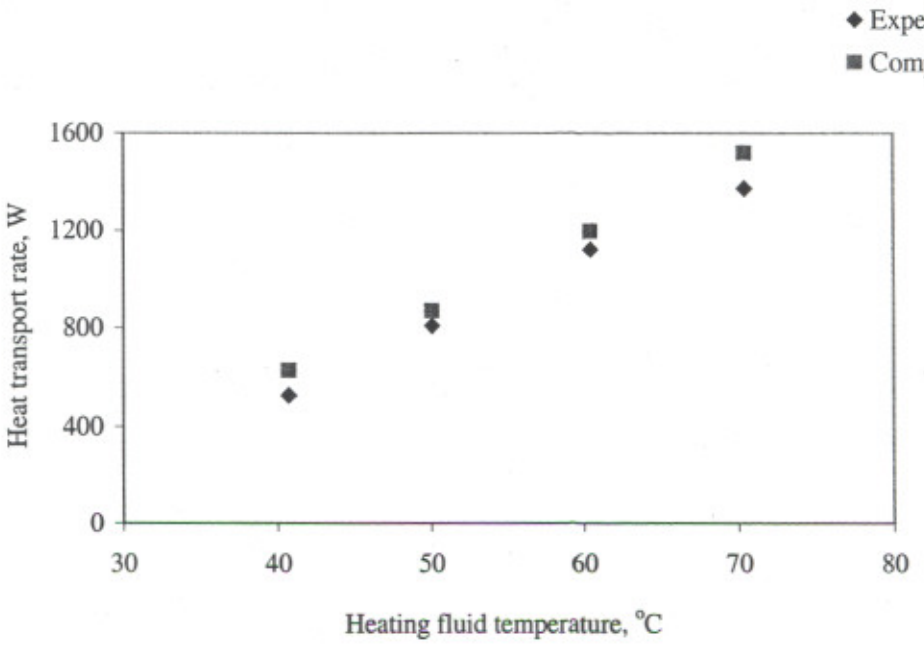

Figure 5.35: A comparison between computed and experimental heat transport rate of the HPHE at 630 lph

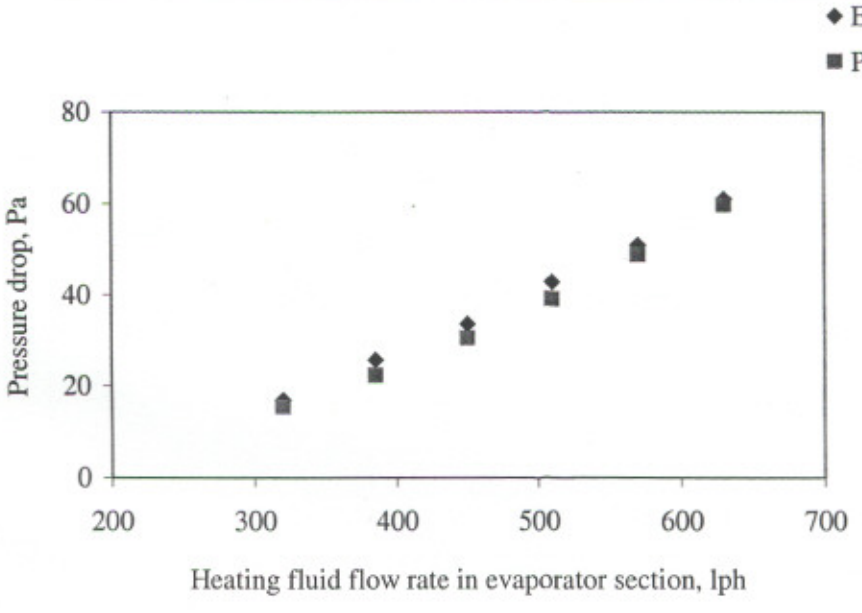

Figure 5.36: Effect of heating fluid flow rate on pressure drop in the evaporator section of the HPHE

CHAPTER 6

CONCLUSIONS

An analytical model has been developed to evaluate thermal performance of the heat pipe as well as for the HPHE under natural convection cooling conditions. The model evaluates the rate of heat transport of a single heat pipe as well as for the HPHE. In addition, it calculates the pressure drop across the evaporator of the HPHE. Experimental studies have been carried out to characterize the heat pipe and the HPHE. Some typical experimental results, obtained at 25° tilt angle for the heat pipe and the HPHE, have been compared with the results predicted by the analytical model for validating the model. The significant observations and conclusions obtained from the present investigation are summarized in the following paragraphs.

For a single heat pipe it is found that:

1. Tilt angle and heating fluid temperature influence the heat transport rate of the heat pipe under natural convection conditions. The maximum and minimum temperature drops between evaporator and condenser end of the heat pipe have been observed at 70.3 °C and 40.9 °C heating fluid temperature, respectively, at a constant tilt angle. At varying tilt angles, the maximum temperature drop between evaporator and condenser end of the heat pipe has been observed at 15° and that of minimum at 90° tilt angle. At 70.3 °C heating fluid temperature, the maximum heat transport rate is obtained at a tilt angle of 25°, which may be due to the lowest overall thermal resistance and the minimum heat transport rate at 15° due to the highest overall thermal resistance.

2. For tilt angles varying from 15° to 25°, the overall heat transfer coefficient of the heat pipe increases as the heating fluid temperature at the inlet of evaporator section increases from 40 °C to 60 °C. The rate of increase in heat transport decreases beyond 60 °C. The maximum overall heat transfer coefficient of the heat pipe is obtained at a heating fluid temperature of 60 °C and 25° tilt angle.

3. The evaporator heat transfer coefficient predicted by Fand's correlation [20] is approximately 3 times less as compared to the experimental value. The evaporator heat transfer coefficient predicted by Dobson & Kröger's correlation [21] has close agreement (within 15 %) with the experimental value, therefore, the predicted evaporator surface temperature is in good agreement (within 1 °C) with experimental value.

4. The internal heat transfer coefficient of the heat pipe predicted by the methodology provided by Chi [3] is 3.5 to 4.6 times more as compared to the experimental value, therefore, the predicted condenser temperature of the external surface differs from the experimental value in the range of 3.1 °C to 5.6 °C.

5. The heat transfer coefficient on the condenser side predicted by Churchill and Chu's correlation for all range of Rayleigh numbers [28] is close to the experimental value (within - 1 % to 12 %).

6. The overall heat transfer coefficient of a single heat pipe predicted by the analytical model is also in good agreement with the experimental value and the variation lies in the range of 1 % to 8 %, even though, there is a large deviation in theoretically computed value of internal heat transfer coefficient. In fact, the condenser heat transfer coefficient is the lowest and it influences the overall heat transfer coefficient decisively, whose prediction is close to the experimental value.

For the HPHE the conclusions are as under:

1. As the flow rate of the heating fluid increases at the inlet of evaporator section, the heat transport rate of the HPHE increases marginally, which is due to fact that the condenser side heat transfer coefficient does not increase significantly. At constant flow rate of the heating fluid, the heat transport rate of the HPHE increases as the heating fluid temperature increases from 40 °C to 70 °C.

2. The heat transport rate of the HPHE increases as the tilt angle increases from 15° to 25°, and it starts decreasing beyond 25°. The best thermal performance of the HPHE has been obtained at 25° tilt angle. The minimum heat transport rate has been obtained at 90°.

3. The heat transport rate of the HPHE predicted by the analytical model is 7 % to 27 % more than the value of the heat transport rate obtained experimentally at different heating fluid temperatures varying from 40 °C to 70 °C. The higher heat transport rate prediction is due to computation of higher condenser temperature, which results in more temperature drop between the condenser and ambient. The deviation between the experimental and the analytical result is less as the heating fluid temperature exceeds 60 °C.

4. The pressure drop across tube bundle is small in magnitude. The predicted pressure drop across inlet and outlet of evaporator section and the experimental value varied within the range of 2 % to 13 %.

5. The analytical model and the experimental results show reasonably good agreement, therefore, the model can be used to predict the heat transport rate of the HPHE under natural convection conditions.

CHAPTER 7

SUGGESTIONS FOR FUTURE STUDIES

The followings are the suggested work for future:

1. The study can be carried out using different heating fluids in the evaporator section of the HPHE, such as transformer oil and industrial fluids, so that such system can be employed for cooling of oil cooled electrical transformers and other industrial equipments.

2. The study can be conducted to improve the thermal performance of the heat pipe by reducing thermal contact resistance between fin and tube under natural convective condition. The study can be focused on the effects of interstitial materials and coatings at the interface of tube and fin on heat transfer.

Table A-2: Properties of water at a temperature of 373 K

Sl. No.	Description	Unit	Value
1.	Surface tension of water, σ	N/m	5.84×10^{-2}
2.	Liquid thermal conductivity, k_l	W/(m-k)	0.68
3.	Heat of vaporization, λ	J/kg	2254×10^{3}
4.	Liquid density, ρ_l	kg/m^3	961
5.	Vapour density, ρ_v	kg/m^3	0.58
6.	Liquid viscosity, μ_l	kg/(m-s)	2.82×10^{-4}
7.	Vapour viscosity, μ_v	kg/(m-s)	1.28×10^{-5}

A.1.1 Capillary Heat Transport Limit

Capillary radius $= \frac{1}{2N} = \frac{1}{2 \times 4937} = 1.0127 \times 10^{-4}$ m

Maximum capillary pumping pressure, $P_{cm} = 2 \times \frac{\sigma}{r_c} = \frac{\left(2 \times 5.84 \times 10^{-2}\right)}{1.0127 \times 10^{-4}} = 1153$ Pa

Vapour dia, $d_v = d_i - (8 \times 8.5 \times 10^{-5}) = 22.00 \times 10^{-3} - 6.8 \times 10^{-4} = 2.132 \times 10^{-2}$ m

Angle of inclination, $\psi = -25^{\circ} = -0.436$ Radian (from the horizontal)

Normal hydrostatic pressure, $\Delta P_{\perp} = \rho_l g d_v \cos\psi$

$\Delta P_{\perp} = 961 \times 9.81 \times 2.132 \times 10^{-2}$ x cos (-0.436) = 182 Pa

Axial hydrostatic pressure, $\rho_l g L_t \sin(-0.436) = -3185$ Pa

Maximum effective pumping pressure, $P_{pm} = P_{cm} - \Delta P_{\perp} - \rho_l g L_t \sin\psi$

$= 1153 - 182 + 3185 = 4156$ Pa

Wick cross section area, $A_w = \left(\frac{\Pi}{4}\right) \times (d_i^2 - d_v^2)$

$$= \left(\frac{3.14}{4}\right) \times ((22.0 \times 10^{-3})^2 - (21.32 \times 10^{-3})^2)$$

$$= 2.31359 \times 10^{-5} \text{ m}^2$$

Wick crimping factor, S = 1.05

Porosity, $\varepsilon_o = 1 - \left(\frac{\pi SNd}{4}\right) = 1 - (0.7853 \times 1.05 \times 4937 \times 8.5 \text{ x } 10^{-5}) = 0.6539$

Wick permeability, $K = \frac{d^2 \times \varepsilon_o^{\ 3}}{(122 \times (1 - \varepsilon_o)^2)} = (8.5 \times 10^{-5})^2 \times \frac{0.6539^3}{(122 \times (1 - 0.6539)^2)}$

$= 1.3823 \times 10^{-10} \text{ m}^2$

Liquid frictional coefficient, $F_l = \frac{\mu_l}{(K A_w \rho_l \lambda)}$

$$= \frac{2.82 \times 10^{-4}}{(1.3823 \times 10^{-10} \times 2.31359 \times 10^{-5} \times 961 \times 2254 \times 10^3)} = 40.70 \text{ Pa/(W-m)}$$

Vapor cross sectional area, $A_v = \frac{\Pi}{4} \times (d_v^2) = \frac{\Pi}{4} \times (2.132 \times 10^{-2})^2 = 3.569 \times 10^{-4} \text{ m}^2$

Vapour frictional coefficient, $F_v = \frac{(f_v Re_v) \mu_v}{2 \times A_v r_{h,v}^2 \rho_v \lambda}$

Vapor core hydraulic radius, $r_{h,v} = 1.066 \times 10^{-2}$ m

Drag coefficient, $(f_v Re_v) = 16$

$$F_v = \frac{(16 \times 1.28 \times 10^{-5})}{(2 \times 3.569 \times 10^{-4} \times (1.066 \times 10^{-2})^2 \times 0.58 \times 2254 \times 10^3)} = 1.93 \times 10^{-3} \text{ Pa/(W-m)}$$

Capillary heat transport factor, $(QL)_{c,max} = \frac{P_{pm}}{(F_l + F_v)} = \frac{4156}{(40.70 + 1.93 \times 10^{-3})} = 102.1$ W-m

Capillary heat transport limit, $Q_{c,max} = \dfrac{(QL)_{c,max}}{(0.5L_c + L_a + 0.5L_e)}$

$L_e = 0.33$ m

$L_a = 0.07$ m

$L_c = 0.40$ m

$$Q_{c,max} = \frac{102.1}{(0.5\times0.33+0.07+0.5\times0.39)} = \frac{102.1}{0.43} = 237.4 \text{ W}$$

A.1.2 Sonic Limit

Sonic limit, $Q_{s,max} = A_v \rho_v \lambda \left(\dfrac{\gamma_v R_v T}{2(\gamma_v + 1)} \right)^{1/2}$

Vapour molecular weight, M = 18 g/mol

Vapour specific heat ratio = 1.33

Universal gas constant, $R = 8.314\times10^3$ J/(kg-mol-K)

Vapour constant, $R_v = \dfrac{8.314\times10^3}{18} = 462$ J/kg-K

$$Q_{s,max} = \frac{3.569\times10^{-4}\times0.58\times2254\times10^3\times(1.33\times462\times373.15)^{1/2}}{(2(1.33+1))^{1/2}} = 1.03\times10^5 \text{ W}$$

A.1.3 Entrainment Limit

Wick surface pore hydraulic radius, $r_{h,s}$

$$= \frac{1}{2N} - \frac{d}{2} = 1.0127\times10^{-4} - 4.25\times10^{-5} = 5.877\times10^{-5} \text{ m}$$

$$Q_{e,max} = A_v \lambda \left(\frac{\sigma \rho_v}{2r_{h,s}} \right)^{1/2}$$

$$= \frac{3.569\times10^{-4}\times2254\times10^3\times(5.84\times10^{-2}\times0.58)^{1/2}}{(2\times5.877\times10^{-5})^{1/2}} = 1.36\times10^4 \text{ W}$$

A.1.4 Boiling Limit

$$Q_{b,max} = \left(\frac{2\pi L_e k_{e,e} T_v}{\lambda \rho_v \ln(r_i/r_v)}\right)\left(\frac{2\sigma}{r_n}\right)$$

Effective thermal conductivity of the liquid-saturated wick, $k_{e,e}$

$$k_{e,e} = \frac{k_l[k_l + k_w - (1-\varepsilon_o)(k_l - k_w)]}{[k_l + k_w + (1-\varepsilon_o)(k_l - k_w)]}$$

Liquid thermal conductivity, $k_l = 0.68$ W/(m-K)

Thermal conductivity of Bronze, $k_w = 52$ W/(m-K)

ε_o = porosity of screen wick

$$k_{e,e} = \frac{0.68 \times [0.68 + 52 - (1-0.6539) \times (0.68 - 52)]}{[0.68 + 52 + (1-0.6539) \times (0.68 - 52))]} = 1.36 \text{ W/(m-K)}$$

Nucleation radius, $r_n = 2.54 \times 10^{-7}$ m

$$\text{Critical pressure} = 2\sigma / r_n = \frac{2 \times 5.84 \times 10^{-2}}{2.54 \times 10^{-7}} = 4.59 \times 10^5 \text{ Pa}$$

$L_e = 0.33$ m

$$Q_{b,max} = \frac{2 \times \Pi \times 0.33 \times 1.36 \times 373.15 \times 4.59 \times 10^5}{2254 \times 10^3 \times 0.58 \times (\ln(0.011/0.01066))} = 1.17 \times 10^4 \text{ W}$$

A.1.5 Viscous Limit

Vapor pressure, $P_v = 1{,}01{,}350$ Pa

$$\text{Viscous limit, } Q_{v,max} = (d_v^2 \lambda A_v) \times \left(\frac{P_v \rho_v}{4 f_v Re_v L_e \mu_v}\right)$$

$$= ((2.132 \times 10^{-2})^2 \times 2254 \times 10^3 \times 3.569 \times 10^{-4}) \times \left(\frac{101350 \times 0.58}{4 \times 16 \times 0.33 \times 1.28 \times 10^{-5}}\right)$$

$$= 8.72 \times 10^7 \text{ W}$$

The heat transport limits of the heat pipe at different evaporator temperatures, as computed from programme at 0° & 25° tilt angle, are presented in Table A-3 and graphically it is shown in Figure A.1 at 25° tilt angle.

Table A-3: Heat transport limitations of the heat pipe at different temperatures

Sl. No.	Operating limit		Heat transport limit, W							
			30 °C	40 °C	50 °C	60 °C	70 °C	80 °C	90 °C	100 °C
1.	Capil-lary	0° tilt*	26.3	30.9	35.7	40.4	44.6	48.3	51.2	53.6
		25° tilt*	99.4	118.8	139.5	160.6	180.9	199.6	216.4	231.9
2.	Sonic		6.0E3	9.4E3	1.4E4	2.2E4	3.4E4	5.1E4	7.5E4	1.1E5
3.	Entrainment		4.0E3	4.8E3	5.9E3	7.1E3	8.6E3	1.0E4	1.2E4	1.4E4
4.	Boiling		1.7E6	1.1E5	7.5E4	5.0E4	3.4E4	2.3E4	1.6E4	1.1E4
5.	Viscous		6.5E6	9.6E6	1.4E7	2.0E7	3.0E7	4.3E7	6.0E7	8.3E7

(* From horizontal axis)

A.2 Working Fluid Inventory

Mass of working fluid = $A_v L_t \rho_v + A_w \varepsilon_o L_t \rho_l$

= $3.569 \times 10^{-4} \times 0.80 \times 0.58 + 2.31359 \times 10^{-5} \times 0.6539 \times 0.80 \times 961$

= 0.01179 kg = 11.8×10^{-3} kg

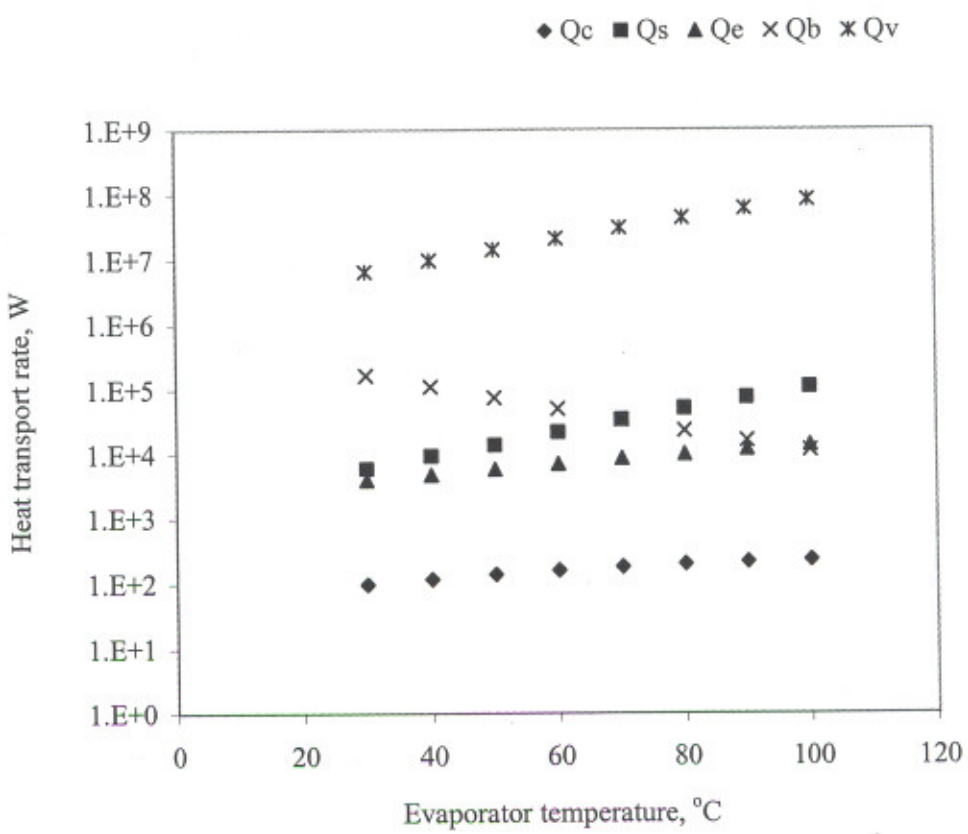

Figure A.1: Effect of evaporator temperature on different operating limits

APPENDIX - B-I

LIST OF EQUIPMENTS USED FOR HEAT PIPE EXPERIMENTS

Table B-1: Detail of instruments used for heat pipe's experimentation

Sl. No.	Instrument	Utility	Make	Specification
1.	Micrometer	To measure the thickness of wire diameter of wire screen	Mitutoyo, Japan	Least count: 0.01 mm Range: 0 mm to 25 mm
2.	Vernier caliper	To determine inner and outer diameter of copper pipe	Mitutoyo, Japan	Least count: 0.05 mm Range: 0 mm to 200 mm
3.	Image analyzer attached with Optiphot metallurgical microscope	To determine mesh number of wire screen Magnification of wire screen	Soft Imaging System Gmbh, Germany Nikon, Japan	Magnification: 1000X (up to 1000 times) X: Magnification
4.	Vacuum pumping system	For evacuation	Hind High Vacuum Company Pvt. Ltd., Bangalore, India	Capacity: 306 lpm Operating pressure Range: 10^{-3} to 10^{-6} mili bar
5.	Helium mass spectrometer	For leak detection	Hind High Vacuum Company Pvt. Ltd., Bangalore, India	Sensitivity: 6×10^{-11} (std) cc/sec Leakage range: $3x10^{-6}$ to 3×10^{-9} cc/sec
6.	Temperature data logger	For recording temperature data at different locations of heat pipe and hot fluid temperature.	Hewlett Packard, USA	Model – 34970 Data acquisition unit Accuracy: ± 0.03 %
7.	Dimmerstat	To vary the power input to electrical heater	Automatic Electric Ltd., Mumbai, India	Model: 15D-IP Range: Up to 4.05 kVA
8.	Rotameter	For flow measurement of hot water	Eureka Industrial Equipments Pvt. Ltd., Pune, India	Range: 20 to 200 lph
9.	Load manager	Power input measurement to electric heater	Elcontrol Energy s.p.a., Italy	Voltage: 200 - 240 V Current: 0 - 120 A

Sl. No.	Instrument/ sensor	Utility	Make	Specification
10.	Centrifugal pump	For circulating hot water	Stuart Turner Ltd, England	Lift : 6.0 m Power: 60 W Discharge: 500 lph
11.	Digital micro voltmeter	For heat flux measurement	Scientific Equipment, Roorkee, India	Model DMV – 001 Range: 1 μV to 10 V
12.	Thermocouple	For temperature measurement at different locations	RS component, UK	T-type, 219-4680 Accuracy: ± 1 °C or 0.0075*T
13.	Micro-foil heat flux sensor	Heat flux measurement	RdF corporation, USA	Model: 20455-3 Nominal Sensitivity: 6.30 μV/W/m^2

APPENDIX - B-II

LIST OF EQUIPMENTS USED FOR HPHE EXPERIMENTS

Table B-2: Detail of equipments used in experimental set-up of HPHE

Sl. No.	Equipment/ sensor	Utility	Make	Specification
1.	Temperature data logger	For recording temperature data at different locations of heat pipe and hot fluid temperature.	Hewlett Packard, USA	Model – 34970 Data acquisition unit accuracy: ± 0.05 %
2.	Dimmerstat	To vary the power input to electrical heater	Automatic Electric Ltd., Mumbai, India	Model: 15D-IP Range: Up to 4.05 kVA
3.	Digital micro voltmeter	For heat flux measurement	Scientific Equipment, Roorkee, India	Model DMV – 001 Range: 1 μV to 10 V
4.	Load manager	Power input measurement to electric heater	Elcontrol Energy s.p.a., Italy	Voltage: 200 - 240 V Current: 0 - 120 A
5.	Thermocouple	For temperature measurement at different locations	RS component, UK	T-type, 219-4680 Accuracy: ± 1 °C or 0.0075*T
6.	Micro-foil heat flux sensor	Heat flux measurement	RdF corporation, USA	Model: 20455-3 Nominal Sensitivity: 6.30 μV/W/m^2
7.	Rotameter	For flow measurement of hot water	Eureka Industrial Equipments Pvt. Ltd., Pune, India	Range: 200 to 2000 lph
8.	Centrifugal pump	For hot water circulation	Crompton Greaves Ltd., Mumbai, India	Lift : 6.0 m Discharge: 2400 lph Power: 0.37 kW

APPENDIX - B-III

SAMPLE CALCULATON FOR HEAT TRANSPORT RATE OF HPHE

A. Input Data

A.1 Experimentally measured values

1. Volumetric flow rate of water : 320±5.7 lph (8.9×10^{-5} m^3/s)
2. Temperature of hot water at evaporator inlet : 70.3±0.25 °C
3. Temperature of hot water at evaporator outlet : 66.4±0.18 °C
4. Average wooden box surface temperature : 33.0±0.3 °C
5. Average top plate surface temperature : 62.9±1.48 °C
6. Ambient temperature : 22±0.2 °C
7. Average heat transfer coefficient of wooden box surface (determined using heat flux sensor) : 8.6±0.25 W/(m^2-K)
8. Average heat transfer coefficient of top plate (determined using heat flux sensor) : 12.3±0.42 W/(m^2-K)

A.2 Theoretically calculated values

1. Specific heat of water : 4267 J/(kg-K)
2. Density of water at 68 °C : 979 kg/m^3
3. Wooden box surface area : 1.1 m^2
4. Top plate surface area : 0.22 m^2

B. Heat Transport Rate Calculation

B.1 Heat input to the evaporator

= mass flow rate of water x specific heat x temperature difference

$= 8.9 \times 10^{-5} \times 979 \times 4267 \times (70.3 - 66.4)$

$= 1450 \pm 45$ W

B.2 Heat loss from wooden box

= average heat transfer coefficient x surface area x temperature difference

$= 8.6 \times 1.1 \times (33 - 22)$

$= 104 \pm 5.5$ W

B.3 Heat loss from top plate

$= 12.3 \times 0.22 \times (63 - 22)$

$= 111 \pm 7.5$ W

B.4 Total heat losses

$= 104 + 111$

$= 215 \pm 8.4$ W

B.5 Heat transport rate of the HPHE = Heat input - (losses from wooden box and top plate)

$= 1450 - 215$

$= 1235 \pm 51$ W

C. Error Estimation

Standard deviation and arithmetic mean are calculated as follows [76, 77]:

C.1 Standard Deviation

$$\sigma = \sqrt{\frac{\sum_{1}^{N} (x_i - \overline{X})^2}{(N-1)}} \qquad \text{(B.1)}$$

C.2 Arithmetic mean

$$\overline{X} = \frac{\sum_{1}^{N} x_i}{N} \qquad \text{(B.2)}$$

where:

I = point number of the series

N = total number of measurements

x_i = value of the measurement at i_{th} point

$\overline{X}$ = arithmetic mean of the measurement

D. Sample Calculation for Standard Deviations

Volumetric flow rate of heating water (lph): 327, 314, 318, 316, 325

Number of measurements: 5

Mean value ($\overline{X}$) = 320 lph

Deviation with respect to mean value, $\sum_{1}^{N}(x_i - \overline{X})^2 = 130$

Standard Deviation, $\sigma = \sqrt{\frac{130}{4}} = 5.7$

APPENDIX - C

EVAPORATION AND CONDENSATION HEAT TRANSFER COEFFICIENT

The average heat transfer coefficients in the evaporator and condenser sections are calculated by using Nusselt's correlation [1]:

$$\bar{h}_e = \frac{4}{3}\left[\frac{\rho_l^2 \, k_l^3 \, g \, \lambda}{4 \, \mu_l \, (T_{w,e} - T_{sat}) \, L_e}\right]^{1/4} \tag{C.1}$$

$$\bar{h}_c = \frac{4}{3}\left[\frac{\rho_l^2 \, k_l^3 \, g \, \lambda}{4 \, \mu_l \, (T_{sat} - T_{w,c}) \, L_c}\right]^{1/4} \tag{C.2}$$

The heat transfer rate through the evaporator and condenser sections under steady state is equal.

$$\bar{h}_c L_c (T_{sat} - T_{w,c}) = \bar{h}_e L_e (T_{w,e} - T_{sat}) \tag{C.3}$$

Based on the above equations, the vapour saturation temperature is calculated as:

$$T_{sat} = \frac{T_{w,e} L_e + T_{w,c} L_c}{L_c + L_e} \tag{C.4}$$

The mean evaporation heat transfer coefficient of the heat pipe obtained experimentally under different operating conditions is presented in Table C-1.

Table C-1: Evaporation heat transfer coefficient of the heat pipe at different heating fluid temperatures & tilt angles

Sl. No.	Tilt angle (Degree)	Evaporation heat transfer coefficient ($W/(m^2-K)$)			
		Heating fluid temperature			
		40.9 °C	49.5 °C	60.0 °C	70.3 °C
1.	15	9,016	9,375	8,862	9,017
2.	20	9,272	9,628	9,006	9,422
3.	25	9,508	9,619	9,390	9,626
4.	30	9,444	9,529	9,529	10,016
5.	35	9,405	9,956	10,048	10,084
6.	90	10,131	10,612	10,346	11,466

The mean condensation heat transfer coefficient is found to be the same as the evaporation heat transfer coefficient because the saturation temperature is the same for calculation of the evaporation & condensation heat transfer coefficient under steady state condition.

REFERENCES

1. Faghri, Amir, "Heat pipe science and technology", Taylor & Francis, Washington, 1995.

2. Dunn, P.D. and Reay, D.A., "Heat pipes", Pergamon Press, New York, 1982.

3. Chi, S.W., "Heat pipe theory and practice: a sourcebook", Hemisphere Publishing Corporation, Washington, 1976.

4. Shah, R.K., "Heat exchanger design methodology - an overview", Heat Exchangers: Thermal-Hydraulic Fundamentals and Design, Hemisphere Publishing Corporation, Washington, 1980, pp. 455-460.

5. Peterson, G.P., "An introduction to heat pipes", John Wiley & Sons, Inc., New York, 1994.

6. Romestant, C., Alexandre, A., and Bonhomme, C., "Power diode cooling by heat pipe module", Proceedings of the 11th Intl. Heat Pipe Conference, Tokyo, Japan, Vol. 2, 1999, pp. 26-31.

7. Hwan Moon, Seok, Kim, Chul Ju, Kim, Bon Hoon, Hong, Sung Eun, and Lee, Jin Sung, "An experimental study on the performance limitation of a micro heat pipe with triangular cross-section", Proceedings of the 11th Intl. Heat Pipe Conference, Tokyo, Japan, Vol. 1, 1999, pp. 15-19.

8. Kim, Kwang Soo, Moon, Seok Hwan, and Choi, Choon Gi, "Cooling characteristics of miniature heat pipes with woven-wired wick", Proceedings of the 11th Intl. Heat Pipe Conference, Tokyo, Japan, Vol. 1, 1999, pp. 20-25.

9. Tathgir, R.G., Kumar, A., and Gangacharyulu, D., "Performance characteristics of a carbon steel heat pipe at low temperature range", Proceedings of the 11th Intl. Heat Pipe Conference, Tokyo, Japan, Vol. 2, 1999, pp. 26-31.

10. Negishi, K., Kaneko, K., Matsuoka, T., Hirashima M., Nishikawa, Y., and Taguchi, M., "Heat-transfer performance of a corrugated-tube thermosyphon - part 1, evaporator performance", Heat Transfer - Japanese Research, Vol. 20, No. 2, 1991, pp. 144-157.

11. Terdtoon, P., Tantakom, P., and Buddajan, K., "Plastic thermosyphon", Proceedings of the 11th Intl. Heat Pipe Conference, Tokyo, Japan, Vol. 2, 1999, pp. 16-19.

12. Shiraishi, Masao, Kim, Young In, Murakami, Masahide, and Terdtoon, P., "A correlation for the critical heat transfer rate in an inclined closed thermosyphon", Proceedings of the 5th Intl. Heat Pipe Symposium, Melbourne, Australia, 1996, pp. 248-254.

13. Terdtoon, P., Rithidej, Sumpun, and Shiraishi, M., "Effect of aspect ratio and Bond number on heat transfer characteristics of an inclined two phase closed thermosyphon at normal operating condition", Proceedings of the 5th Intl. Heat Pipe Symposium, Melbourne, Australia, 1996, pp. 261-266.

14. Abhat, A. and Nguyenchi, H., "Investigation of performance of gravity assisted copper-water heat pipes", Proceedings of the 2nd Intl. Heat Pipe Conference, Vol.1, Bologna, Italy, 1976.

15. Wilkins, E. S. and Al-left, A. A., "Experimental study of gravity-assisted heat pipes", Kerntechnik, Vol. 55, No. 4, 1990, pp. 235-238.

16. Maziuk, V., Kulakov, Rabetsky, and Vasiliev, L, "Miniature heat pipe thermal performance prediction tool - software development", Proceedings of the 11th Intl. Heat Pipe Conference, Tokyo, Japan, Vol. 1, 1999, pp. 26-33.

17. Lee, Yung, Rhi, Seok-Ho, and Kim, Won-Tae, "Simulation of cooling systems using two phase closed thermosyphons for telecomunication multi-chip modules", Proceedings of the 5th Intl. Heat Pipe Symposium, Melbourne, Australia, 1996, pp. 22-31.

18. Lee. Y. and Rhi, S.H., "Limitation of computer simulation for two-phase closed and loop thermosyphons", Proceedings of the 11th Intl. Heat Pipe Conference, Tokyo, Japan, Vol. 3, 1999, pp. 31-37.

19. Howard, A.H. and Peterson, G.P., "Investigation of a heat pipe array for convective cooling", J. of Electronic Packaging, Transactions of the ASME, Vol. 117, No. 3, 1995, pp. 208-214.

20. Fand, R.M., "Heat transfer by forced convection from a cylinder to water in crossflow", Intl. J. of Heat Mass Transfer, Vol. 8, 1965, pp. 995.

21. Dobson, R.T. and Kröger, D.G., "Evaporator heat transfer coefficient and maximum heat transfer rate of an inclined two phase closed-thermosyphon", Proceedings of the 11th Intl. Heat Pipe Conference, Tokyo, Japan, Vol. 2, 1999, pp. 34-39.

22. Abhat, A. and Seban, R.A., "Boiling and evaporation from heat pipe wicks with water and acetone", J. of Heat Transfer, 1974.

23. Davis, M.J. and Chaffey, G.H., "Development and demonstration of improved gas to gas heat exchanger for the recovery of residual heat", Report EUR 7127, Commission of the European Communities, 1981.

24. Zukauskas, A., "Heat transfer from tubes in cross flow", Adv. Heat Transfer, Vol. 8, 1972, pp. 93-162.

25. Churchill, S.W. and Bernstein, M., "A correlating equation for forced convection from gases and liquid to circular cylinders in cross flow", J. of Heat Transfer, Vol. 99, 1977, pp. 300-306.

26. Chapman, Alan J., "Fundamentals of heat transfer", Macmillan Publishing Company, New York, 1987.

27. Holman, J.P., "Heat Transfer", McGraw Hill, Inc., New York, 8th Edition, 1997.

28. Churchill, S.W. and Chu, H.H.S., "Correlating equations for laminar & turbulent free convection from a vertical plate", Intl. J. of Heat Mass Transfer, Vol. 18, 1975, pp. 1323.

29. Sparrow, E.M. and Gregg, J.L., "Laminar free convection heat transfer from outer surface of a vertical circular cylinder", Transactions of the ASME, Vol. 78, 1956, pp. 1823.

30. Fujii, T. and Imura, H., "Natural convection from a plate with arbitrary inclination", Intl. J. of Heat Mass Transfer, Vol. 55, 1972, pp. 755-767.

31. Yildiz, Ş. and Yüncü, H., "An experimental investigation on performance of annular fins on a horizontal cylinder in free convection heat transfer", Heat & Mass Transfer, Vol. 40, No. 3-4, 2004, pp. 239-251.

32. Zelko, Miroslav and Polasek, Frantisek, "Cooling of power electronics by heat pipes", Proceedings of the 5th Intl. Heat Pipe Symposium, Melbourne, Australia, 1996, pp. 199-207.

33. Murase, T., Tanaka, S., and Ishida, S., "Natural convection type long heat pipe heat sink powerkicker for the cooling of GTO thyristor", Proceedings of the 6th Heat Pipe Conference, Grenoble, France, 1987, pp. 537-542.

34. Krishnamoorthy, S. and Pillai, B.C., "Heat pipes for transformer cooling", National Seminar on Heat Pipe for Rural & Industrial Applications, National Physical Laboratory, New Delhi, India, 1993, pp. 19-26.

35. Saaski, E.W. and Franklin, J.L., "The use of two-phase heat transfer for improved transformer cooling", Electric Power Research Institute, Research Report, California, USA, 1997.

36. Waldon, P.L. and Bennett, R.E., "Electrical apparatus with heat pipe cooling", US Patent, No. 4,009, 417, 1977.

37. Polasek, F, "Cooling of A.C. motor by heat pipe", Proceedings of the Ist Intl. Heat Pipe Conference, Stuttgart, Germany, 1973.

38. Groll, M., Krähling, H., and Münzel, W.D., "Heat pipe for cooling of an electric motor", 3rd Intl. Heat Pipe Conference, Palo Alto, USA, 1978.

39. Bradford, M. and Highgate, D., "Heat pipes in rotating machines", Technical Report, ERA Technology Ltd., Surrey, England, 1988.

40. Ponnappan, R. and Leland, J. E., "High speed rotating heat pipe for aircraft applications", SAE Aerospace Atlantic Conference, Dayton, USA, 1995.

41. Yerkes, K. L. and Beam, J. E., "Arterial heat pipe performance in a transient heat flux and body force environment", SAE Aerotech Conference, Anaheim, USA, 1992.

42. Gottschlich, J. M. and Meininger, M., "Heat pipe turbine vane cooling", 27th Intersociety Energy Conversion Engineering Conference, San Diego, USA, 1992.

43. Silverstein, C. C., Gottschlich, J. M., and Meininger, M., "Feasibility of heat pipe turbine vane cooling", Transactions of the ASME, 1994, pp. 1-7.

44. Cao, Yiding and Wang, Qian, "Reciprocating heat pipes and their applications", J. of Heat Transfer, Vol. 117, 1995, pp. 1094-1096.

45. Tan, J.O. and Liu, C.Y., "Predicting the performance of a heat-pipe heat exchanger using the effectiveness-NTU method", Intl. J. of Heat and Fluid Flow, Vol. 11, No. 4, 1990, pp. 376-379.

46. Hsieh, Shou-Shing, "A generalized correlation for thermal design data of heat pipe heat exchanger", Intl. J. of Heat Mass Transfer, Vol. 5, 1985, pp. 89-99.

47. Hsieh, S. and Huang, D., "Thermal performance and pressure drop of counter-flow and parallel heat pipe heat exchangers with aligned rows", Heat Recovery Systems & CHP, Vol. 8, No. 4, 1988, pp. 343-354.

48. Hsieh, S. and Huang, D., "Comparisons of thermal performance and pressure drop of counterflow and parallel-flow heat-pipe heat exchangers with aligned/staggered tube rows", Energy Conversion and Management, Vol. 30, No. 4, 1990, pp. 357-368.

49. Peretz, R. and Horbaniuc, B., "Optimal heat pipe heat exchanger design", Heat Recovery Systems & CHP, Vol. 4, No. 1, 1984, pp. 9-24.

50. Tan, J.O., Liu, C.Y., and Wong, Y.W., "Heat pipe heat exchanger optimization", J. of Heat Recovery Systems & CHP, Vol. 11, No. 4, 1991, pp. 313-319.

51. Swanson, L. W., "External parameter selection for countercurrent heat pipe heat exchangers", Transactions of the ASME, Heat Transfer Division, Vol. 118, 1989, pp. 25-30.

52. Azad, E., Bahar, F., and Moztarzadeh, F., "Design of water to air gravity-assisted heat pipe heat exchanger", Heat Recovery Systems & CHP, Vol. 5, No. 2, 1985, pp. 89-99.

53. Azad, E. and Gibbs, B.M., "Analysis of air-to-water heat pipe heat exchanger", Heat Recovery Systems & CHP, Vol. 7, No. 4, 1987, pp. 351-358.

54. Peretz, R. and Bendescu, J., "The influence of the heat pipe heat exchanger's geometry on its heat transfer effectiveness", Heat Recovery Systems & CHP, Vol. 3, No. 1, 1983, pp. 23-34.

55. Azad, E. and Geoola, F., "A design procedure for gravity-assisted heat pipe heat exchanger", Heat Recovery Systems & CHP, Vol. 7, No. 4, 1987, pp. 101-111.

56. Azad, E., Mohammadieh, F., and Moztarzadeh, F., "Effect of different arrangement of performance of heat pipe heat recovery system", Heat Recovery Systems & CHP, Vol. 6, No. 2, 1986, pp. 143-149.

57. Shah, R.K. and Giovannelli, A.D., "Heat pipe heat exchanger design theory", National Chemical Laboratory, Pune, India, 1986, pp. 6.132-6.168.

58. Liu, C.Y., Ying, W.M., and Tan, J.O., "Note on method of analysis for heat pipe heat exchanger", Intl. J. of Heat Mass Transfer, Vol. 33, No. 8, 1990, pp. 1774-1775.

59. Gnielinski, V., "Equations for calculating heat transfer in single tube-rows and banks in transverse flow", Intl. Chem. Engg., Vol. 19, 1979, pp. 380-391.

60. Feldman, K.T. and Lu, D.C., "Preliminary design study of heat pipe heat exchangers", Proceedings of the 2nd Intl. Heat Pipe Conference, Bologna, Italy, Vol. 1, 1976.

61. Gamal, M.G., Muftah, A.A., Yuan, Ha, Hu, Yacai, and Tu, Chuanjing, "Heat transfer analysis of heat pipe heat exchanger for nuclear heating supply system", Proceedings of the 5th Intl. Heat Pipe Symposium, Melbourne, Australia, 1996, pp. 310-315.

62. Wakiyama, Y., Harada, K., Inoue, S., Fujita, J., and Suematsu, H., "Heat transfer characteristics of a gas to gas heat exchanger using heat pipes", Heat Transfer-Japanese Research, Vol. 7, No. 1, 1978, pp. 23-29.

63. Wen, Guoping, Ao, Jianjum, Shenghe, Gu, Senghe, and Sun, Quanping, "The development and the application of the large integrative heat pipe air preheater", Proceedings of the 5th Intl. Heat Pipe Symposium, Melbourne, Australia, 1996, pp. 317-322.

64. Dube, V., Sauciuc, I., Akbarzadeh, A., and Davis, A., "Design, construction and testing of thermosyphon heat exchanger for medium temperature heat recovery", Proceedings of the 5th Intl. Heat Pipe Symposium, Melbourne, Australia, 1996, pp. 273-279.

65. Wadowski, T., Akbarzadeh, A., and Johnson, P., "Characteristics of a gravity assisted heat pipe based heat exchanger", Heat Recovery Systems & CHP, Vol. 11, No. 1, 1991, pp. 69-71.

66. Terdtoon, P., Chaitep, S., Soponpis, N., and Groll, M., "Thermosyphon economiser for package boilers: a case study in northern Thailand", Proceedings of the 5th Intl. Heat Pipe Symposium, Melbourne, Australia, 1996, pp. 267-272.

67. Hill, J. M. and Lau, A. S., "Performance of supermarket air-conditioning systems equipped with heat pipe heat exchangers", ASHRAE Transactions, Vol. 99 (1), 1993, pp. 1315.

68. Wasim, Saman, "Performance of a thermosyphon heat exchanger in an evaporative air conditioning system", Proceedings of the 5th Intl. Heat Pipe Symposium, Melbourne, Australia, 1996, pp. 296-300.

69. Danielewicz, Jan, "Two phase closed thermosyphon heat exchangers for heat recovery in HVAC systems", Proceedings of the 11th Intl. Heat Pipe Conference, Tokyo, Japan, Vol. 1, 1999, pp. 158-161.

70. Khantha, Pattnapong and Terdtoon, Pradit, "Heat pipe air preheater and its application in gypsum drying", Proceedings of the 11th Intl. Heat Pipe Conference, Tokyo, Japan, Vol. 2, 1999, pp. 256-261.

71. Bhatt, H.T. and Vora, S.M., "Stoichiometry", Tata Mcgraw Hill, 2nd Edition, 1984.

72. Somerscales, E.F.C., "Fouling of heat transfer equipment", Hemisphere Publishing Corporation, Washington, 1981.

73. Standards of the tubular exchanger manufacturers association (TEMA), 7th Edition, New York, USA, 1988.

74. McKinney, Billy Grant, "An experimental and analytical study of water heat pipes for moderate temperature range", University of Alabama, Ph.D. Thesis, USA, 1969.

75. Saunders, E.A.D., "Heat exchangers: selection, design, and construction", Longman Scientific & Technical, New York, 1988.

76. Squires, G.L., Taylor, J.R., Brandt, S., and Bevington, P.R., "Experimental uncertainties(errors)", http://physics.indiana.edu/~meyer1/p309s04/documents/errors.pdf.

77. Bejan, Adrian and Kraus, Allan D., "Heat Transfer Handbook", John Wiley & Sons, New York, 2003.

Thapar Institute of Engg: & Tech
PATIALA-147001
CENTRAL LIBRARY
92082 27 MAY 2005